EXPLORATION OF A CONDITION MONITORING SYSTEM FOR ROLLING BEARING BASED ON A WIRELESS SENSOR NETWORK

Mustafa Omran Aliwan

A Thesis Submitted to the University of Huddersfield
in Partial Fulfilment of the Requirements for
the Degree of Doctor of Philosophy

April 2016

TABLE OF CONTENTS

LIST OF FIGURES

LIST OF TABLES

LIST OF ABBREVIATIONS

AC	Alternating Current
ADC	Analog to Digital Converter
AIN0	Analog Input
AM	Amplitude Modulation
ANFIS	Adaptive Neuro-Fuzzy Inference System
CBM	Condition Based Monitoring
CCS	Code Composer Studio
CFFT	Complex FFT
CM	Condition Monitoring
CMSIS	Cortex Microcontroller Software Interface Standard
CPU	Central Processing Unit
CTS	Clear-To-Send
DAC	Data Acquisition Card
DC	Direct Current
DFT	Discrete Fourier Transform
DMA	Direct Memory Access
DSP	Digital Signal Processor
EMD	Empirical Mode Decomposition
EMI	Electromagnetic Interference
FAT	File Allocation Table
FFT	Fast Fourier Transform
FIFO	First-in, First-out
FIR	Finite Impulse Response
FMEA	Failure Modes and Effects Analysis
FPU	Floating Point Unit
FRF	Frequency Response function
GND	Ground
GPIO	General-purpose input/output
GPTM	General-Purpose Timer Module

GUI	Graphic User Interface
HHT	Hilbert Huang transform
HP	HorsePower
HT	Hilbert Transform
HV	High Voltage
IC	Integrated Circuit
IC	Integrated Circuit
ICDI	In-Circuit Debug Interface
IEPE	Integrated Electronics Piezo-Electric
IIR	Infinite Impulse Response
ISR	Interrupt Service Routine
KW	Kilo Watt
LAN	Local Area Network
LV	Low Voltage
MAC	Medium Access Network
MCU	Microcontroller Unit
MEMS	Micro-Electro-Mechanical Systems
MV	Medium Voltage
NFC	Near-Field Communication
NVIC	Nested Vectored Interrupt Controller
PE	Piezo-Electric
RAM	Random-Access Memory
RFI	Radio Frequency Interference
RFID	Radio Frequency Identification
RMS	Root Mean Square
ROV	RTOS Object Viewer
RPS	Revolutions per Second
RTC	Real-Time Clock
RTS	Request-To-Send
SES	Squared Envelope Spectrum
SF	Sample Frequency
SNR	Signal-to-Noise Ratio
SRAM	Static Random-Access Memory

SRS	Shaft Rotational Speed
STFT	Short Time Fourier Transform
TI	Texas Instrument
TI-RTOS	Texas Instrument -Real Time Operating System
U1CTS	UART1 Clear To Send
U1RTS	UART1 Request to Send
U1RX	UART1 Receiver
U1TX	UART1 Transmitter
UART	Universal Asynchronous Receiver/Transmitter
USB	Universal Serial Bus
WA	Wavelet Analysis
WLAN	Wireless Local Area Network
WMAN	Wireless Metropolitan Area Network
WPAN	Wireless Personal Area Network
WT	Wavelet Transform
WWAN	Wireless Wide Area Network
µDMA	Micro Direct Memory Access Unit
ARAM	Autoregressive Moving Average
TSA	Time Synchronous Average

ABSTRACT

In recent years, wireless sensor networks (WSN) have attracted attention in machine condition monitoring (CM) fields for a more efficient system based on the inherent advantages of WSN, including ease of installation and relocation, lower maintenance cost and the ability to be installed in places not easily accessible. As critical components of rotating machines, bearings account for more than 40% of the various types of failures, causing considerable unpredicted breakdowns of a plant. Thus, this thesis intends to develop a cost-effective and reliable wireless measurement system for rolling bearing condition monitoring.

Based on the investigation of various wireless protocols, Zigbee has been taken as a the most promising candidate for establishing the wireless condition monitoring system as it can have an acceptable bandwidth at low power consumption. However, a comparison made between wired and wireless measurement system has found that the Zigbee based wireless measurement system is deficient in streaming long continuous data of raw vibration signals from typical application environment with inevitable ambient interference. As a result, data loss can happen from time to time.

To solve this issue, an on-board processing scheme is proposed by implementing advanced signal processing algorithms on the sensor side and only transmitting the processed results with a much smaller data size via the wireless sensor network. On this basis, a wireless sensor node prototype based on the state-of-the-art Cortex-M4F is designed to embed customizable signal processing algorithms. As an extensively employed algorithm for bearing fault diagnosis, envelope analysis is chosen as the on-board signal processing algorithm. Therefore, the procedure of envelope analysis and considerations for implementing it on a memory limited embedded processor are discussed in detail. With the optimization, an automatic data acquisition mechanism is achieved, which combines Timer, ADC and DMA to reduce the interference of CPU and thus to improve the efficiency for intensive computation. A 2048-point envelope analysis in single floating point format is realized on the processor with only 32kB memory.

Experimental evaluation results show that the embedded envelope analysis algorithm can successfully diagnose the simulated bearing faults and the data transmission throughput can be reduced by at least 95% per frame compared with that of the raw data; this allows a large number of sensor nodes to be deployed in the network for real time monitoring.

Furthermore, a computation efficient amplitude based optimal band selection algorithm is proposed for choosing an optimal band-pass filter for envelope analysis. Requiring only a small number of arithmetical operations, it can be embedded on the wireless sensor node to yield the desired performance of bearing fault detection and diagnosis.

Keywords: *Wireless sensor network, Zigbee, rolling bearing, local data processing, envelope analysis, Hilbert transform, Cortex-M4F.*

DECLARATION

No portion of the work referred to in this thesis has been submitted in support of an application for another degree or qualification of the University of Huddersfield or any other university or other institute of learning.

COPYRIGHT

ACKNOWLEDGMENT

Firstly and foremost, I would like to thank Almighty God for providing the strength to complete my PhD and His guidance throughout my life.

This work has been carried out within the School of Computing and Engineering, Department of Mechanical engineering at the University of Huddersfield, UK. It was financially funded by Libyan higher education through the Libyan cultural affairs in London. I am very grateful to their support during this project.

I would like to thank my supervisor, Prof. Andrew D. Ball, for all his guidance and help during this research. I am especially grateful to Dr. Fengshou Gu, for his sincere and warm-hearted support and encouragement. This work would never have been accomplished without his very often interesting discussions and multi-disciplinary research expertise.

Special thanks my friend Mr. Guojin Feng who has shared with me the ideas regarding our research and encouraged me throughout my research time. I also appreciate the help from all my friends I have met in Huddersfield. They have made my time here both enjoyable and unforgettable.

I also give thanks to my mum, Mabrouka, my dad, Omran and my brothers and sisters for their love, support and motivation throughout my life.

I would like to thank my wife for her love, patience and unlimited encouragement throughout my study. My deepest thanks go to my lovely daughter and sons for their love.

Finally, I would like to thank all my relatives back home who supported me throughout my study and many thanks to all my friends back home.

PUBLICATIONS

Aliwan M., Gu F., and Ball A., (2012) A Study of Wireless Vibration Sensors for Monitoring Bearing Faults. The 2nd International Workshop and Congress on eMaintenance, Luleå University Technology, Luleå, Sweden.

G. Feng, A. Mustafa, D. Zhen, F. Gu and A. D. Ball (2013) The Real-time Implementation of Envelope Analysis for Bearing Fault Diagnosis Based on Wireless Sensor Network, Proceedings of the 19th International Conference on Automation & Computing, Brunel University, London, UK.

G. Feng, M. Aliwan , J. Xi Gu, D. Zhen, F. Gu and A. Ball (2014) The Implementation of Envelope Analysis on a Wireless Condition Monitoring System for Bearing Fault Diagnosis, Manchester, UK.

G. Feng, D. Zhen, M. Aliwan, F. Gu, and A. Ball (2013). Investigation of Wireless Protocols for Remote Condition Monitoring, in Proceedings of Computing and Engineering Annual Researchers' Conference 2013, G. Lucas, Ed. Huddersfield: University of Huddersfield, 2013, pp. 19–24.

M. Hamed , B. Tesfa, Aliwan M., Gu F., and Ball A., (2012) The influence of vehicle tires pressure on the suspension system response by applying the time-frequency approach, Proceedings of the 19th International Conference on Automation & Computing, Brunel University, London, UK.

Chapter 1
INTRODUCTION

As the modern industrial process becomes more complicated, the maintenance tasks become more important and the relevant costs quickly. This chapter starts with a consideration of the general current situation in maintenance development. Then, the maintenance strategies and popular condition monitoring techniques are explained. This is followed by a detailed description of the motivation, aims and objectives of the research. Finally, the outlines of the thesis are described.

1.1 Introduction of Machinery Maintenance

Most industrial processes are involving hundreds of pieces of equipment. The sudden breakdowns of individual items not only incurs damages to the equipment itself but also may cause economic loss due to the interruption of the plant's operation.

Rotating machinery is a crucial part of every manufacturing process. Motors, gearboxes, bearing, pumps, compressors, etc. are relied upon to operate efficiently to maintain a steady stream of production at maximum throughput. The duration of every piece of machinery is limited by the speed at which it is operating, the load to which it is subjected, the quality of its components, assembly and installation, its environment and the level of maintenance [1].

In recent years this view has been changed to one/off maintenance where the management of maintenance becomes an integral part of the operation and production subsequently bringing profits to the company [2]. This change has resulted in the development of several philosophies that aim to establish the most appropriate maintenance strategy for defined failure modes. One of the most widely used of these techniques is condition based maintenance. This technique defines maintenance actions based upon the change within one or a group of defined monitoring parameters. The principal parameter used is vibration which often provides a direct relevance to the condition of rotating machinery and its diagnostic value.

The manufacturing of bearings is one of the most important processes involved in rotating machinery. In recent years, a variety of ways have been proposed to monitor their health condition for which, the wireless sensor networks based on condition; in this area, wireless sensor networks consist of many distributed sensors called nodes. These nodes are used to monitor or detect various kinds of change in vibration, pressure, temperature or movement etc. This research deals with the development of a vibration monitoring system for a bearing manufacturing machine tool based on wireless sensor networks (WSNs).

Currently, WSN technology has been successfully applied in many commercial areas such as environmental monitoring, construction health monitoring, temperature monitoring in product distribution, and debris flow monitoring [3].

Many industrial applications have unsuitable building layouts or walls that cannot be wired for various reasons making it difficult or impossible to build a wired network. Wireless networking in these environments is a very cost effective alternative and also provides future flexibility [3].

1.2 Maintenance Strategies and Condition Monitoring Techniques

The main objective for investment for many companies and industries are to achieve maximum profit from a minimum spends on plant and equipment. This means increasing machine throughput, reducing maintenance costs per machine and preventing unscheduled delays.

Condition monitoring differs generally from one machine to another in relation to the maintenance goals. For example, visual inspections may be suitable to assess the state of a simple production process, but for complex processes a condition monitoring structure may be demanded. Condition monitoring techniques should take into account both the monitoring objectives and cost. In recent years, the obvious benefits obtained by the application of condition monitoring have led to the development of an enormous number of new methods for condition monitoring. Some of the most commonly used machine and process condition monitoring techniques are discussed in the following section.[4],[5].

1.2.1 Breakdown Maintenance

In this technique, the machinery is simply run to failure then maintenance takes place. No predetermined action is taken to prevent failure and the emphasis is given on corrective maintenance. This can be done by repairing or replacing the failed components. This is the most costly of maintenance strategies when applied in critical equipment [6].

1.2.2 Preventative Monitoring

In this strategy the maintenance is based upon specific time intervals and relies on human senses, including sight, touch and sound, to assess the condition of machine. This can lead to savings in maintenance cost over breakdown maintenance [7] [8]. The amount of cost saving depends upon particular applications.

1.2.2.1 Visual Inspection

This technique again uses human senses to assess the condition of machine. Visual inspection alone might be able to detect the machine defects without the necessity for further inspections [8]. Visual inspection uses different types of tools, including simple magnifying glasses, low power microscopes, and devices like stroboscopes. It is commonly applied in several areas to detect cracks, sub-surface defects, corrosion and leakage. Visual monitoring may use dye penetrants to present clearer pictures of cracks or fractures that may have taken place on the surfaces of machines [9]. In addition, different methods of visual inspection provide a flexible and immediate assessment of condition and require low level inspection skills. The problem is that different results may be found for the same machine by different inspectors due to the individual nature of their personal skills, although the use of appropriate instruments is more likely to give consistent results even with different operators. Also, the machine's performance is monitored and how it is designed to perform required functions, such as converting energy from one energy form to another and producing products. The data or information which is collected about performance monitoring can be indicative of the state of machine components [4].

The difficulty with this issue of monitoring is that its information may not be received on time or be clear enough in advance before the fault occurs.

1.2.2.2 Performance Monitoring

This refers to the machine performance and how it is designed to perform required functions. This monitoring technique uses targets to confirm that it performs certain functions such converting energy from one energy form to another and producing products. The data or information which is collected about performance monitoring can be indicative of the state of machine components. For example, tool wear may result in an increase of product dimensions and hence by checking the product quality, the extent of tool wear can be assessed. Performance monitoring employs a variety of transducers to detect changes in power, pressure, speed, load, temperature and flow [4].

1.2.3 Online condition monitoring

Online condition monitoring assesses the condition of all dynamic systems changes with time; these changes in the system signal provide information about the system. CM

emphasis on applying signal processing techniques to separate significant trends from random variation signals to diagnose the fault at an early stage. In the following sections there are more details about CM parameters including vibration and noise, acoustic emission and temperature.

1.2.3.1 Vibration and Noise Analysis

Table 1-1 Common parameters are used as indicators of machine condition [8].

Machine Fault	Vibration	Temperature	Oil Analysis
Out of Balance	X		
Misalignment/Bent Shaft	X		
Damaged Rolling Element Bearing	X		X
Damaged Journal Bearing	X	X	X
Damaged or Worn Gears	X		X
Mechanical Looseness	X		

Vibration analysis is gaining popularity because of its nature. . Unfortunately, no single technique has been found that is able to detect all machine faults. Vibration measurement is the most widely used CM technique in industry, because of its proven ability to detect the early presence of faults: however, it can identify only 60% to 70% of machine faults. Vibration analysis is now usually performed online via a computer-based machine CM system and does not require the shutdown of the machinery. **Error! Reference source not found.** compares vibration analysis against two monitoring parameters, temperature and oil analysis, which whilst not as powerful and versatile as vibration measurement, can be used to provide warning of an impending machine breakdown [10] [11].

In practice, it is often difficult to extract meaningful information from vibration spectra based on Fourier Transform (FT) of time-domain to frequency-domain. In the early stages of fault development, important defining frequencies have low amplitude and can be masked by other vibration sources or buried in background noise. This is particularly relevant because the individual vibration impulses generated by rolling bearing defects typically tend to be of short duration, causing the corresponding frequency pulse to spread over a wide frequency band with low amplitude. It can also be very difficult to identify a particular frequency indicative of a defect when a large number of spectral components are present [12].

Vibration monitoring and analysis vibration levels on machine frames and bearing housings and relative movements between shaft journals and bearings provide a useful guide to such faults as imbalance, misalignment, etc. By implementing vibration analysis, this will improve the reliability of the machines and lead to better machine efficiency and reduced down time by eliminating mechanical or electrical failures.

In recent years, continuous vibration monitoring of process plants has become an accepted practice often using permanent electronic installations. It is known that vibrations would have special features under normal or abnormal conditions. It is not only the vibration amplitude which should be known but also the frequencies of vibrations which are important [13]. Li used neural networks to perform motor bearing fault diagnosis based vibration signals. The results show that neural networks can be effectively used in the diagnosis of various motor bearing faults [14]. Monavar et al described the suitability of vibration monitoring and analysis techniques to detect defects in roller bearings [15].

As an example, unbalance results in vibrations which have a frequency equal to that of running speed, while misalignment or looseness results in frequencies which are multiples of running speed. For frequency analysis, it is necessary to analyze the vibration signal using filters and a spectrum analyser. This analyzer is the real time analyzer or a Fast Fourier Transform Analyzer (FFT) which gives an instantaneous picture of amplitude vs. frequency. For example if the outer race of the roller bearing has a fault, because of one of the failure mechanisms, each time one of the balls rolls over the flaw, a high-level short duration (impulsive) force is incurred that causes the bearing to vibrate. The bearing responds by "ringing" at its natural frequency, a response that decays quickly because of damping. The excitation and response occur each time when one of the balls rolls over the flaw, so that the fundamental frequency of the response waveforms is the rate at which the elements roll over the flaw. It is the fundamental frequency which is of interest in the detection of bearing faults, not the resonance frequency at which the bearing rings. The resonance frequency can be predicted from the bearing geometry and the speeds at which the inner and outer races rotate. Different frequencies are obtained for flaws in an outer race, inner race, on one of the balls, or in the cage.

1.2.3.2 Acoustic Emission

Acoustic emission has been successfully used in a number of applications including the testing of pressure vessels, detection of leaks, cavitation detection, corrosion fatigue crack detection, seal failure detection and detection of damage in rolling [16].

Acoustic emission (AE) is the phenomena of transient elastic wave generation due to a rapid release of strain energy caused by a structural alteration in a solid material under mechanical or thermal stresses. AE technology should be able to detect the cracks under the surface of a rolling race before the defect in the surface forms. While vibration signals only shows significant changes when defects are present, the AE method may be able to detect the fault propagation earlier. AE and vibration signals share similar features of involving periodic impact and resonance. The difference is that the resonance excited by the impulse in the AE has a high frequency above 100 kHz, while the resonance in vibration signal has a lower frequency below 20 kHz [17].

In Comparative studies of various vibration and acoustic emission measurement methods [18], [19], [20], measurements were conducted on good new bearings and bearings with simulated defects in their elements. Vibration measurements included the overall vibration acceleration, envelope-detected acceleration, kurtosis, crest factor and shock pulse; acoustic emission measurements included ring down counts, event duration and peak amplitude. The results indicated that, in general, the detection of defects at lower speeds is highest with acoustic emission and lowest with the vibration shock pulse method. James (1995) and Miettinen et al. (2000) carried out experiments using acoustic emission for bearing monitoring. They found that AE is an effective condition monitoring method for early fault detection in bearings. The results showed that the appearance of distinct random transients indicated the degradation of bearing condition. As degradation intensified the number of bursts and the mean signal level also rose. The dramatic reduction of AE events was achieved when pump bearings were re-greased [21], [22] .

Tandon and Choudhury reviewed the vibration and acoustic measurement method for the detection of defects in rolling element bearings. Vibration measurement in both time and frequency domains along with signal processing techniques such as the high-frequency resonance technique have been covered [23].

Xiaoqin Liu, et al. comparing AE signals to vibration signals with three conditions of different shaft speeds, found that at the same fault condition, with higher rotary speed, the AE method is superior to vibration method; but at lower speed, the AE is overtaken by the vibration method. High frequency components above 50 kHz are almost completely absent in the experimental AE signals. The higher frequency band in the AE signal declines more when rotary speed slows down. The AE shows no significant advantage over vibration on detecting small fault at low speed. This may due to two factors[24].

1.2.3.3 Temperature Monitoring

Thermocouples and resistance thermometers are used for measuring bearing temperatures. Useful warning of failure may be obtained by monitoring maximum bearing surface temperature. Excessive bearing temperature is followed by failure, within hours. Infrared thermography techniques are used to monitor both the temperatures and temperature pattern of equipment in operation. This information along with data on physical construction of the component and the thermodynamic state of equipment is used to evaluate the degree of deterioration of an item of process plant. Thermography is used to locate the increased surface temperature associated with corrosion damage in furnaces and stacks.

1.3 Motivation to Conduct Wireless Condition Monitoring

This research is motivated by both the potential benefits and the great challenges of implementing a wireless network for remote condition based maintenance. Wireless networks are used in the industry field have certain advantages such as [25], [26]:

Installation: Wireless networks can be easy to use and cost-effective for areas such as hazardous plants and where high-assets protection applications are used; they are also ideal for areas that present access problems such as across rivers or in mountainous or rural areas. Installation of a wireless network can eliminate the need for long cabling for any communication system [27].

Maintenance: Recent advances and the cost of cabling can be the highest cost of a project. For example, in dangerous and non-reachable places, some cabling can cost around $2,000 per foot (£4,134 per meter) [28]. As the wires age, they can crack or fail. It

needs a great deal of time and labour to inspect and trouble shoot. The maintenance of these cables and sensors is usually much more expensive than the cost of the sensors themselves [29].

Mobility and Flexibility: The ease of relocation is another advantage of using a wireless network. Since there are no wires, the plant managers can better track materials and reconfigure assembly lines to meet changing customer demands. Wireless sensor networks can be installed without going into the complexities of planning the cabling routes for the wired networks. [25].

Security: Industrial wireless network must be more secure to protect the data. Preventing intrusion and malicious jamming of frequencies are primary concerns when applying wireless technology [30]. The wired network has some inherent advantages in security over the existing wireless network. However, the advances in modern encryption and identity recognition can solve this problem and are making wireless networks much safer.

1.4 Research Aims and Objectives

The aim of this research is to explore a cost-effective, reliable and practical wireless measurement system to monitor the health status of rolling bearings. To achieve this aim, the objectives are listed below.

- Investigate the popular condition monitoring techniques and select an effective one to monitor the health status of the bearing.
- Investigate the fundamentals of rolling bearings, including bearing types, components and common failures, and explore the fault generation mechanisms.
- Review the popular signal processing algorithms and select effective signal processing algorithms for bearing fault feature extraction and diagnosis.
- Study the current popular wireless protocols and their applications for condition monitoring and choose a suitable wireless protocol suitable for the industrial environment.
- Make a comparison test between a wired and wireless condition monitoring system and evaluate the performance of the wireless measurement system.
- On-board local data processing is an effective way to reduce the data throughput of the wireless network and thus solve the bandwidth limitations of the Zigbee

network. In order to implement customizable signal processing algorithms, the wireless sensor node needs to be redesigned.

- Study the implementation procedure of envelope analysis algorithm and realize it on an embedded processor with limited memory and computing capability.
- Implement and optimize the envelope analysis on the designed wireless sensor node.
- Evaluate the wireless sensor node with embedded envelope analysis and examine its performance for bearing fault diagnosis.

1.5 Outline of Thesis

This thesis comprises 10 chapters according to the logical connection involved in achieving the research objectives. The following is a brief description of each chapter:

Chapter one:

This chapter begins with a general situation about current maintenance development. Then, the maintenance strategies and popular condition monitoring techniques are explained. This is followed by a detailed description of the motivation, aims and objectives of the research. Finally, the outlines of the thesis are described.

Chapter two:

This chapter firstly reviews the machinery failure report. Then, various bearing types and their application areas are studied. As a typical example, the rolling bearing is specially studied. Finally, common bearing faults and bearing fault signal characteristics are summarised.

Chapter three:

In this chapter, the current popular signal processing methods are investigated in three main categories: time-domain, frequency domain and time-frequency. Their applications to extracting or diagnosing bearing faults are specifically explored.

Chapter four:

This chapter reviews the main features of the most popular wireless techniques and their typical applications in the condition monitoring fields. Then, a comparison is made with

a specific purpose for machinery condition monitoring. Finally, the requirements and challenges for employing wireless techniques in the industrial field are discussed.

Chapter five:

In this chapter, a cost-effective commercially available wireless measurement system is employed to collect the vibration signal of a bearing test rig. As a comparison, a wired data acquisition system is used to collect the vibration signal as well. Then, both signals from the wired and wireless system are processed by using the envelope analysis method.

Chapter six

This chapter presents a hardware design for a wireless sensor node, on which some local processing algorithms can be implemented so as to reduce the data output requirement. By doing this, the transmission load of the wireless measurement system is hoped to be reduced and thus multiple sensor nodes can coexist in the same wireless network.

Chapter seven:

This chapter gives an introduction to the sensor node development. It explains the programs of the embedded processor which were developed under the powerful integrated code composer studio (CCS) environment. It also gives more details about implementation and optimization of data acquisition to improve the CPU efficiency by using four methods. Finally, the signal processing is optimized by applying FFT and Hilbert Transform.

Chapter eight:

This chapter explains the software development work involved on the wireless sensor node, including the data acquisition process, the implementation of envelope analysis and data transmission. The programs of the embedded processor are developed under the integrated environment code composer studio (CCS) and the real time operating system TI-RTOS is employed to handle the task scheduling.

Chapter nine

In this chapter, the middle processing results of the implemented algorithm are analyzed online in the CCS development environment. Then, they are further employed to evaluate two other kinds of bearing faults (inner race and roller element). Based on the

experiments, a practical and effective band-pass filter selection algorithm is developed to automatically select the effective pass band on the wireless sensor node.

Chapter ten

This chapter presents the conclusions and reviews the achievements of the project against the aim and objectives, describes the contribution to knowledge made by the research, and suggests possible future work.

Chapter 2
OVERVIEW OF ROLLING BEARING AND ITS FAULT GENERATION MECHANISM

Being an important part of the rotating machines, bearing plays a crucial role in the modern industrial manufacturing process. According to the investigation, bearing accounts for a rather high percentage of failure among the various types of machinery components. This chapter firstly reviews the machinery failure report followed by the studies on the various bearing types and their application areas. This chapter also provides a summary on the common bearing faults and the bearing fault signal characteristics.

2.1 Introduction to Rolling Bearing

Rolling bearings play an important role in rotating machines, which are extensively used in chemical industries, manufacturing plant, nuclear power stations, etc. The failure of rolling bearings is one of the major causes of machine breakdown, thus, many researches have been carried out on the rolling bearing fault detection and diagnosis over the past decades [31],[32],[33].

Machines with moving parts must have some ways to link those parts and guide their motions. It is used to enable rotational or linear movement, while reducing friction and handling stress. The working state of rolling bearings determines whether or not the equipment can be used normally. Vibration is unavoidable in the rolling bearing running state [34].

A survey conducted in 2008 reviewed condition monitoring methods for rotating electrical machines based on the literature of the past 30 years. The paper takes a holistic view of the subject and describes the methods in relation to the structure of machines and their usefulness as shown in Table 2-1 [35].

Previous study has shown that most engine or machinery problems are caused by bearing failure. In 1995 an IEEE survey covered petrochemical and similar industries. Other differences with the 1985 survey include a focus on machines ranging from 200 to 10,000 hp. The primary difference is identified in Figure 2.1 where various faults found in the machines were substantially different. It is noted that the EPRI study focused on utility motors that were 100 hp and larger, while the IEEE study related to machines of 10kW (~15 HP) and larger at 50 Hz and 60 Hz. The IEEE in Figure 2.1 shows 51% of survey bearing faults and EPRI study 41% of bearing fault [36].

Table 2-1 Distribution of failed subassemblies in electrical machines obtained from the literature

Subassemblies	Predicted by an OEM through FMEA[a] techniques, 1995-7	MOD[f] survey, Tavner, 1999 [37]	IEEE large Motor survey, 1985, 'Donnell, 1985 [38]	Motors in Utility Applications, Albrecht, 1986 [39]	Motor Survey Offshore and Petrochemical, Thorsen, 1995 [40]	Proportion of 80 Journal Papers published in IEEE and IEE on these subject areas over the past 26years
Types of machines	Small to medium LV[b] motors and generators, 150 kW[e], generally squirrel cage induction motors	Small LV[b] motors and generators , 750 kW[e], generally squirrel cage induction motors	Motors greater Than 150 kW[e] generally MV[c] and HV[d] induction motors	Motors greater than 75 kW[e] generally MV[c] & HV[d] induction motors	Motors greater than 11 kW[e] generally MV[c] & HV[d] induction motors	All machines
Bearings	75%	95%	41%	41%	42%	21%
Stator related	9%	2%	37%	36%	13%	35%
Rotor related	6%	1%	10%	9%	8%	44%
Others	10%	2%	12%	14%	38%	—

Notes: a) FMEA means Failure Modes and Effects Analysis.
b) LV means Low Voltage.
c) MV means Medium Voltage.
d) HV means High Voltage.
e) KW means Kilo Watt.
f) MOD means Ministry of Defence.

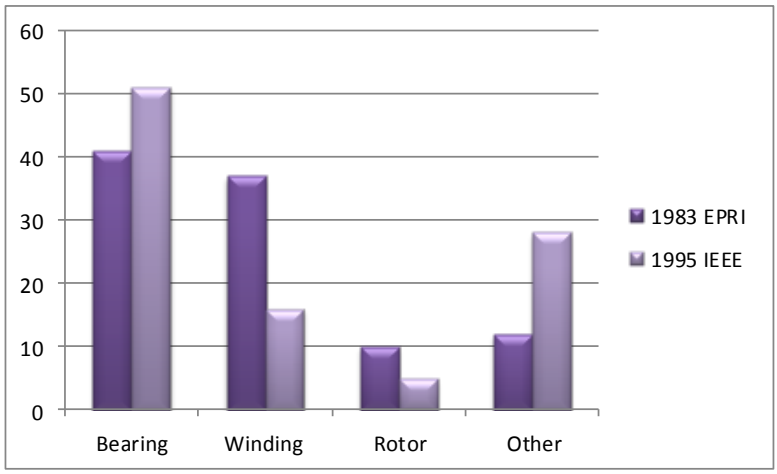

Figure 2.1 The comparison between 1983 EPRI study and 1995 IEEE survey [41]

Unexpected bearing failures can interrupt the production, cause unscheduled downtime and economic losses. So development of fault diagnosis and monitoring to prevent malfunctioning and failure of rolling bearings during operation is necessary. However, it is a great challenge to extract early bearing fault signatures from collected signals because components such as inner races, outer races, rollers, and cages in a rolling element bearing result in the complicated bearing vibration signals. Furthermore, the collected signal is covered by background noises and mixed with vibration signals of shafts, gears, and other mechanical components. Many diagnosis methods of rolling bearings have been developed for detection and diagnosis of bearing defects in recent years such as those based on vibration, acoustics, temperature measurements and wear debris analysis, the vibration analysis is the most frequently used technique for condition monitoring of rolling bearings, to determine the mechanical condition of machinery [42].

2.2 Rolling Bearing Types

As shown in Figure 2.2, rolling bearings can be divided into two main classifications: ball bearings and roller bearings. Ball bearings can be further classified according to their bearing ring configurations: deep groove, angular contact and thrust types. Roller bearings on the other hand are classified according to the shape of the rollers: cylindrical, needle, taper and spherical. Rolling bearings can be further classified according to the direction in which the load is applied; radial bearings carry radial loads and thrust bearings carry axial loads.

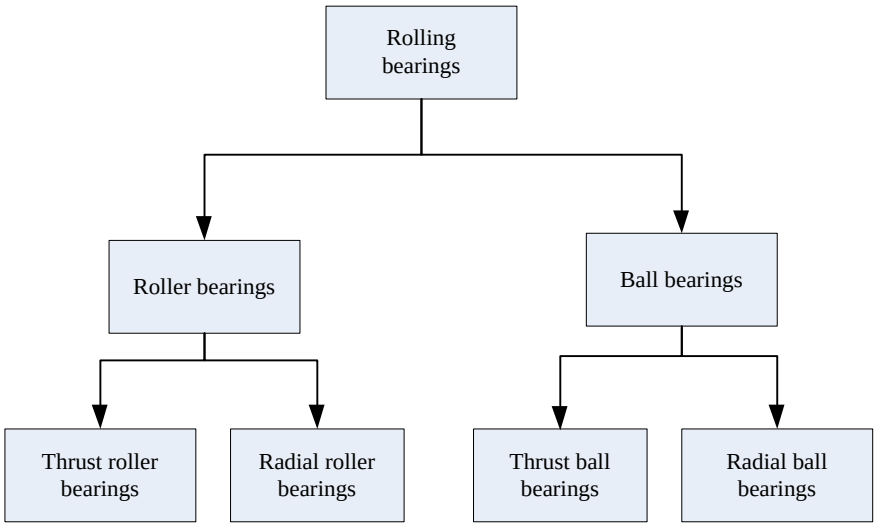

Figure 2.2 Classification of rolling bearings [43]

Figure 2.3 shows the picture of several common types of rolling bearings. Some of these rolling bearing are briefly introduced below.

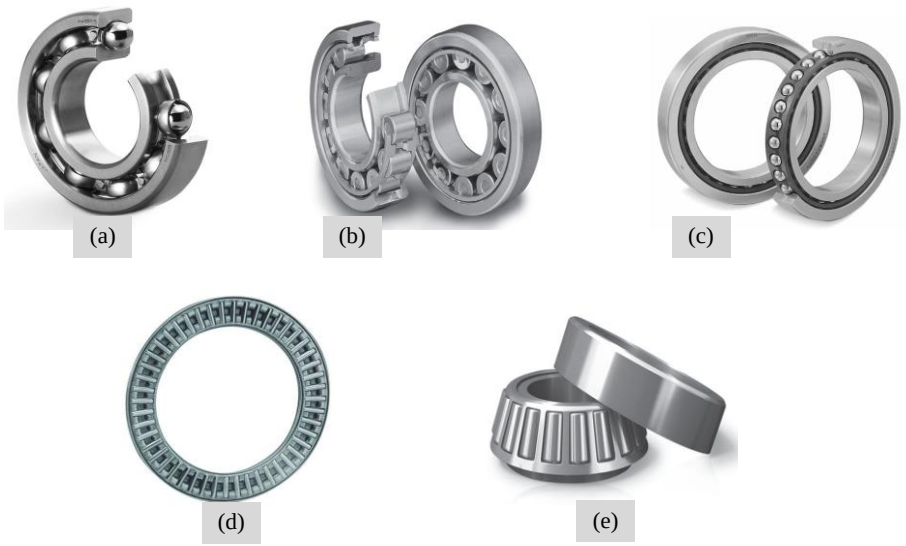

Figure 2.3 Types of rolling bearings. (a) ball bearing. (b) roller bearing (c) thrust bearing (d) needle roller thrust bearings (e) tapered roller bearing [44]

- **Ball Bearing**

Ball bearings are used in a wide array of machines for rotary motion. Ball bearings support rotary parts and reduce friction to facilitate the smooth operation of machines. Figure 2.3 (a) shows the ball bearing architecture. They are found in a widespread array of uses, such as roller blades and even hard drives. These bearings can handle both radial and thrust loads, and are usually found in applications where the load is quite small. The standard geometric shapes of rolling elements that create the rolling element

bearings include: balls, cylindrical rollers, needle rollers, tapered rollers, and spherical rollers. In a ball bearing, the load is conveyed from the outer race to the ball and from the ball to the inner race. Since the ball is a sphere, it only links the inner and outer race at a very small point, which helps it rotate very smoothly. But it also means that there is small contact area holding that load, so if the bearing is overloaded, the balls can deform, crush or destroy the bearing. Ball thrust bearing; the kinds of ball bearings as shown in Figure 2.3(c), are designed to carry almost exclusively thrust loads in low-speed low-weight applications. Bar stools, for example, make use of ball thrust bearings to support the seat.

- **Roller Bearing**

The purpose of a roller bearing is to reduce rotational friction and support radial and axial loads. Compared to ball bearings, roller bearings can support heavy radial loads and limited axial loads. The primary roller is a cylinder, which means the load is distributed over a larger area, enabling the bearing to handle much amounts of load see Figure 2.3 (b). Roller bearings are used in car and vehicle wheel bearings where they must cope simultaneously with large vertical (radial) and horizontal (axial) forces. Most of pumps and small to medium size motors run with roller bearings [45]. The roller is a cylinder, so the contact between the inner and outer race is not a point but a line. This spreads the load out over a larger area, allowing the bearing to handle much greater loads than a ball bearing. However, this type of bearing is not designed to handle much thrust loading. Some of the advantages of rolling contact bearings include exact shaft guiding, lower start-up torque, and fewer leakage and maintenance problems [46].

Roller thrust bearings are one of the roller bearings (see Figure 2.3(d)), which can carry thrust loads. The difference, however, lies in the amount of weight. Roller thrust bearings can support much amounts of thrust load, therefore is used in car transmissions, between gears, and between the housing and the rotating shafts. The helical gears used in most transmissions have angled teeth. This causes a thrust load that is supported by a bearing. As shown in Figure 2.3(e), tapered roller bearings are also designed to handle large radial and thrust loads. Tapered roller bearings are used in car hubs, where they are usually mounted in pairs facing opposite directions so that they can handle thrust in both directions.

2.3 Rolling Bearing Components

A rolling bearing as shown in Figure 2.4 mainly composes of four parts: inner race, outer race, rolling elements, and the cage [47]. Some special bearings may have additional components such as the guide race and seals. Typically, the inner race of the bearing is mounted on a rotating shaft, and the outer race is mounted to a stationary housing. The rolling elements may be balls or rollers. The balls in a ball bearing transfer the load over a very small surface on the raceways. The load-carrying capacity of a ball bearing is, therefore, lower than that of a roller bearing in which the rollers transfer the load via line contact with the raceways. The cage separates the rolling elements, preventing contact between them during operation, which also helps to prevent poor lubrication conditions and hold the bearing together during handling.

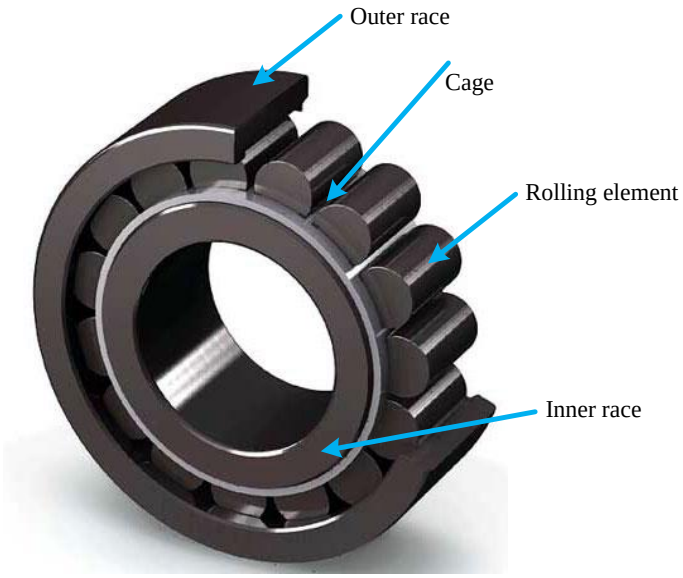

Figure 2.4 Components of a rolling bearing [47]

- **Inner race**

The inner race is the rotating part in most cases since it is mounted on the shaft of the machine. The inner race against which the rolling elements run have various forms depending on the type of rolling elements. The forms of the raceways may be spherical, cylindrical, or tapered. The defect on the inner raceway will create a series of high pulses at a rate same as the ball pass frequency relative to the inner raceway. Because the inner ring is rotating, the defect will enter and leave the load zone causing a variation in the rolling element-raceway contact force, hence deflections. While in the

load zone the amplitudes of the pulses will be highest but then reduce as the defect leaves the load zone resulting in a signal, which is amplitude-modulated at inner ring rotational frequency.

- **Outer race**

The outer race is mounted in the housing of the machine and in many cases it does not rotate. The raceways against which the rolling elements run have different forms such as cylindrical, spherical, or tapered, depending on the type of rolling elements. The fault on the outer raceway will generate a series of high energy pulses at a rate equal to the ball pass frequency relative to the outer race. Because the outer race is stationary the amplitude of the pulse will remain theoretically the same, and hence will appear as a single discrete peak within the frequency domain.

- **Rolling elements**

The types of rolling elements used in rolling bearings are classified as ball bearings and roller bearings. The balls in a ball bearing transfer the load by point contact with the raceway. The load-carrying capacity is therefore lower than that of a roller bearing, where rollers transfer the load via line contact with the raceways. The rolling elements are usually made of carbon chromium steel, also called bearing steel [45].

- **Cage**

Cages function to keep rolling elements at a uniform pitch so load is never applied directly to the cage and to avoid the rolling elements from falling out when handling the bearing. The cage separates the rolling elements to inhibit frictional contact between them during operation that would cause poor lubrication conditions. Cages are prepared from cold rolled steel strip. The bearing cage tends to rotate at typically 0.4 times inner ring speed, has a low mass and therefore, unless there is a fault from the manufacturing process, is generally not observable. Unlike raceway defects, cage failures do not usually excite specific ringing frequencies and this limits the effectiveness of the envelope spectrum. In the case of cage failure, the signature is likely to have random bursts of vibration as the balls slide [45].

Excessive clearance can lead to vibration at the fundamental train frequency (FTF) as the rolling elements accelerate via the load zone, which can result in large impact forces

between the rolling elements and cage.

- **Seal**

Seals are essential for a long and reliable life of a bearing. They protect the bearing from contamination and keep the lubricant inside the bearings.

- **Guide races**

Guide races are used in some spherical roller bearings that demand extremely high quality. The main function of the guide races is to lead the rollers in the bearings so that they can rotate parallel to the shaft and distribute the load evenly to the raceway.

2.4 Rolling Bearing Faults and Causes

There has been extensive research on rolling element bearings over many years to improve their reliability. Common rolling bearing faults and their mechanisms can lead to bearing damage, including mechanical damage, crack damage, and wear damage, lubricant deficiency, and corrosion. Abusive handling can induce nicks and dents, which are particularly harmful when located in areas traced by the rolling elements. When the smooth rolling contact surfaces are damaged, higher stress conditions are forced on the surface, reducing bearing lifetime considerably. Permanent indentation produced by rolling element overload is called brinelling. A crack in a bearing component may begin as a manufacturing-related defect or be induced by operating stress via overload or cyclic loading. Figure 2.5 shows the some common types of faults in a rolling bearing.

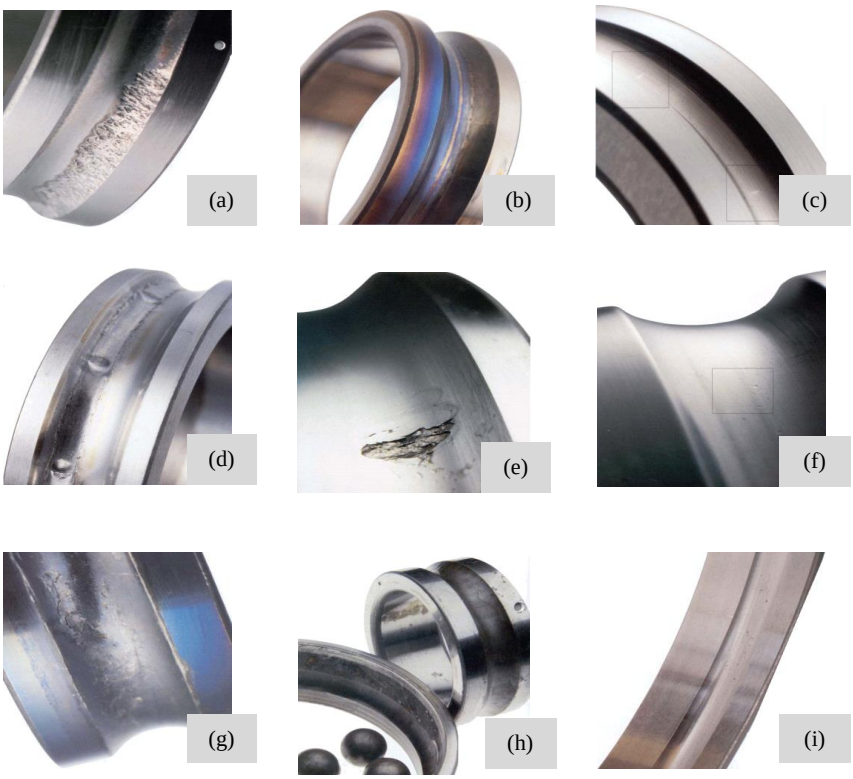

Figure 2.5 Common rolling bearing faults faults

(a) severe spalling due to excessive load.(b) blue/black and silver/gold result of overheating. (c) false brinell marks are bright and surrounded by debris (d) using hammers to remove or install bearings.(e) normal fatigue failure. (f) contamination failure area. g) lubricant failure. h) corrosion results from the chemical attack on metal. i) misalignment [48].

There are several mechanisms that can lead to bearing failure, including mechanical damage, crack damage, wear damage, lubricant deficiency, and corrosion [49],[48].

- **Fatigue**

Any bearing that is subjected to alternating normal loads could fail due to material fatigue after a certain operation time. Fatigue damage starts with the formation of tiny cracks below the bearing surface. As operating continues, the cracks progress to the surface where they cause material to break loose in the contact areas. The actual failure can manifest itself as pitting or flaking of the bearing races or rolling elements. If the bearing carries out in service, the deterioration will increase, especially in the vicinity of the defect due to stress concentration. The damaged surface disturbs the nominal motion of the rolling elements by introducing short time impacts repeated at the characteristic rolling element defect frequencies. As the damage continues to spread the impacts will diminish as the motion of the rolling element becomes so irregular and disturbed that it is

impossible to differentiate between individual impacts. If the bearing was to continue in service, the damage may spread to the other components, which will lead to a complete breakdown.

- **Corrosion**

Corrosion damage occurs when water or other contaminants in the oil enter the bearing components. This can be caused by damaged seals, acidic lubricants or condensation that happens when bearings are suddenly cooled from a higher operating temperature in very humid air. That results in rust on the running surfaces which produces irregular and noisy operations as the rust particles interfere with the lubrication. The rust particles also have an abrasive effect which generates wear [50].

- **Wear**

Wear is another cause of bearing failure. It is caused mainly by rust or any foreign particles entering the bearing through inadequate sealing. The abrasive foreign particles roughen the contacting surfaces. Severe wear changes the raceway as well as rolling elements profiles and increases the bearing clearance. The rolling friction increases considerably and can lead to a high level of slipping and skidding which results in a complete breakdown.

Wear results in a gradual worsening of the bearing components, leading to a loss of dimensioning. When lubrication conditions become insufficient, the friction will be increased. Operating forces can cause enlarged plastic deformation by tearing the locally friction-welded regions from the metal matrix. Lighter adhesive damage is often called scuffing or scoring; whereas, more intensive damage is referred to as seizing or galling. Abrasive wear happens when rigid particles become entrained among the contact surfaces.

- **Lack of lubrication**

Insufficient lubrication is a very common cause of premature bearing failure as it leads to skidding, slippage and bearing breakdown. It accelerates the adhesive wearing progress. Poor lubrication increases bearing component temperatures, which speeds up the deterioration processes. Poor lubrication increases bearing component temperatures, which speeds up the deterioration processes [51].

2.5 Bearing Fault Signal Characteristics

Bearing faults can be divided into two types: distributed and localized faults. Surface roughness, waviness, misaligned races and off-size rolling elements are included in the class of distributed defects. The localized defects, on the other hand, include cracks, pits and spalls caused by fatigue on the rolling surfaces.

Each time a localized defect in a rolling element bearing makes contact under load with another surface in the bearing, an impulse of vibration is generated, as shown Figure 2.6 . The impulse will have an extremely short duration compared to the interval between impulses, and so its energy will be distributed across a very wide frequency range. The result is that various resonances of the bearing and the surrounding structure will be excited by the impacts. The excitation will normally be repetitive because the contacts between the defect and the mating surfaces in the bearing are essentially periodic [52]. If the defect is in a different position, the impulse rate will be different.

For a constant rotational speed, the frequency of impulse, termed the ‘‘characteristic defect frequency’’, can be determined uniquely by the location of the defect; whether it is on the inner race, outer race or on one of the rolling elements [53], [54]. Thus, it is possible not only to detect the presence of a defect by the excitation of the resonance but also to diagnose the component of the bearing where the defect is.

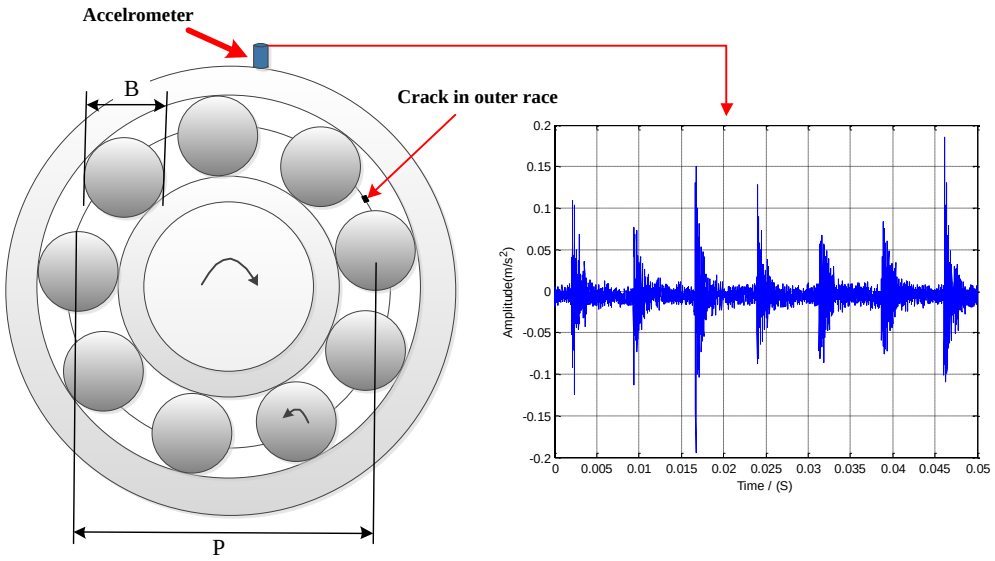

Figure 2.6 Ideal vibration signature due to fault in outer bearing race [51].

For an angular contact ball bearing in which the inner race rotates and the outer race is stationary, the four characteristic frequencies are:

Fundamental Train or Cage Frequency (FTF)

$$\mathrm{FTF(Hz)} = \frac{S}{2}\left(1 - \frac{B}{P}\cos\emptyset\right), \tag{2-1}$$

Ball Pass Frequency. Outer race (BPFO)

$$\mathrm{BPFO(Hz)} = \frac{NS}{2}\left(1 - \frac{B}{P}\cos\emptyset\right), \tag{2-2}$$

Ball Pass Frequency. Inner race (BPFI)

$$\mathrm{BPFI(Hz)} = \frac{NS}{2}\left(1 + \frac{B}{P}\cos\emptyset\right), \text{ and} \tag{2-3}$$

Ball Spin Frequency. Inner race (BSF)

$$\mathrm{BSF(Hz)} = \frac{PS}{2B}\left(1 - \frac{B^2}{P^2}\cos^2\emptyset\right) \tag{2-4}$$

Where B is the roller diameter; P is the pitch diameter; N is the number of balls, S is the shaft rotation rate in Hertz, and Ø the contact angle of the roller with the races (Ø equals to zero for the bearing employed in this thesis).

2.6 Summary

A brief review of bearing-related faults and their diagnosis are presented in this chapter. There are many types of bearings which are used for different purposes. These include ball bearings and roller bearings. There are different types of faults which are caused by the bearing components. Common rolling bearing faults and their mechanisms can lead to bearing failure, including mechanical damage, crack damage, lubricant deficiency, wear damage and corrosion. Bearing fault characteristic frequencies for outer race, inner race, balls and cage are also discussed.

Chapter 3
SIGNAL PROCESSING TECHNIQUES FOR BEARING FAULT DIAGNOSIS

For different signal processing algorithms, they can reveal some unique features of the signal. In this chapter, the current popular signal processing methods are investigated in three main categories: time-domain, frequency domain and time-frequency. Their applications on extracting or diagnosing bearing faults are especially explored.

3.1 Time-domain Analysis

The time domain is considered the most fundamental form of data collection for CM. Statistical methods are widely used to investigate the random characteristics of a physical system. It is important to be able to summarize the data obtained and be able to draw meaningful and useful features. Time domain analysis is one of the simplest methods for detecting incipient bearing faults. It is the traditional way of observing signals and viewing them in the time domain [55]. The time domain is a record of what happened to a parameter of the system versus time. It can be done by applying some statistical parameters such as root mean square value, crest factor, and kurtosis value, etc. Other time domain parameters include clearance factor, impulse factor and shape factor. These three non-dimensional vibration amplitude parameters were found to be useful under simulation conditions using a Gaussian probability density function model of fatigue spall. The clearance and impulse factors were the most useful with the clearance factor being the most sensitive and generally robust for detection of incipient fatigue spall.

Fabio and Marco investigated the statistical properties of machine signals in order to identify in what bandwidth that disturbance is more suitable to appear [56]. This approach is believed to be more effective for the specific characteristics of generalized-roughness faults. The most common parameters used to describe the time domain signal are the RMS value of the signal, which describes the energy contained in the signal, the peak value which describes the maximum value of the signal, and crest factor and kurtosis value are explained below.

3.1.1 Root Mean Square

The most common form of time data manipulation is to calculate a simple RMS value. The RMS value of a vibration signal is a time analysis feature that is the measure of the power content in the vibration signature. This feature is good to track the overall noise level, but it will not provide any information on which component is failing. It can be very effective in detecting a major out-of-balance in rotating systems. Equation (3-1) gives the equation that is used to calculate the root mean square value of a data series x_n over length$N$.

$$RMS = \sqrt{\frac{1}{N} * \sum_{n=1}^{N} x_n^2} \tag{3-1}$$

From this definition it is clear that RMS is not sensitive to sudden short duration, isolated peaks in the signal, and thus is often not sensitive enough to detect incipient tooth failure. RMS becomes more useful as tooth failure progresses and is a measure of the overall vibration level of the system. It is therefore considered as a very good descriptor of the overall condition of bearing and is sensitive to changes in operational conditions such as load and speed [57].

3.1.2 Crest Factor

The crest factor is used to measure defects in the time domain. However, the RMS level may not show small changes in the early stages of bearing damage. A better method is to use "crest factor" (CF) which is defined as the ratio of the peak level of the input signal to the RMS level. Therefore, peaks in the time series signal will result in an increase in the crest factor value. For normal operations, crest factor may reach between 2 and 6 [58]. A value above 6 is usually associated with machinery problems. This method is used to detect the alert in the signal pattern due to impulsive vibration sources such as outer race of a bearing damage or tooth breakage on a gear. Equation (3-2) shows the equation for the crest factor [58].

The peak value of the impulsive signal will increase as the defect grows while the RMS level of the overall acceleration (vibration) will only have a small change because the time over which the impulse acts does not significantly increase. CF is good for detecting discrete impulses above the background signal which do not occur frequently or have enough duration to significantly increase the RMS level.

$$Crest\ Factor = \frac{V_P}{V_{RMS}} \tag{3-2}$$

Where V_{RMS} is the root mean square of the raw data and V_P the peak level of the raw time series.

The Crest Factor is a fast and useful calculation that gives the analyst an idea of how much pulse is occurring in a time spectra. Spikes are often related with roller bearing

wear, cavitation and gear tooth wear. There are also some studies on signal analysis in time domain using crest factor technique, for example: Dron et al. studied the interest of spectral subtraction for the improvement of the sensitivity of scalar indicators (crest factor, kurtosis) within the application of conditional maintenance by vibratory analysis on ball bearings [59].

3.1.3 Kurtosis value

Kurtosis is defined as the fourth moment of the distribution and measures the relative peakedness or flatness of a distribution as compared to a normal distribution. Kurtosis provides a measure of the size of the tails of distribution and is used as an indicator of major peaks in a set of data. As a gear wears and breaks this feature should signal an error due to the increased level of vibration. The equation for kurtosis is given by:

$$\gamma = \frac{1}{N}\sum_{n=1}^{N}\frac{(x(n)-\mu)^4}{\delta^4} \tag{3-3}$$

Where $x(n)$ is the raw time series at point n, μ is the mean of the data, $\mu^2$is the variance of the data, and N is the number of data points in the data sequence.

The higher the kurtosis value the sharper the peak(s), and the longer the tails of the signal. The lower the kurtosis, the more rounded the peak(s). When the vibration signal is random noise, then it follows Gaussian (Normal) distribution and has a kurtosis value equal to 3.0 and 1.5 for a pure sine wave [60]. A signal with Gaussian data distribution, for example the acceleration, has Kurtosis value =3 while, in presence of impulsive phenomena, the distribution of the data has not Gaussian shape and its Kurtosis value is>3. During bearing condition monitoring the increasing of value of Kurtosis from 3 to 3.23 it would be enough to underline a change in bearing running [61].

This is primarily due to impulses (isolated peaks with high amplitude) generated by the affected bearing [62]. Consequently, kurtosis is commonly used as a parameter for the detection of bearing faults. Besides, there are also some advanced signal analysis techniques in the time domain, such as time synchronous average (TSA) and autoregressive moving average (ARMA) model [63]. The idea of TSA is to use the ensemble average of the raw signal over a number of evolutions in an attempt to remove or reduce noises and effects from other sources, so as to enhance the signal components

of interest. The main idea of the ARMA model is fitting the waveform data to a parametric time series model and extracting features based on this parametric model.

3.2 Frequency-domain Analysis

The frequency domain refers to the display or analysis of the vibration data based on the frequency. The time domain vibration signal is typically processed into the frequency domain by the application of the Fourier transform. The principle advantage of this method is that the repetitive nature of the vibration signals is clearly displaced as peaks in the frequency spectrum at the frequency where the repetition takes place.

Frequency-domain analysis is a powerful conventional technique for vibration analysis and has been demonstrated as a useful tool for detection and diagnosis of faults in simple rotating machinery [64],[65]. Frequency-domain analysis is based upon the transformed signal in the frequency domain, which gives spectral information of the signals and often used for data analysis. It is realized by transforming the signals from the time domain into the frequency domain. The advantage of frequency-domain analysis over time-domain analysis is the ability to easily identify and isolate certain frequency components of interest. The most widely used conventional analysis is the spectrum analysis by means of fast Fourier transform (FFT).The main idea of spectrum analysis is to either look at the whole spectrum or look closely at certain frequency components of interest and thus extract features from the signal [88, 89] The most commonly used tool in spectrum analysis is the power spectrum, whose definition is given in Equation (3-4).

$$P = E[X(f) * X^*(f)] \tag{3-4}$$

where $X(f)$ the Fourier transforms of signal$x(t)$; $X^*(f)$ is the complex conjugate of$X(f)$; E denotes expectation.

3.2.1 Envelope Analysis

Envelope analysis has been widely used in health monitoring and fault diagnosis of rolling element bearings [66],[67]. It was discovered in the early 1970's by Mechanical Technology Inc. and was originally called the high frequency resonance technique (HFRT). Besides, it has been known by a number of other names including amplitude

demodulation, demodulated resonance analysis, narrow band envelope analysis or simply just envelope, which now seems to be the more popular designation.

Envelope analysis is able to find the localized bearing faults at an early stage and thus has been widely employed in different the industrial areas and continuously improved by many researchers. Envelope analysis can extract periodic impacts, such as those made within a deteriorating rolling element bearing, from a machine's vibration signal. It can do this even when the impacts may be low in energy and buried within the other vibrations from the machine. Envelope analysis can thus differentiate between the periodic impacting of rolling bearing fault and the random impacts of other phenomena [68]. The results of envelope analysis will depend on the band pass filters selection to include those frequencies where the defect signal is high. Nevertheless, the band may not be known initially and also may change as the bearing operating condition change. So envelope analysis is likely to be more successful if the operator has prior knowledge of the carrier frequencies before selecting the band pass filters, however, the raw signal can be very noisy and even after band pass filtering may still contain undesirable components which increase the difficulty of identifying the envelope spectrum. Envelope analysis is unsuitable for use with bearings with severe faults as the damage is likely to have spread to such a degree that the dynamic response is more random noise than clear impact [69].

Quite a few researchers have explored the envelope analysis for bearing fault diagnosis. For example, Yuan etc. used Hilbert transform for analysis of the demodulation and spectral refining of the signal [70]. Patel, V. N., et al studied local defect detection on the races of test bearing in the presence of external vibrations. For effective and efficient detections of the defects, features of envelope analysis and Duffing oscillator have been identified and adopted in this investigation. The envelope analysis has been accomplished using Hilbert transform [71]. Sheen Yuh-Tay, applied the resonance frequency in the first-vibration-mode in the envelope detection for the bearing vibration. According to the experimental study, the envelope detection method for the first-vibration-mode resonance frequency could be effectively applied in the signal processing for the bearing defect diagnosis [72].

Figure 3.1 shows the process of using envelope analysis on a vibration signal from a bearing with inner race fault. The raw signal in the time domain (Figure 3.1 (a)) shows a series of periodical impulses, which indicate that there might exist a fault in the bearing. The signal is then sent through a band pass filter set for an appropriate resonance frequency to improve the signal to noise ratio (SNR) as shown in Figure 3.1 (b). Then, the filtered signal is demodulated to obtain its envelope as shown in Figure 3.1(c). Finally, the frequency spectrum of the envelope is presented in Figure 3.1(d), from which the impulse frequencies can be viewed clearly. Recall the bearing fault signal characteristics in Section 2.5, each fault localization has an unique characteristic frequency. Therefore, from the envelope spectrum, it can verify the existence of any bearing defects and the location of the defect on the bearing components.

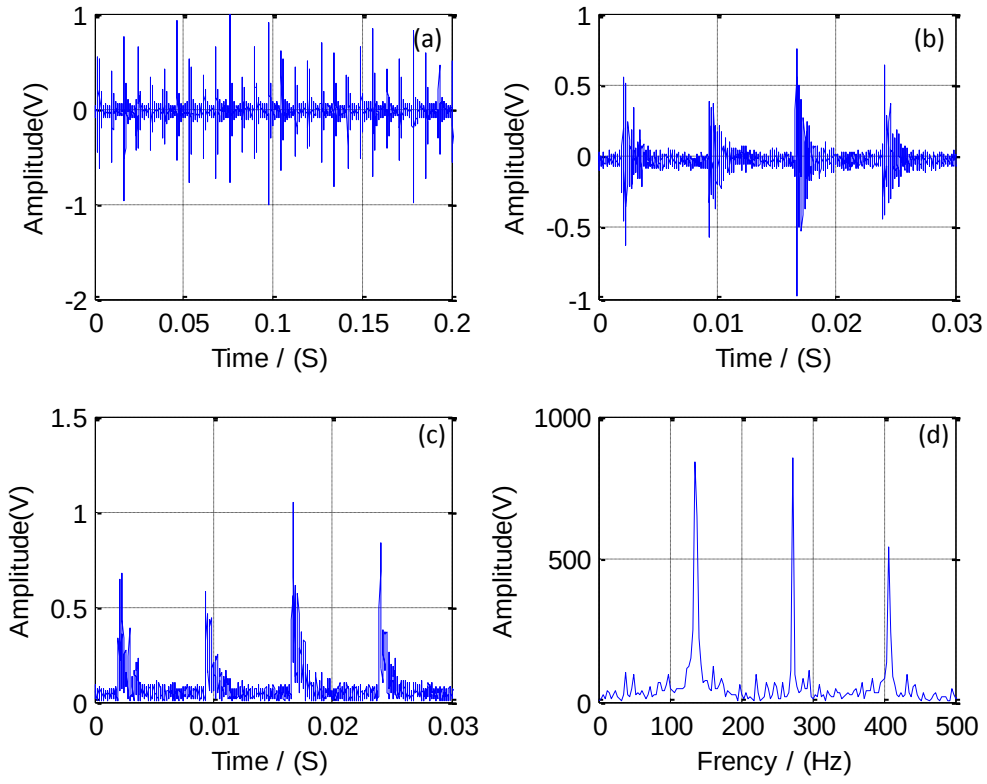

Figure 3.1 Envelope analysis on an inner race fault signal for rolling bearing (a) time domain signal (b) band-pass filtered time signal (c) envelope of band-pass filtered signal (d) envelope spectrum

3.3 Time–frequency Analysis

Detection of signals in a noisy area is a common problem in Signal Processing. Noise is measured as an unwanted signal that interferes with the information signal. Unfortunately, the FFT-based methods are not suitable for non-stationary signal analysis and are not able to reveal the inherent information of non-stationary signals. Time frequency analysis methods, such as Short Time Fourier Transform (STFT) or Wavelets are considered more appropriate to handle non-stationary signals. Thus they are frequently used for real signal de-noising either in time or frequency domain. The popular time–frequency analysis method includes STFT, Wavelet Transform, Empirical Mode Decomposition and Hilbert Huang transform.

3.3.1 Short time Fourier Transform

This technique is known as short-time Fourier transform (STFT), or windowing technique. The STFT provides some information about the time- and frequency-based views and represents a sort of compromise between them. However, this information can only be obtained with limited precision, which is determined by the size of the window. The fixed size of the window is the main disadvantage of the STFT. The problem with STFT is that it provides constant resolution for all frequencies since it uses the same window for the analysis of the entire signal. This means that if we want to obtain a good frequency resolution using wide windows, which is desired for the analysis of low-frequency components, we would not be able to obtain good time resolution, which is desired for the analysis of high-frequency components. Therefore, the STFT is suitable for the quasi-stationary signal analysis (stationary at the scale of the window but not the real stationary signals). Moreover, there exist no orthogonal bases for STFT; therefore it is difficult to find a fast and effective algorithm to calculate STFT [73].

3.3.2 Wavelet Transform

The different from the STFT and the wavelet transform can be used for multi-scale analysis of a signal through dilation and translation, so it can extract time–frequency features of a signal effectively. Wavelet theory has been quickly developed in the past

decade and has varied application [74]. A continuous wavelet transform is defined as Equation (3-5).

$$W(a,b) = \frac{1}{\sqrt{a}} \int_{-\infty}^{\infty} x(t) \psi^*(\frac{t-b}{a})\, dt \qquad (3\text{-}5)$$

Where $x(t)$ is the waveform signal, a is the scale parameter, b is the time parameter and $\psi(\cdot)$ is a wavelet, which is a zero average oscillatory function centred on with a finite energy, and "*" denotes complex conjugate.

Similar to Fourier transform, wavelet transform also has its discrete form which is obtained by discretizing a and b, expressing $x(t)$ in discrete form. Similar to FFT, a fast wavelet transform is also available for the calculation. Wavelet analysis of a waveform signal expresses the signal in a series of oscillatory functions with different frequencies at different time by dilations via the scale parameter a and translations via the time parameter b. Similar to power spectrum and phase spectrum in Fourier analysis, a scalogram defined as $|W(a,b)|^2$ and a wavelet phase spectrum defined as the phase angle of the complex variable $W(a,b)$ are used to interpret the signal.

One main advantage of wavelet transform is its ability to produce a high frequency resolution at low frequencies and a high time resolution at high frequencies for signals with long duration low frequencies and short duration high frequencies. Another advantage of wavelet transform is its ability to reduce noise in raw signals [75]. Wavelet analysis is able to decompose a signal into different scales corresponding to different frequency bandwidth and has been used to extract machine fault signatures. Researchers have applied many applications to detect bearing faults [32]. Altmann and Mathew used ANFIS (Adaptive Neuro-Fuzzy Inference System**)** for automated selection of wavelet packets containing bearing fault related features[76]. Xinsheng Lou et al developed a new scheme for the diagnosis of localised defects in ball bearings based on the wavelet transform and neuro-fuzzy classification. The technique is based on statistical analysis, the discrete wavelet transform, and pattern classification techniques such as neuro-fuzzy inference [77].

There are many types of wavelet functions available for different purposes, such as the Harr, Dabechies, Gaussian, Meyer Mexican Hat, and Morlet functions. Generally, continuous WA (Wavelet Analysis) is preferable for vibration-based machine fault

diagnosis, as the resolution is higher compared to the dyadic type of Wavelet Analysis [78].

3.3.3 Hilbert–Huang Transform (HHT)

The Hilbert-Huang transform (HHT), a recently developed method by Huang et al [79]. is an adaptive data analysis method designed specifically for analyzing data from nonlinear and non-stationary processes. It mainly consists of two parts: empirical mode decomposition (EMD) and Hilbert spectral analysis (HSA). The EMD method decomposes the input dataset into a finite and often small number of components, called intrinsic mode functions (IMF). With the Hilbert transform, the IMF's yield instantaneous frequencies as functions of time that give sharp identifications of embedded structures [80]. The final presentation of the results is an energy-frequency-time distribution, designated as the Hilbert spectrum.

EMD was effectively used for signal de-noising in a wide range of applications, such as biomedical signals, acoustic signals, and ionosphere signals [81], [82]. Junsheng, Dejie and Yu propose a new fault feature extraction approach based on empirical mode decomposition (EMD) method and autoregressive (AR) model for roller bearings. [83]. Maio et al. used EMD to transform one set of one-dimensional series into multiple sets of one-dimensional series for pre-processing.

In addition, the HHT revealed true physical meanings in many of the data examined. Powerful as it is, the method is entirely empirical. In order to make the method more robust and rigorous, many outstanding mathematical problems related to the HHT method need to be resolved. Z.K. Peng et al improved HHT’s performance in rolling bearing fault detection by comparing with the wavelet based scalogram through experimental case studies [84].

3.4 Summary

This chapter has attempted to review fundamentals and practical techniques for bearing fault detection. In summary, the signal processing techniques for bearing fault provide many different of choices to extract the faults in rolling bearing. RMS, Kurtosis and crest factor are quite straightforward and their calculated amounts are not large, which means they could be achieved on the WSN node with low computing capability and

small memories. Meanwhile, the algorithms such as FFT, envelope analysis and Wavelet are quite complicated, in which case the WSN node should have relatively higher computing capability and larger memories in order to realize them in real time. These signal processing techniques have their unique advantages in extracting some specific features.

Chapter 4
INVESTIGATION OF WIRELESS TECHNOLOGY FOR CONDITION MONITORING

With the rapid development of electronics technology, wireless communication techniques have been growing especially fast. Various wireless communications have been developed for satisfying different application requirements. This chapter reviews the main features of the most popular wireless techniques and their typical applications in the condition monitoring fields. Then, a comparison is made with a specific purpose for machinery condition monitoring. Finally, the requirements and challenges for employing wireless techniques in the industrial field are discussed.

4.1 Introduction to Wireless Sensor Network for Condition Monitoring

Applying wireless sensors to industrial applications faces several challenges and predictive maintenance applications sometime need high-resolution data sampling, particularly vibration analysis, but the wireless sensor network hardware platforms do not readily support such data intensive sampling or provide sufficiently reliable end-to-end communication [85].

Wireless sensor networks at the beginning are tested in small industrial monitoring applications to monitor the rotating machines. Condition-based monitoring is alarm based methodologies to monitor states of a machine and its applications have advantages from various sensing points. Precise applications of wireless sensor networks include motor analysis and machine tool performance.

Wireless sensor networks enable condition monitoring systems for small electric motors [86]. Moreover, wireless sensor networks enable new in-situ motor analysis opportunities previously not possible with wired sensors including agent-based steady-state motor analysis [87]. Applications to machine tool monitoring include temperature measurement sensors for end-mill inserts [88] and vibration-based condition monitoring for tool breakage [89].

The advantages of wireless technology has been utilized to overcome these barriers and to facilitate applications that in the past were impractical, such as temporary installations for troubleshooting and remote monitoring. On the other hand the challenges to Wireless Vibration Monitoring present unique demands on wireless devices, networks and associated components. High bandwidth is needed, due to the relatively large amounts of data that need to be sent over the wireless link. In addition, good dynamic range, low noise levels and higher-level processing capabilities, and the ability to capture data at the right time are also key requirements. Battery-powered devices that are required to provide on board power must satisfy customer demands for long service life. The devices and sensors, as well as the wireless network components, must also cope with conditions commonly found in the industrial environment.

There are many issues, including packet loss which is caused by network congestion. It occurs when one or more packets of data travelling across a computer network fail to

reach their destination. Dropping of packets acts as an implicit signal that the network is congested, and may cause senders to reduce the amount of bandwidth consumed. This research work on improving WSN data transmission by applying the new techniques inside the processor is used to compress the raw data through extracting the features of the measured signals using the designed algorithm and compact the optimal dataset for transmission by wireless transceiver unit. This work demonstrates the feasibility of on-sensor node diagnosis the faults of bearing [89].

4.2 Review on Wireless Techniques for Condition Monitoring

Wireless network technology has made enormous developments in the past few years and a variety of wireless protocols have been developed for different kinds of applications, such as 2G/3G/4G mobile communication, Wi-Fi, Bluetooth, NFC, RFID, Zigbee, etc. These kinds of technologies bring great benefits to our routine work and daily lives, as well as the industrial fields. Condition-based maintenance is one of such areas that produce significant benefits. The use of wireless network technology in CBM area is a part of the wireless sensor network WSN.

Wireless network standards can be divided into four specific groups according to its application area and signal range [88]: wireless personal area network (WPAN), wireless local area network (WLAN), wireless metropolitan area network (WMAN), and wireless wide area network (WWAN), as is shown in Figure 4.1. In general, the power consumption and cost increases with its signal range and bandwidth are discussed.

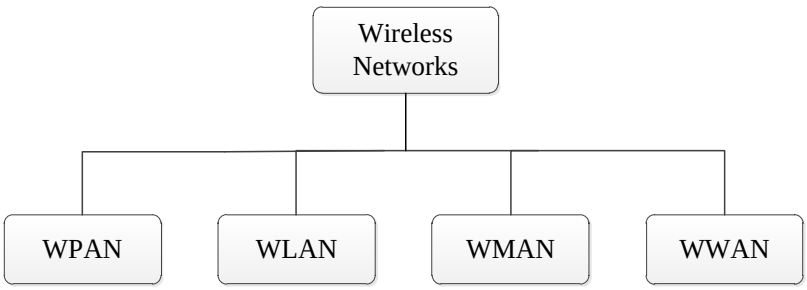

Figure 4.1 Wireless networks division

4.2.1 Wireless Wide Area Network (WWAN)

When talking about wireless networks, a cellular network is the most familiar protocol to be used, which is a kind of WWAN. WWAN provides for users the possibility to create wireless connections in a wide geographic area with remote public or private networks. Cellular networks are the most commercially successful wireless networks. The maximum data speed for different cellular networks is given in Table 4-1.

While a number of competing cellular networks were operating throughout the world, eventually, the standard referred to as Global System for Mobile communications (GSM) became the most popular. This standard often referred to as 2G, short for second generation, initially only supported voice communication and not digital packet data transmissions. However, it did eventually evolve to support data transmissions. The General Packet Radio Service (GPRS) is a packet data communications built on top of the GSM technology. GPRS offers maximum download and upload speeds of 114 kbps and 40kbps respectively. A further enhancement on GSM was Enhanced Data rates for GSM Evolution (EDGE), which improved the theoretical maximum possible download and upload speed to 384 kbps and 60 kbps respectively. While encryption is implemented in GSM, GPRS and EDGE, several weaknesses have been shown to exist with it [28].

Table 4-1 Maximum data speeds for cellular network standards [28].

Protocol	Standard	Download	Upload
2.5G	GPRS	114Kbps	20Kbps
2.75G	EDGE	384Kbps	60Kbps
3G	UMTS	384Kbps	64Kbps
	W-CDMA	2Mbps	153Kbps
	HSPA 3.6	3.6Mbps	348Kbps
	HSPA 7.2	7.2Mbps	2Mbps
Pre-4G	HSPA 14	14 Mbps	5.7 Mbps
	HSPA+	56 Mbps	22 Mbps
	WiMAX	75 Mbps	30 Mbps
	LTE	100 Mbps	50 Mbps
4G	WiMAX2	1 Gbps	500 Mbps
	LTE Advanced	1 Gbps	500 Mbps

Third generation (3G) cellular networks have brought much higher data rates, but limited coverage is offered throughout most countries, generally limited to major urban areas.

A competing technology is High-Speed Packet Access (HSPA) 7.2, which supports maximum possible download and upload speeds of 7.2 Mbps and 5.76 Mbps, respectively.

Further, going to the fourth generation (4G) cellular networks, the data rates will be even higher, which can reach theoretical peak download data rates up to 1 Gbps and 500 Mbps during upload.

When considering the usage of mobile communication technologies, some practical problems need to be paid attention to. While a country's coverage by cellular networks is generally very high, certain remote locations might not be covered. Thus, an understanding of the reliable data rate for each location would be needed if a high data rate CBM application is required by a utility. It should also be noted that the achievable data rate, at a particular location, also depends on the number of users at that location. Every cellular base station can serve a specific number of users, which will depend on a number of factors including the users total data rate. It is unclear how "fair" to its users a base station will be in response to a surge of user requests for downloading or uploading data.

A wireless sensor for monitoring temperature, humidity, 3-phase current and voltage at distribution level prefabricated substations was proposed in [11]. Such a wireless sensor was developed and tested in [86], where the load current and transformer oil temperature of the prefabricated substations were monitored. Once threshold values were exceeded, Short Message Service (SMS) were sent to a cellular phone, informing the operator of the condition of the substation.

4.2.2 Wireless Metropolitan Area Network (WMAN)

WMAN is the official name trademarked by the IEEE 802.16 Working Group on Broadband Wireless Access Standards (BWA) for its wireless metropolitan area network. Although the 802.16 family of standards is officially called WirelessMAN, the expression Worldwide Interoperability for Microwave Access (WiMAX) by an industry group called the WiMAX Forum is frequently used. The aim of the WiMAX is the

providing the broadband internet connectivity for WLANs and LANs with the wireless access point. The WiMAX technology is often called the technology for the Last Mile Access.

Maximum theoretical data rates for WiMAX are 75Mbps, with this number dropping with respect to distance from the base station. While WiMAX is a likely contender to be used by utilities for their CBM communication needs, no published information has been found relating to its so use. From the Table 4-1, it can be seen that WiMAX is included in the 4G mobile communication.

4.2.3 Wireless Local Area Network (WLAN)

The IEEE standard for WLAN is IEEE 802.11. Comparing to WLAN, Wi-Fi is used much more often in the real world. Wi-Fi is defined by Wi-Fi Alliance as any "wireless local area network (WLAN) products that are based on the IEEE802.11 standards". However, since most modern WLANs are based on these standards, the term "Wi-Fi" is used in general English as a synonym for "WLAN". Only Wi-Fi products that complete Wi-Fi Alliance interoperability certification testing successfully may use the "Wi-Fi CERTIFIED" trademark.

The 802.11.x term is used to denote the set of amendments to the standard. WLANs have a restricted signal range within the scope of the one building and one room (indoor range is approximately 40 meters). The WLAN is created for example by means of the connection of two computers together [90].

Second only to cellular networks, WLAN are the most commercially successful wireless data networks. The 802.11 standard describes an over-the-air interface between a wireless client, referred to as a station (STA) and a base station, referred to as a wireless access point (WAP). A large number of 802.11x standard amendments have been published since 1997 and many others are at various stages of being ratified. The most commercially successful and widely used standard amendments are shown in Table 4-2 below, with some of their respective specifications.

Table 4-2 Basic IEEE 802.11(a/b/g/n) standard details [90]

IEEE standard amendment	Approval data	Operating frequency (GHz)	Maximum theoretical data rate (Mbps)	Maximum outdoor range (m)
802.11a	1999	5	54	120
802.11b	1999	2.4	11	140
802.11g	2003	2.4	54	140
802.11n	2009	2.4/5	600	250

The 802.11(a/b/g/n) devices all use the Industrial, Scientific and Medical (ISM) license free frequency bands. The ISM radio portions used by 802.11 devices change slightly from country to country, but the European Telecommunications Standards Institute (ETSI) defines them at 2.4-2.5 GHz and 5.47-5.725 GHz. In the real world, these frequencies may also be used by some other devices and would be interfered with when operating at the same frequency. A number of options are available to 802.11 network users to mitigate this interference, like forcing an 802.11 network to change frequency channel. Figure 4.2 below shows the 802.11 channels available in the 2.4GHz band. While different 802.11 networks operating on the same channel have mechanisms designed to share the ISM frequency spectrum between them, the channel sharing is contentious. While any of 13 channels are available for use in Europe, it is most common for channel 1, 6, or 11 to be used. One reason for this is frequency overlapping between adjacent 802.11 channels causes a reduction in data rate [28].

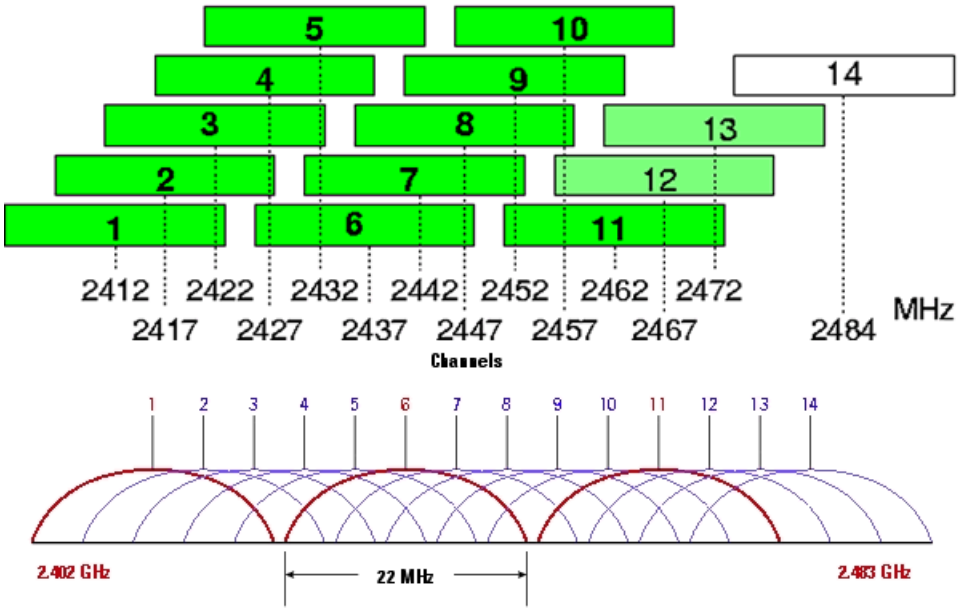

Figure 4.2 Graphical representation of 802.11 channels in 2.4GHz band [28].

The WiVib 4/4 Wireless Surveillance Pod [91] from diagnostic solutions adopts the IEEE802.11b protocol and is capable of processing four channels of vibration with its maximum frequency increments at 20kHz. The product is shown in Figure 4.3.

Figure 4.3 WiVib 4/4 Wireless surveillance pod [91]

4.2.4 Wireless Personal Area Network (WPAN)

Wireless personal area networks are usually characterized by short-range and low-power. The possibility of the ad-hoc mode connection is an advantage of these networks. Because of these advantages, they have been widely used and gained success in the area of wireless sensor networks (WSNs), which mainly features on low rate, low cost, restricted energy and short distance transmission [13].

IEEE defined a group of standards as IEEE802.15 for WPAN. IEEE802.15.1 (e.g. Bluetooth), IEEE802.15.3 (e.g. Ultra-band width) and IEEE802.15.4 (e.g. Zigbee, WirelessHART) are the most popular protocols among them. Besides, there are also some popular short-range and low-power protocols beyond the scope of IEEE, such as RFID, NFC, IRDA, etc. The following gives a brief introduction of these wireless network protocols [92].

IEEE 802.15.4 standard can trace back to the low-rate wireless personal area networks (LR-WPAN) standard, which was fuelled by the need to enable inexpensive WSNs for remote monitoring and control of noncritical functions in the residential, commercial, and industrial applications. While other wireless network standards aim to achieve long distance, large throughput, and high quality of service level, the IEEE 802.15.4 is

designed to provide simple wireless communications with relatively short range, limited power, relaxed data throughput, low production cost, and small size, which, however, are sufficient to satisfy the requirements of most remote monitoring system for industrial applications.

A number of protocols have been developed to work with the 802.15.4 standard [93]. ZigBee, WirelessHART and ISA100.11a are currently the most well-known. As is shown in Table 4-3, the IEEE 802.15.4 supports two frequency bands, which are a low band at 868/915 MHz and a high band at 2.4 GHz. The low band defines one channel with a raw data rate of 20 kbps near 868 MHz and ten channels with a raw data rate of 40 kbps near 915 MHz. The high band defines 16 channels with a raw data rate of 250 kbps. While 802.15.4 wireless sensors can use one of three different frequency ranges, the most commonly used is the 2400-2483.5MHz. This data rate is fairly enough when multiple machines are monitored, where the processed data (such as the algorithm results, e.g., fault alarms) instead of real-time continuous data (such as continuous motor raw data samples) are transmitted [93].

Table 4-3 Basic IEEE 802.15.4 standard details [93].

Frequency band (MHz)	Coverage	Maximum theoretical data rate (kbps)	Channels
868.0-868.6	Europe	20	1
902-928	Americas	40	10
2400-2483.5	Worldwide	250	16

One of the major benefits of 802.15.4 sensors is that they can form a mesh network, where each sensor does not only transmit its own data, but also serve as a relay for other sensors.

4.2.5 Comparison of Different Wireless Protocols

There have been some trial applications using the WWAN, WLAN and WPAN protocols for industrial condition monitoring. According to the investigations, they may find different kinds of application areas due to their own features.

Wireless sensors based on WWAN (cellular networks) and WLAN (Wi-Fi), having large power consumption and high data rates are more suitable for multiple or even continuous CBM measurements, powered by an AC/DC power supply. Meanwhile, the relative low cost and low power consumption features of WPAN make it more suitable

for CBM measurements, especially for battery powered applications. Below in section 4.4, the protocols in WPAN will be further compared.

4.3 Requirements and Challenges for Industrial Applications

Currently, WSN technology, especially the IEEE802.15.4 network, has been successfully applied in many commercial areas such as environmental monitoring [94], construction health monitoring [95], temperature monitoring in product distribution [96], and debris flow monitoring [97]. However, industrial processes and devices have their unique characteristics, which make further demands on industrial WSNs (IWSNs), such as higher sampling rates, faster data transmission rates, and higher reliability. In addition, compared with wired monitoring systems, WSN monitoring systems have constrained resources, including limited radio bandwidth, computational ability, and battery energy. Therefore, a key question to be addressed in this research is how to achieve these higher system requirements using resource-constrained IWSNs.

Some requirements of IWSN monitoring systems are presented below.

1) **Higher sampling rate**: The sampling rate of IWSNs has to be much higher than the sampling rate of WSNs for environmental or structural applications because of the need to perform accurate monitoring for dynamic signals such as vibration signals.

2) **Fast transmission rate**: The fast transmission rate needs to be taken into account when a higher sampling rate produces large amounts of data. Often the limited wireless bandwidth impedes high-speed data collection and transmission.

3) **Energy efficiency**: To achieve wireless connection, the nodes of IWSNs are usually powered by battery, and this often determines the lifetime of the whole network. However, higher sampling rate and large amounts of transmission data from the above requirements will increase the energy consumption. So energy efficiency needs to be factored into the design of node hardware and communication protocols.

4) **Higher reliability data transmission**: Machinery applications are more intolerant to loss of data and thus the communications has to be more reliable. However, the higher sampling rates make retransmission, which is usually used for enhancing the reliability, more difficult.

5) **Accurate time synchronization**: Fault diagnosis and multi-sensor fusion algorithms require the joint study of the signals of several sensors. So the time synchronization, skew rates and clock drift become important for machine monitoring.

6) **Processing heterogeneous sensor signals**: An industrial monitoring system usually needs to measure several parameters, including static signals like temperature, and dynamic signals like vibration. IWSNs usually need the capability of acquiring and processing heterogeneous sensors signals, and then transmitting the data.

4.4 Protocols for IWSN

Recently, because of these demanding requirements, significant standardization efforts related to IWSNs have been conducted. Four industrial wireless network standards, ZigBee, WirelessHART, 6LoWPAN and ISA100.11a, have been ratified, which are all based on the IEEE 802.15.4 physical layer.

4.4.1 ZigBee

ZigBee is a mesh-networking standard based on IEEE 802.15.4 radio technology targeted at industrial control and monitoring, building and home automation, embedded sensing, and energy system automation. ZigBee is supported by a large group of industry players. The good characteristics of the ZigBee are extremely low energy consumption and help for a number of different topologies, which makes it a good candidate for several sensor network applications [98]. However, in [99], it is reported that ZigBee cannot meet all the requirements for at least some industrial applications. For example, it cannot serve the high number of nodes within the specified cycle time.

Currently, there are many chip vendors, including TI, NXP, Freescale, producing commercially available products adopting the ZigBee specification. Due to Zigbee's wide application, some companies have published wireless data acquisition products based on it, such as GST [100].

4.4.2 WirelessHART

WirelessHART is an extension of the HART protocol and is an open and interoperable wireless communication standard designed to address the critical needs of industry for reliable, robust and secure wireless communication in real-time industrial process

measurement and control applications. WirelessHART was added to the overall HART protocol suite as part of the HART 7 Specification, which was approved by the HART Communication Foundation in June 2007.

The protocol utilizes a time synchronized, self-organizing, and self-healing mesh architecture and supports operation in the 2.4 GHz ISM band using IEEE 802.15.4 standard radios[101]. In April 2010, WirelessHART was approved by the International Electrotechnical Commission (IEC) unanimously, making it the first wireless international standard, as IEC 62591 [101].

Currently, WirelessHART is supported by many instrumentation suppliers, such as ABB [92] and Emerson [98]. As an interoperable standard, WirelessHART provides an easy way to set up, operate, and maintain a WSN.

4.4.3 6LoWPAN

6LoWPAN aims for standard IP communication over low power wireless IEEE 802.15.4 networks utilizing IP version 6 (IPv6) [102]. The advantages of 6LoWPAN from the industrial point of view are its ability to communicate directly with other IP devices locally or via an IP network (e.g., Internet, Ethernet), existing architecture and security, established application level data models and services (e.g., HTTP, HTML, XML), established network-management tools, transport protocols, and existing support for an IP option in most industrial wireless standards.

4.4.4 ISA100.11a

ISA 100.11a is a wireless system standard for industrial automation, which is intended to provide a reliable and secure wireless operation for noncritical monitoring or control applications in industrial applications. ISA100.11a adopts a hybrid medium access control layer, which combines time division multiple access and CSMA/CA [103]. The time slots of ISA100.11a are flexible with configurable length, which provides more flexibility for different system requirements. Frequency hopping and channel blacklisting techniques are also supported in ISA100.11a to ensure the robustness of wireless communications. ISA100.11a can be mixed with existing wired networks, including Modbus, PROFIBUS, Foundation fieldbus, and HART, using tunneling techniques [104].

Currently, there are some commercial ISA100.11a productions from different suppliers, for example, GE and Honeywell [105]. However, there are technical challenges to implement the full ISA100.11a stack architecture on low-cost hardware [106].

There are some similarities and dissimilarities between these four standards. All standards are based on IEEE 802.15.4 standards and the same frequency, which is 2.4 GHz. ISA100.11a, 6LoWPAN and WirelessHART are able to communicate simultaneously with current wired protocols and can be easily integrated with other wired protocols while Zigbee doesn't support wired protocols. Furthermore, WirelessHART and the ISA 100 standard incorporate several strategies that are used simultaneously to optimize coexistence with other users of the 2.4 GHz radio spectrum [89]. These comparisons indicate that WirelessHART and ISA.100.11a are more suitable for industrial applications.

4.5 Summary

It is evident that each technology has its specific advantages and disadvantages and can be used for specific applications of Asset Management but no one-fits-all solution exists at this time. The IEEE802.15.4 proves to be the most suitable standard for the WSN applications. However, the hostile environment of the industrial machines has brought more challenges for industrial WSNs. Therefore, several more advanced protocols based on the IEEE802.15.4 have been proposed to solve this problem, among which the ISA100.11a and WirelessHART are the outstanding ones.

Chapter 5
COMPARISON OF WIRELESS AND WIRED MEASUREMENT SYSTEM FOR BEARING CONDITIONING MONITORING

In this chapter, a cost-effective commercially available wireless measurement system is employed to collect the vibration signal of a bearing test rig. As a comparison, a wired data acquisition system is used to collect the vibration signal as well. Then, both signals from the wired and wireless system are processed by using the envelope analysis method. During the test, both the healthy and faulty bearings are acquired for analysis. The results of the analysis show that the seeded outer race fault can be successfully detected by both the wired and wireless system. However, there does have reliability problems on the wireless measurement system.

5.1 Experimental Setup

In order to evaluate the performance of the wireless measurement system for bearing fault diagnosis, a bearing test rig is set up and the vibration signals are measured by a wired data acquisition system and a wireless measurement system separately and processed using the same algorithms.

5.1.1 Bearing Test Rig

The aim of this study was to detect specific faults introduced into given roller bearings and to diagnose differences between the wireless sensor network and wired network. This will be done by monitoring the vibration signal from an accelerometer placed on the bearing housing. Two bearing chosen for this experiment was a NSK type N406 cylindrical roller bearing which is typical of many used in industry. However, the test rig had to be designed so that bearing faults could be introduced as required. The instrumentation and equipment used were selected and the test rig is located in our lab at Huddersfield University. It is established for simulating the bearing fault signals as shown in Figure 5.1. It consists of five main parts: electrical induction motor, couplings, bearing, shaft and DC generator.

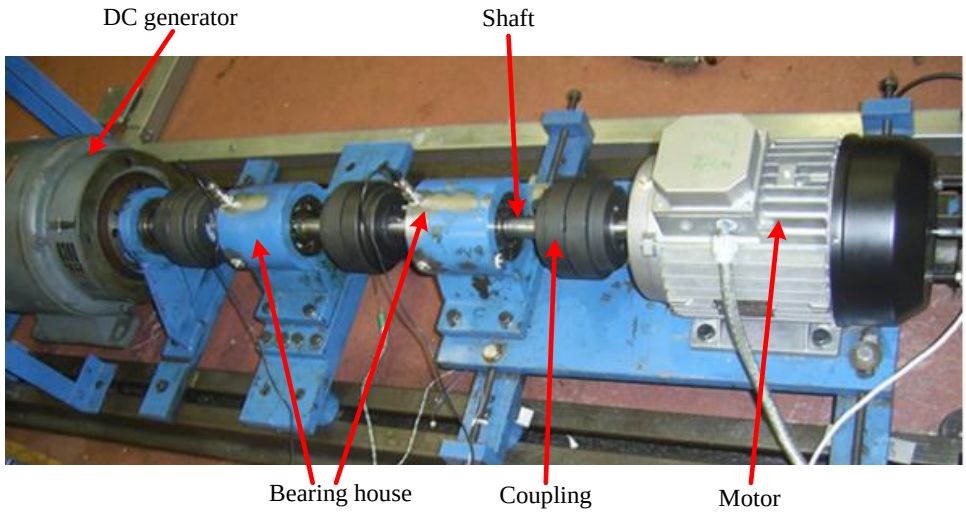

Figure 5.1 Picture of the bearing test rig

Our development during the test, two same type bearings but one healthy and the other one faulty are placed in two bearing houses, in which way the healthy and faulty bearing signals can be obtained in the same time. Moreover, the signals are obtained under very identical running environment with the same shaft speed and load. A faulty

rolling bearing is put inside the bearing house near the DC generator and a PE sensor (piezoelectric sensor) is mounted vertically to the bearing housing. This test was repeated three times with three faults (Inner race fault, Outer race fault and Roller fault).

The model of the bearing used in the test is N406 and the simulation fault is a flaw on the outer race inner race and rolling bearing element, as shown in Figure 5.2.

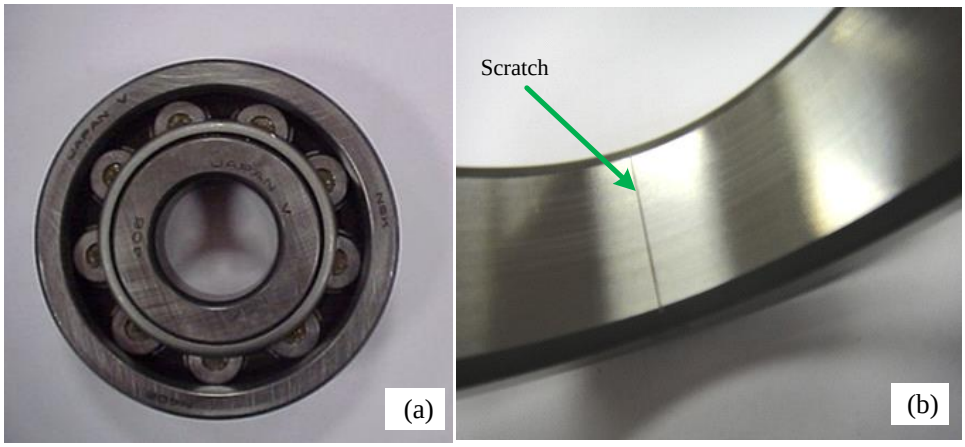

Figure 5.2 Healthy bearing and outer race bearing fault. (a) healthy condition, (b) outer race fault.

The scratch will be rolled over periodically when the bearing is running, which results in a fault signal modulated by a carrier signal at the resonant frequency of the bearing house, as explained in Section 2.5.

In this test, two NSK type N406 cylindrical roller bearings were used and their specifications are shown in Table 5-1.

Table 5-1 Specification of NSK type N406 cylindrical roller bearing

Parameter	Measurement
Pitch Diameter (*P*)	59 mm
Roller Diameter (*B*)	14 mm
Roller Number (*N*)	9
Contact Angle (∅)	0

During the test, the shaft runs at 1461.6 RPM, i.e. 24.36 Hz. The four common fault frequencies of the N406 bearing [49] can be calculated according to (2-1) - (2-4) and listed out in Table 5-2.

Table 5-2 Fault frequencies for bearing (N406) running at 1460 rpm.

Defect position	Fault frequency (Hz)
Ball Pass Frequency of the Inner Race (BPFI)	135.5
Ball Pass Frequency of the Outer Race (BPFO)	83.5
Ball Spin Frequency (BSF)	48.4
Train or Cage Frequency (FTF)	9.3

5.1.2 Wireless Measurement System

A wireless measurement system from Beetech Ltd [107] is employed to acquire the vibration signal. A piezoelectric (PE) type of accelerometer is mounted on the bearing house and connected to the wireless sensor node via an insulted cable. The popular Zigbee protocol is employed in this wireless system, which consists of a gateway and several sensor nodes, as shown in Figure 5.3 separately.

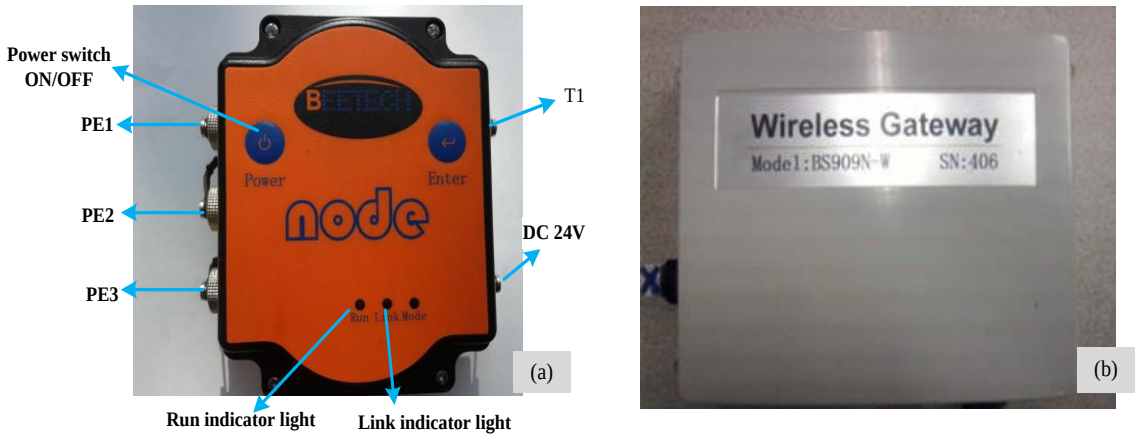

Figure 5.3 Picture of the wireless measurement system (a) sensor node (b) gateway

The structure of the wireless measurement system is shown in Figure 5.4. The Zigbee network is composed of several sensor nodes that are capable of measuring different kinds of signals. The collected data in the Zigbee network are converged to the gateway which is connected to the Internet. Finally, the data arrive at the user.

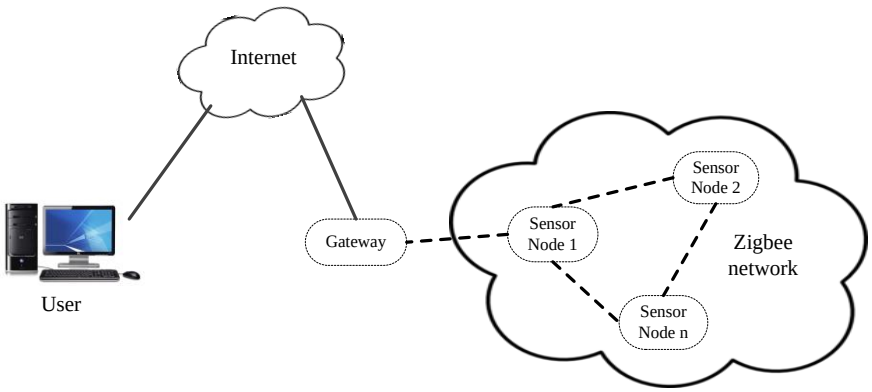

Figure 5.4 Structure of the wireless measurement system

The model of the sensor node adopted is A302, which is designed especially for collecting vibration signals. It can obtain three channels of vibration signals with as high as 16bit resolution and 10 kHz sampling rate. The model of the gateway is BS909N, which integrates a Zigbee coordinator and an Ethernet controller. Thus, the gateway can transmit the sensor data from the Zigbee network to the Internet and send the commands from the Internet to the Zigbee network.

Figure 5.5 Picture of the PE accelerometer CA-YD-127T

The sensor node can accept the vibration signal from piezoelectric (PE) type of accelerometer. The PE sensor adopted is CA-YD-127 (shown in Figure 5.5) and its specification is shown in Table 5-3. It is because the maximum sampling rate of the sensor node is 10 kHz, a PE sensor with low bandwidth is selected to satisfy the Nyquist sampling theory. During the test, one of the sensors is put on the bearing house with a healthy bearing and the other one on the bearing house with a faulty bearing.

Table 5-3 Specification of the sensor used for WSN

Accelerometer model	CA-YD-127	
Serial No.	01055	01067
Sensitivity (mV/ms2)	13.82	16.62
Frequency Range (Hz)	0.2-3000	0.2-3000
Weight (g)	38	38

5.1.3 Wired Measurement System

As a comparison with the wireless measurement system, the vibration signals from the bearing test rig are also collected by a wired measurement system. A dynamic data acquisition (DAQ) system YE6232B is adopted, as shown in Figure 5.6. This device is capable of measuring 16 channels of signals simultaneously with 16 bit resolution and a maximum sampling rate of 96 kHz per channel. The detailed specification of YE6232B is shown in Table 5-4. The collected data from the YE6232B are transmitted to the PC via the USB interface.

Figure 5.6 Picture of YE6232B DAQ system

Table 5-4 Specification of the YE6232B DAQ system

Number of Channels	**16 (selectable)**
A/D Conversion resolution	24 bit
Sampling rate (maximum)	96kHz per channel, Parallel sampling
Input range	±10 V
Gain	×1, ×10, ×100
Filter	Anti-aliasing
Interface	USB 2.0

Similar to the wireless measurement system, a PE type accelerometer is employed to collect the vibration signals. The model of the PE sensor is CA-YD-104T (shown in Figure 5.7) and its specification is shown Table 5-5.

Figure 5.7 Picture of the PE accelerometer CA-YD-104T

Table 5-5 Specification of the sensor used for wired network

Accelerometer model	CA-YD-104T	
Serial No.	07300	07223
Charge Sensitivity (mV/ms2)	3.77	3.70
Frequency Range (Hz)	0.5-7000	0.5-7000
Weight (g)	32	32

5.2 Test Procedure

During the data acquiring process the number of data points and the sampling frequency were set to 12 kHz. Also, the required time to collect this length of data is found to be 20 sec. This test shows the methods and techniques of using both wired and wireless systems to monitor outer race bearing condition. Two bearing conditions were considered, one is connected to the motor side, and the other is connected close to the generator as shown in Figure 5.1. This experiment is implemented to detect the fault on the outer race of the rolling bearing.

The performed test involves placing a scratch that is 100% of the bearing's outer race width (seeded fault), see Figure 5.2 (b). Two bearings are installed on the rotary machine.

The experiment was conducted under a shaft rotational speed (SRS) of 1461.6 rpm or 24.36 Hz. This test was implemented twice to collect the data from a wired network and

a wireless sensor network. There are two channels of vibration signals collected from the accelerometers mounted on the bearing housing in a vertical position one is healthy and the other is outer race fault. This test is installed to monitor the vibration signal via the wired and wireless network.

5.3 Results and Discussion

5.3.1 Results from Wired System

The spectra were calculated using the FFT algorithm and employing a Hanning window. All figures of spectra are plotted in the frequency range of 3900-5800 HZ to filter the signal. The envelope analysis method is implemented and therefore the fault frequencies of high amplitudes with their harmonics will appear in the envelope spectra. Figure 5.9 shows the characteristic outer race fault frequency (83.3 Hz), clearly indicating the presence of an outer race fault.

Root-Mean-Square (RMS) will work as an indicator of average amplitude level of vibration signals. As the energy within a signal is relative to the squared value of vibration amplitude, RMS can also be considered as a directory of vibration energy in this study.

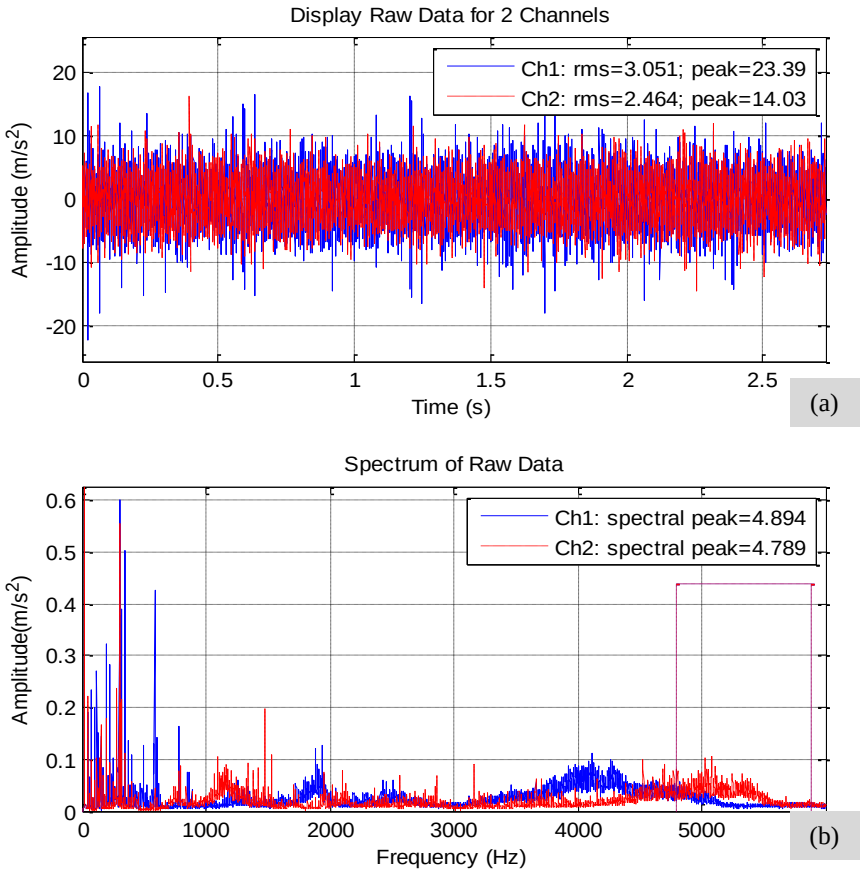

Figure 5.8 Wired signal (a) raw data (b) spectrum of raw data

On the other hand, it can be seen that from the Figure 5.8 (the blue line representing the bearings in normal condition means that the shaft is rotating at a constant speed, supported by healthy bearing). The first impression created by the waveform in Figure 5.8 is that the general vibration level of the signal of the faulty bearing is slightly higher than those of the normal condition with an RMS equivalent to 3.051.

The characteristic frequency of the outer race defect should be obvious in the spectrum as shown in Figure 5.8 (b). Besides, it can be observed that the amplitude between 4.9 KHz and 5.9 KHz is relatively higher, which might be one of the resonant frequencies of the bearing house. Therefore, a band-pass filter with the band width 1 kHz is applied to filter the raw vibration signal. Hilbert transform is then carried out on the filtered signal to obtain the analytic signal. After the Hilbert transform, the envelope is acquired by simply calculating the magnitude of the analytic signal.

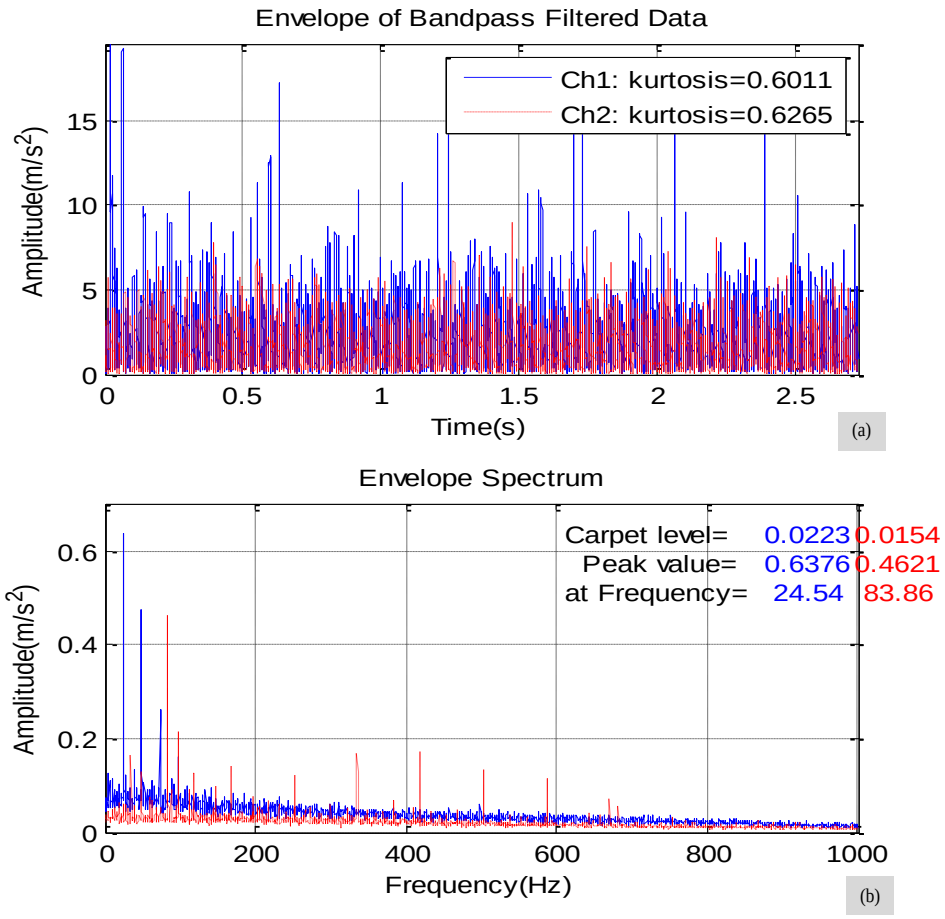

Figure 5.9 Wired signal (a) envelope of band-pass filtered data (b) envelope spectrum

The vibration signal from the early stage of a defective bearing may be masked by machine noise making it difficult to detect the fault by spectrum analysis alone. The main advantage of envelope analysis is its ability to extract the periodic impacts and the modulated random noise from a deteriorating rolling bearing. This is even possible when the signal from the rolling bearing is relatively low in energy and 'buried' within other vibration from the machine. The envelope and envelope spectrum of the band-pass filtered signal are shown in Figure 5.9.

5.3.2 Results from Wireless System

In this experiment, two channels of vibration signals were collected from the accelerometers mounted on bearing housing in a vertical position. The experiment was conducted under a shaft rotational speed (SRS) of 1461.6 revolutions per second (RPS), that is, 24.36 Hz with sample rate 10 kHz.

The collected raw vibration signal and its spectrum are presented in Figure 5.10 (a) and (b), respectively. The time domain spectra shows successive impulses occurring at somewhat similar spacing between one another and the RMS value of the blue spectra is 2.705 and the red spectra are 1.527

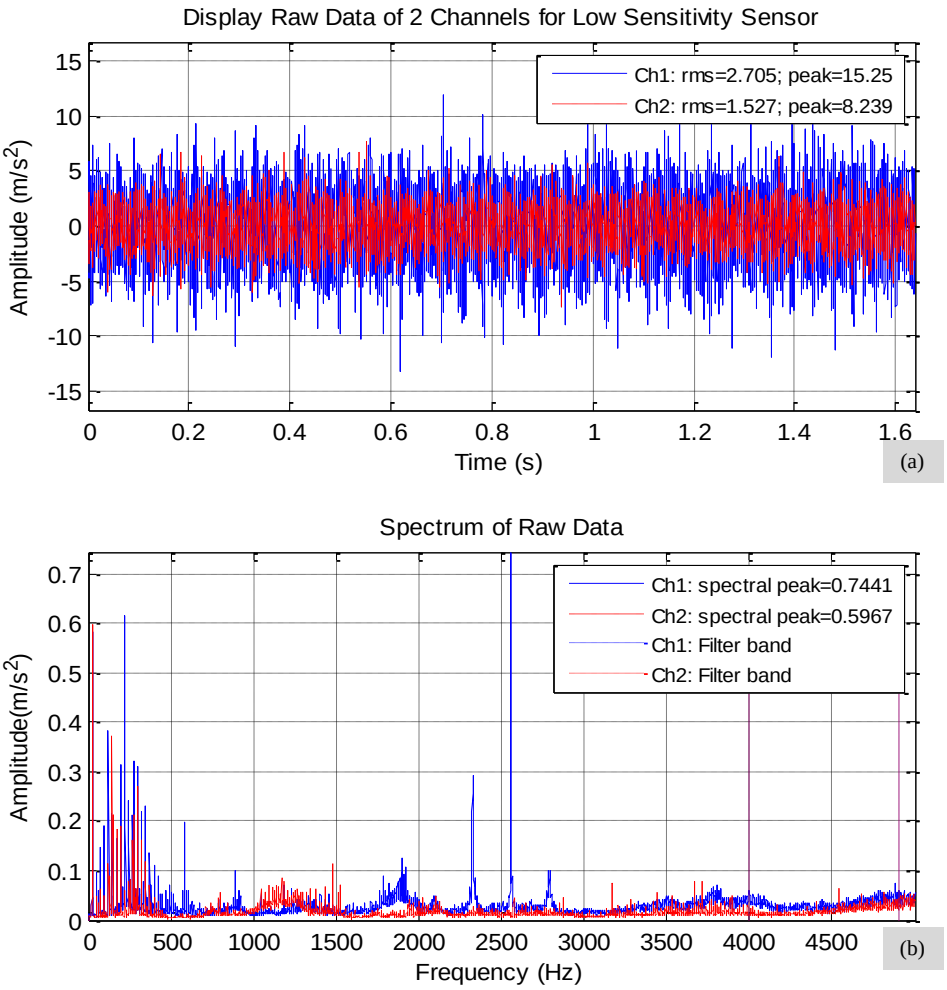

Figure 5.10 Wireless data (a) raw data (b) spectrum of raw data

The Figure 5.10 (b) shows the amplitude between 4 KHz and 5KHz is relatively higher, which might be one of the resonant frequencies of the bearing house. Therefore, a band-pass filter with the pass-band from 1 kHz is applied to filter the raw vibration signal. By applying envelop spectrum on the filtered vibration signals as shown in Figure 5.11(b) it can be seen that the red spectrum has the outer race fault. The frequency spectrum of the vibration signal from the bearing with the outer race defect peaks at 83.6 Hz, 167.2 Hz, and 249.9 Hz. The fundamental frequency for the bearing with the outer race defect from the equation is found to be 81.65 Hz. It also shows that the frequency for

outer race fault around 83.6 kHz has the highest peak with an amplitude which is approximately 0.139.

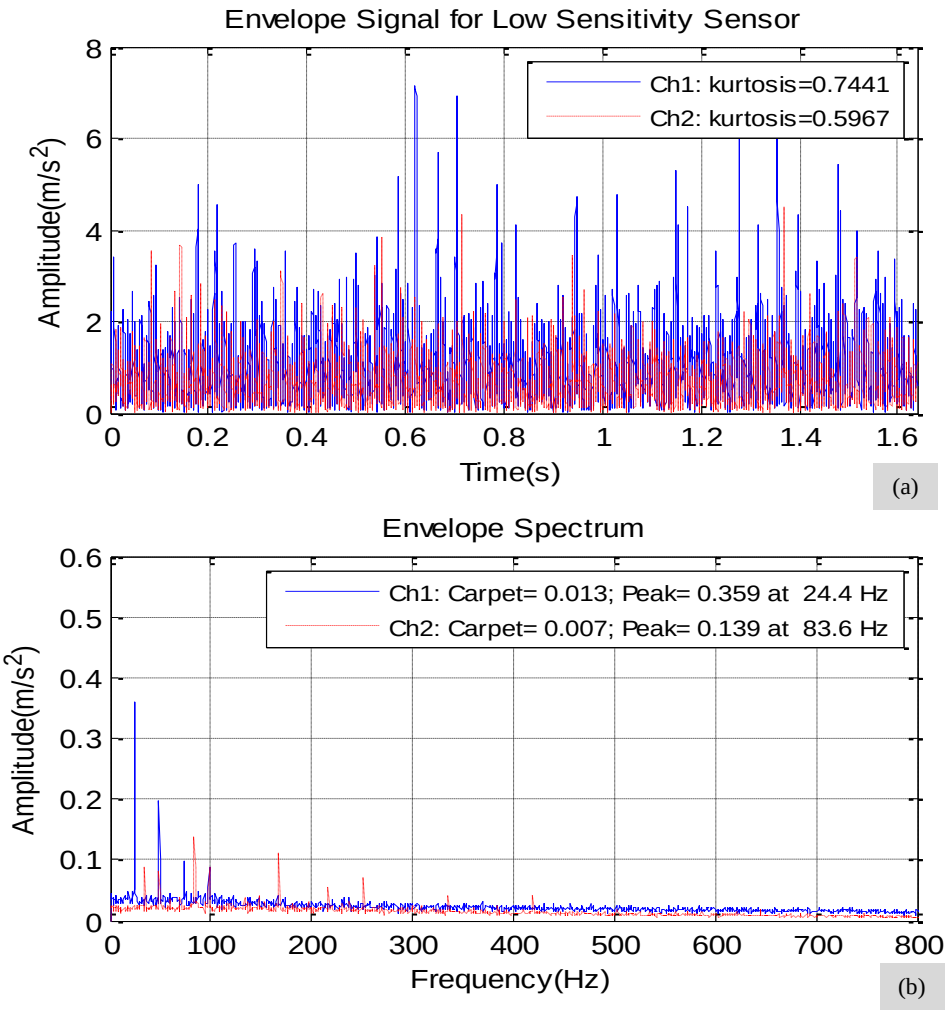

Figure 5.11 Wireless signal (a) envelope of band-pass filtered data (b) envelope spectrum

Wireless transmission of data is by far the most limitation performed by a wireless sensor. It would, thus, be desirable to reduce the amount of transmitted data as much as possible. It is possible to reduce the size of the acquired data, by processing it inside the node before transmission, or by reducing the sampling rate of the ADC. For some condition monitoring applications, it is feasible to process the acquired data in the wireless sensor and only transmit a small portion of the processed data, which is sufficient to show the condition of the bearing. The next chapter will discuss implanting the step of new design to improve the data transmission.

5.4 Summary

Condition Monitoring is important in industry. However, wired measurements have problems in installation. Therefore this chapter investigates the wireless measurement based on CM. Wireless sensors are gaining popularity in condition monitoring applications because of their relatively low cost and ease of installation. Most wireless systems are of the IEEE 802.15.4 standard for communication system. Zigbee is a standard for Wireless Personal Area Network (WPAN) applications that require low data rates and low battery life. To evaluate this communication protocol system in condition monitoring, a vibration node is developed by a supplier and evaluated in the lab. This evaluation is based on a bearing condition monitoring practice. Time waveform and frequency spectrum provide useful information to detect defects in bearings. Time waveform indicates severity of vibration in defective bearings. Frequency domain spectrum identifies amplitudes corresponding to defect frequencies and enables to predict the presence a defects on the outer race. The evaluation results shows that the presence of peaks in the spectrum at the second bearing, were not exact multiples of the shaft rate. This was the first indication that a bearing problem was likely to exist. The presence of peaks around these bearing tones confirmed that this vibration was in fact bearing related, as external vibration would not cause this effect and because this pattern is common to outrace faults. The presence of the same peak is about 83 HZ in the demodulated data from the bearing; therefore, this confirmed that the problem was at the bearing outrace and rolling element. However, some problems with wireless networks are related to the bandwidth rate.

Chapter 6
HARDWARE DESIGN OF THE PROPOSED WIRELESS SENSOR NODE

The previous chapter evaluated the wireless measurement system for bearing fault diagnosis in comparison with a typical wired measurement system. It is observed that the data from the wireless measurement system can diagnose the simulated bearing failure; however, some data may be lost during transmission. This could be the result of conflicts between the relatively high data throughput requirement of the vibration signal and the low bandwidth of the Zigbee protocol. To solve this problem, this chapter presents a hardware design for a wireless sensor node, on which some local processing algorithms can be implemented so as to reduce the data output requirement. By doing this, the transmission load of the wireless measurement system is hoped to be reduced, and thus, multiple sensor nodes can coexist on the same wireless network.

6.1 Overall Structure

According to the investigation in Chapter 4, IEEE802.15.4 is found to be the proper standard for WSN applications mainly because of its inherent features like low power consumption, low cost and the ability to establish a large wireless network. This chapter employs a higher level standard Zigbee based on IEEE802.15.4 and creates a wireless CM (condition monitoring) system with multiple wireless sensor nodes that are capable of realizing some signal processing algorithms.

The structure of the system is illustrated in Figure 6.1. The wireless CM system consists of a sink node and multiple sensor nodes. The sensor node collects data, processes them locally and transmits the results to the sink node via the Zigbee network. Then, the sink node sends the data received from different nodes to the processing center for further analysis via USB, Ethernet, etc. To focus on the algorithm realization, the commercially available wireless module Xbee Pro module is chosen to build the wireless network.

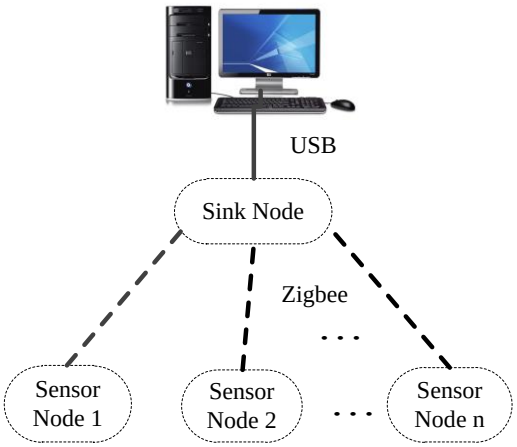

Figure 6.1 Overall structure of the wireless CM system

The work in this design mainly focuses on the wireless sensor node. The sensor node structure is illustrated in Figure 6.2, which is composed of four principal components: a sensor unit, a processing unit, a wireless module and power unit [108]. The sensor unit is used to sense different kinds of signals and convert them to digital signals; therefore, it usually contains a sensor, some signal conditioning circuits and might an analog-to-digital converter (ADC). The processing unit includes a microcontroller, which helps facilitate data capturing, processing while, at the same time, communicating with the wireless module. The wireless module is one microchip

equipped with an antenna, which facilitates the wireless communication of information. The power supply can be any power converter and battery, which acts as the source of energy for the nodes' all components. In some cases, some form of energy harvestings like solar, wind, or vibration system may also belong to the power unit. In the following sectors, the design of each unit will be introduced.

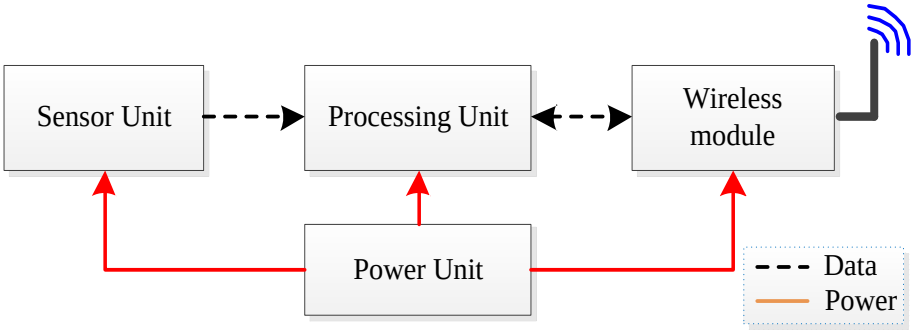

Figure 6.2 Basic components of a WSN node

6.2 Sensor unit

This thesis mainly focuses on the study of the vibration based condition monitoring; the sensor unit includes vibration sensor and its corresponding signal conditioning circuits.

6.2.1 Vibration Sensor

The vibration signal is usually collected using an accelerometer due to its low cost and good frequency response. There are two kinds of accelerometers: Piezo-Electric (PE) accelerometer and Integrated Electronics Piezo-Electric (IEPE) accelerometer. The PE accelerometer can generate an electric charge signal proportional to vibration acceleration, which means it needs no external power supply. However, its output is usually a high impedance signal, which means a foreign charge amplifier is frequently required to convert it to a low impedance voltage signal, and thus the signal could be efficiently collected by the ADC. By contrast, the IEPE accelerometer has a low impedance output due to the use of a built-in preamplifier and the signal could be directly collected by the ADC or be transmitted over long distances. However, it must require excitation power from a constant-current regulated or direct-current (DC) voltage source which is not always readily available.

For low power considerations, PE sensor is selected as the vibration sensor in this design. PE sensor is widely accepted as the best choice for measuring absolute vibration because of its high performance, such as extremely wide dynamic range, low output noise, and wide frequency range. Besides, it can operate in high-temperature environments. There are certain sensors have the potential to withstand temperatures exceeding 1000 ºF (538 ºC). Meanwhile, PE sensor also has some shortcomings. The high impedance output of the PE sensor extremely sensitive to corruption from various environmental factors. Little noise and expensive cabling must be used to reduce radio frequency interference (RFI) and electromagnetic interference (EMI).

Besides these two traditional accelerometers, the Micro-Electro-Mechanical Systems (MEMS) accelerometer is also an option. MEMS have integrated charge amplifiers or even an ADC. Thus, MEMS accelerometers usually allow for a significant reduction in size, power consumption and cost compared to conventional accelerometers. Therefore, they are being used in more and more fields. For example, a digital MEMS accelerometer ADXL345 is used to detect the mechanical looseness and misalignment faults of induction motors in [109]. However, the bandwidth of most current commercially available MEMS accelerometers is restricted within 2kHz while the resonant frequencies discussed in Section 2.5 are often in the several kHz range [110], which is out of the range of the MEMS sensors.

6.2.2 Signal Conditioning Circuit

To convert the high impedance output of the PE sensor to a low impedance signal, a charge amplifier is added after the PE sensor. In this way, the signal can be efficiently collected by the analog to digital converter (ADC). In this design, the on-chip ADC of the core processor is employed to fulfill the conversion for low power and cost considerations and will be introduced later.

Figure 6.3 shows the basic schematic of a charge amplifier for PE signal impedance conversion. As shown in Equation (6-1), the gain of output voltage V_{out} is dependent only upon the ratio of the input charge q to the feedback capacitor C_f. It can be noticed that the smaller the capacitor is, the bigger the gain. The feedback resistor R_f is employed to bias the amplifier. In together with the capacitive C_f, R_f and C_f act as a high-pass filter with the cut-off frequency at f_{HP}, as given in equation (6-2). A group

of typical values for the resistor and capacitors are illustrated in Figure 6.3. According to equation (6-1) and (6-2), the gain of the charge amplifier is 0.303mV/pC, and the cut-off frequency of the high-pass filter is 4.97Hz.

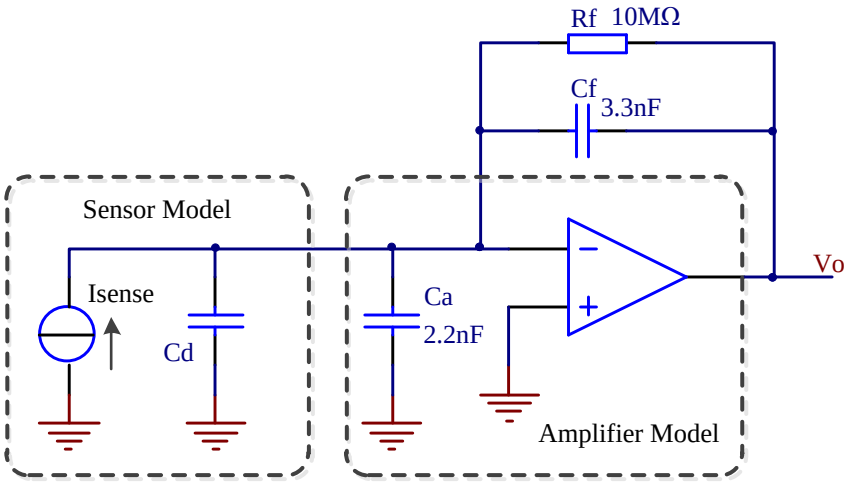

Figure 6.3 Schematic of the charge amplifier

$$V_{out} = \frac{q}{C_f} \tag{6-1}$$

$$f_{HP} = \frac{1}{2\pi R_f C_f} \tag{6-2}$$

6.3 Processor unit

For quick prototyping, a Launchpad board (as shown in Figure 6.4 (a)) from Texas Instrument (TI) is employed as the central processor. The main reason for choosing this board lies in its optimized low power consumption and excellent computing performance. It contains a state-of-the-art 32-bit ARM Cortex-M4F microcontroller TM4C1233H6PM of the Tiva C Series [111]. The function diagram of the processor is presented in Figure 6.4 (b) and the key features of which are listed below.

- ARM Cortex-M4 with floating point unit (FPU) with capabilities for digital signal control applications
- 256 KB Flash, 32 KB SRAM
- 32-channel configurable µDMA controller, providing a way to offload data transfer tasks from the Cortex™-M4 processor, allowing for more efficient use

of the processor and the available bus bandwidth

- 12-bit ADC accuracy is achievable at the full 1-MSPS rating with no hardware averaging
- Generous communication options available: 8 UARTs, 6 I2C, 4 SPI / SSI

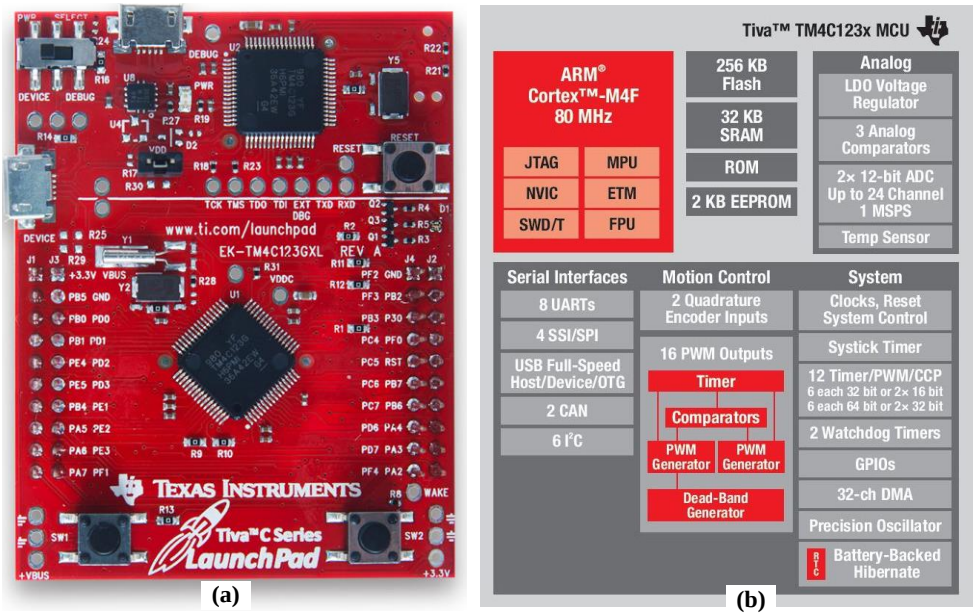

Figure 6.4 (a) Tiva launchpad development board (b) block diagram of Tiva C series MCU [116]

Another reason for choosing this board is that it includes an onboard simulator. This makes the development process much easier and costs effective. Besides, the abundant software resources and libraries can fasten the development process quite a lot and will be introduced in the next chapter.

For microcontrollers to achieve a fast exchange of information with other I/O devices and to be able to detect and respond quickly to physical events that are taking place, dedicated architecture is contained within them. This architecture is divided into logical divisions, generally known as peripherals, which can be accessed by the microcontroller when needed. The microcontroller TM4C1233H6PM has some these built-in peripherals. In this design, we mainly use the Analog-to-digital converter (ADC), Micro Direct Memory Access Unit (µDMA), Interrupt, Timer and Universal Asynchronous Receivers/Transmitters (UART).

6.3.1 Analog-to-digital Converters

Analog-to-digital converters often referred to as A/D converters or simply ADCs, have played an increasingly important role in instrumentation in recent years. The increasing importance of ADCs to instruments has been driven by the development of high-performance integrated circuit (IC) technology. This has enabled higher-speed and higher-resolution ADCs to be designed, manufactured, and sold at reasonable cost. The primary function of an A/D converter is to convert an analog value (typically represented by voltage) into binary bits that give a "good" approximation to that analog value. The ADC converts the conditioned analog signal to a digital signal that can be processed by the microcontroller and transferred over the network.

Here, the on-chip 12-bit ADC is employed to convert the vibration signals. Although the resolution is a bit low for vibration signals, it is competent enough for a demonstration. In this design, only channel 0 of the ADC used. Table 6-1 gives out the related pins on the LaunchPad board. As it shows, the vibration signal will be connected to the J3_9 pin.

Table 6-1 LaunchPad board GPIO pins connected to ADC

Pin number	GPIO	Signal Name
J1_1	---	3.3V
J3_2	---	GND
J3_9	PE3	AIN0

Two ADC modules (ADC0 and ADC1) are integrated on this MCU, and only ADC0 unit is used here. The ADC unit on the TIVA C MCU provides quite a few rather powerful capabilities to suit various data acquisition requirements. Some of the functions used in this design are briefly explained below.

A. Sequencer

The data sampling process is finished automatically by the programmable sequencer without the intervention of the controller. The sample sequencer allows the ADC to collect data from multiple input sources without having to be reconfigured or serviced by the processor. The sample sequencer can be used to configure the input source, trigger events, interrupt generation, and sequencer priority.

For the ADC0 module, it has four sample sequencers, each with configurable trigger events, can be captured. The first sequencer captures up to eight samples, the second and third sequencers capture up to four samples, and the fourth sequencer captures a single specimen. Each sample can be the same channel, different channels, or any combination in any order.

B. Trigger source

The ADC conversion can be triggered by various sources, such as a controller (software), timers, analog comparators or GPIOs. In Section 8.2, we will compare the data acquisition process of employing different trigger sources.

C. Hardware sample averaging

The ADC module provides a hardware sample averaging circuit, which can generate higher precision results with the cost of lower throughput. The circuit can be configured to accumulate up to 64 samples and averaged to form a single data entry in the sequencer FIFO. Throughput is decreased proportionally to the number of samples in the averaging calculation. For example, if the averaging circuit is configured to average eight samples, the performance is reduced by a factor of 8.

D. Interrupt and direct memory access (DMA) operation

When the data conversion is finished, the sample sequencer will generate an interrupt to indicate the CPU to read the conversion results, or it can generate a direct memory access (DMA) event to let the DMA unit to more efficiently move data without the CPU intervention. For each sample sequencer, it has a request signal to the associated dedicated channel of the μDMA controller.

E. Reference voltage

The reference voltage of the ADC is provided by the internal signals VREFP and VREFN, which are connected to VDDA and GNDA pins respectively, as shown in Figure 6.5. On the Launchpad, the VDDA is connected to 3.3V power supply, and GNDA connects to the ground signal. Thus, the reference voltage is 3.3V in this case.

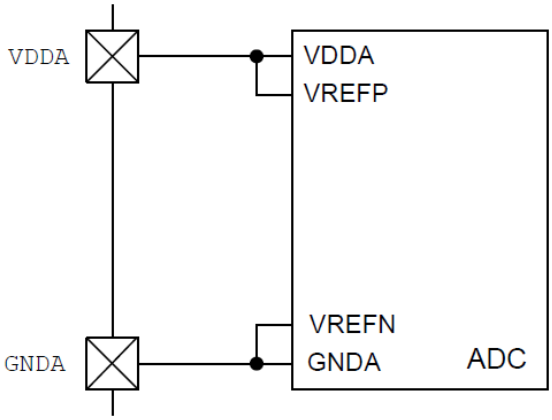

Figure 6.5 ADC voltage reference

The conversion results of the ADC ranges from 0x000 to 0xFFF. In single-ended-input mode (our case), the 0x000 value corresponds to the voltage level on VREFN and the 0xFFF value corresponds to the voltage level on VREFP. Therefore, the resolution v_{res} can be calculated using;

$$v_{res} = \frac{VREFP - VREFN}{4096} = \frac{3.3-0}{4096} = 0.8057 \text{ mV/LSB} \quad (6\text{-}3)$$

Where; LSB the least significant bit.

For the values beyond the input range, the ADC conversations saturate in under-voltage and over-voltage cases. In this case, the analog input voltages above 3.3V soak at 0xFFF while those below 0V saturate at 0x000.

Besides, the ADC unit provides other functions like the digital comparison, internal temperature sensor, differential sampling and phase shifter, etc.

6.3.2 Micro Direct Memory Access Unit (µDMA)

The Micro Direct Memory Access (µDMA) controller is designed to work with the ARM Cortex-M processor and provides an efficient and low-overhead means of transferring blocks of data in the system, allowing for more efficient use of the processor and the available bus bandwidth. It can automatically perform data transfers between memory and peripherals and has dedicated channels for each supported on-chip module. One more thing needs to mention about the µDMA controller is that its usage of the bus is always subordinate to the CPU, so it never holds up a bus transaction by the processor.

The μDMA controller is rather powerful and flexible to be suited for different application requirements. Here below are some of its features:

- Dedicated channels for supported peripherals
- One channel each for receive and transmit for devices with receive and transmit paths
- Dedicated channel for software initiated data transfers
- Channels can be independently configured and operated
- An arbitration scheme that is configurable per channel
- Two levels of priority
- Subordinate to Cortex-M processor bus usage
- Data sizes of 8, 16, or 32 bits
- Address increment of byte, half-word, word, or none
- Maskable device requests
- Optional software initiated transfers on any channel
- Interrupt on transfer completion

The μDMA controller supports several different transfer modes, allowing for various transfer schemes. The following transfer modes are provided:

- **Basic mode**

Basic mode performs a simple transfer when a request is asserted by a device. This mode is appropriate to use with peripherals where the peripheral asserts the request signal whenever data should be transferred. The transfer pauses if the request is de-asserted, even if the transfer is not complete.

- **Auto-request mode**

Auto-request mode performs a simple transfer that is started by a request but always completes the entire transfer, even if the request is de-asserted. This mode is appropriate to use with software-initiated transfers.

- **Ping-Pong mode**

Ping-Pong mode is used to transfer data to or from two buffers, switching from one buffer to the other as each buffer fills. This mode is appropriate to use with peripherals as a way to ensure a continuous flow of data to or from the peripheral. However, it is more complex to set up and requires code to manage the ping-pong buffers in the interrupt

handler.

- **Memory scatter-gather mode**

Memory scatter-gather mode is a complex mode that provides a way to set up a list of transfer "tasks" for the μDMA controller. Blocks of data can be transferred to and from arbitrary locations in memory.

- **Peripheral scatter-gather mode**

The peripheral scatter-gather mode is similar to memory scatter-gather mode except that it is controlled by a peripheral request. A detailed explanation of the various transfer modes is beyond the scope of this document. Please refer to the device data sheet for more information on the operation of the μDMA controller. The μDMA is quite helpful especially in the data acquisition process and will be explained in Section 8.2.

6.3.3 Interrupt and Timer

An interrupt in the microcontroller allows a forced deviation from normal program flow by an external or internal event. The code that is executed when the interrupt occurs is referred to as the Interrupt Service Routine (ISR). An interrupt can be employed to execute some tasks that need the real-time response. For example, in the data acquisition process, an ADC interrupt is utilized to indicate the CPU to read the conversion results. Otherwise, the new conversation results would overwrite the old ones.

The Nested Vectored Interrupt Controller (NVIC) in Handler Mode controls the interrupt on the TIVA C MCU. The processor state is automatically stored to the stack on an exception and automatically restored from the stack at the end of the ISR. For each interrupt, its priority can be programmed as 0-7. A higher level corresponds to a lower priority, so level 0 is the highest interrupt priority.

The programmable timer is an important unit in the MCU, which be used as a counter, timer or to count or time external events that drive the Timer input pins. The timer peripheral on TIVA C is called General-Purpose Timer Module (GPTM), which contains six 16/32-bit GPTM blocks and six 32/64-bit Wide GPTM blocks. For each 16/32-bit GPTM block, it provides two 16-bit timers/counters (referred to as Timer A and Timer B) that can be configured to operate independently or concatenated to

operate as one 32-bit timer. Similarly, each 32/64-bit Wide GPTM block provides 32-bit timers for Timer A and Timer B that can be concatenated to operate as a 64-bit timer.

The timer block can work at different modes for various applications, such as one-shot, periodic, real timer clock (RTC), edge count, edge time and pulse width modulation (PWM). Also, timers can be used to trigger analog-to-digital conversions (ADC) and DMA transfers, which are quite helpful for the data acquisition process and will be proved in Section 8.2. Noticeably, The ADC trigger signals from all of the general-purpose timers are ORed together before reaching the ADC module, so only one timer should be used to trigger ADC events.

6.3.4 Universal Asynchronous Receivers / Transmitters (UART)

The Universal Asynchronous Receivers/Transmitters (UART) is a general-purpose serial communication unit that performs the functions of parallel-to-serial and serial-to-parallel conversions. Because of its simplicity in interface and protocol mechanism, it is widely equipped with the embedded modules, like the Xbee wireless communication module employed in this design.

The TIVA C MCU provides up to eight UART modules with programmable baud-rate generator allowing speeds up to 5 Mbps for regular speed and 10 Mbps for high speed. The data bits, parity mode and stop bit of the UART module are fully configurable for various application needs. Besides, it also includes a 16x12 bit receive FIFO, and a 16x8 bit transmit FIFO to reduce CPU interrupt service loading.

The Universal Asynchronous Receiver/Transmitter (UART) provides a set of functions for using the UART modules. Functions are provided to configure and control the UART modules, to send and receive data, and to manage interrupts for the UART modules.

In this design, UART1 is used to communicate with a wireless module and the relevant pins on the LaunchPad board are listed in Table 6-2. concerning Table 6-2, the U1RX line receives data from wireless module to the microcontroller, while the U1TX line transmits data from the microcontroller to the wireless module. The U1RTS (Request-To-Send) line is used by the microcontroller to inform the PORT module that

it would like to transmit data to it while the U1CTS (Clear-To-Send) line informs the microcontroller that it can send data.

Table 6-2 LaunchPad board GPIO pins For UART

Pin number	GPIO	Signal Name
J1_3	PB0	U1RX
J1_4	PB1	U1TX
J4_5	PC5	U1CTS
J4_4	PC4	U1RTS

6.4 Wireless Module

For quick prototyping, a commercially available module Xbee Pro ®ZB module (shown in Figure 6.6(a)) from Digi International [112], [113] is employed to set up the Zigbee network for the data transmission. This commercial module is valid, reliable and practical for the application [114].

The connection between the processor and the Xbee Pro module is presented in Figure 6.6 (b). As the data throughput is relatively large in this application, the clear to send (CTS) and request to send (RTS) flow control are employed to avoid overflowing the serial buffer on the Xbee Pro module, in which case some data may be lost. RTS and CTS flow control can be enabled using the D6 and D7 commands[115].

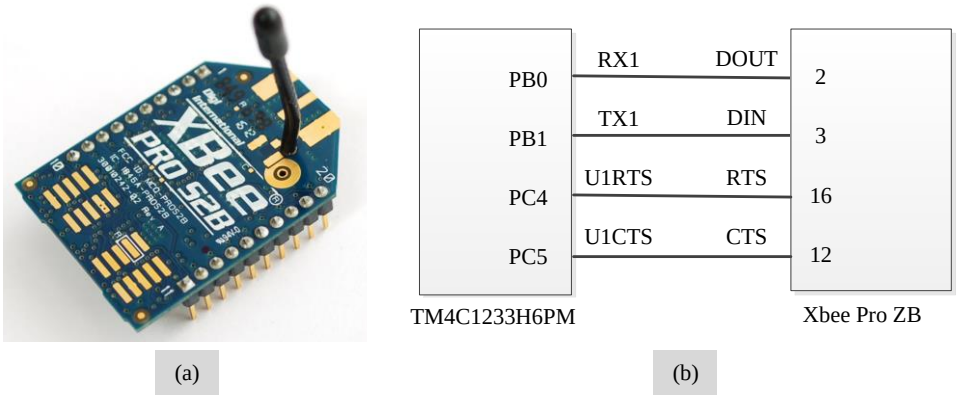

Figure 6.6 Connections between the processor and the Xbee Pro module

The Xbee module can be configured as three kinds of nodes: coordinator, router, and end device. In this case, the Xbee module on the sensor node is configured as a router while the Xbee on the sink node is configured as coordinator. The configuration can be achieved by connecting the Xbee module to a Xbee USB adapter (shown in Figure 6.7

(a)) and then using the X-CTU software provided by the company to configure the parameters. The configuration interface of X-CTU software is shown in Figure 6.7 (b), which is a very straightforward and handy tool.

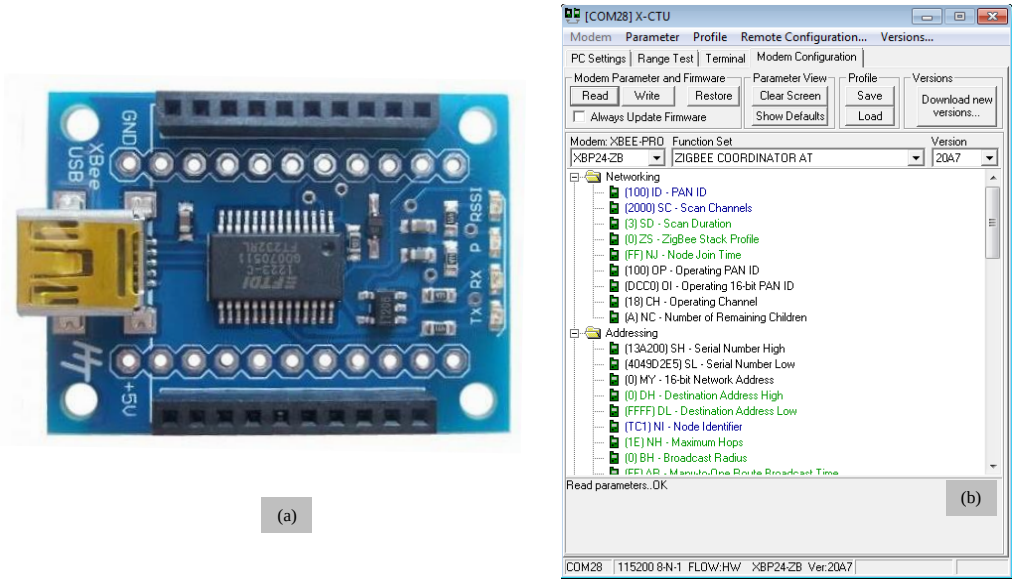

Figure 6.7 (a) Xbee USB adapter and (b) X-CTU configuration interface

6.5 Summary

A prototype wireless CM system is established in this chapter intending to implement local processing algorithms on the wireless sensor node and thus reduce the data throughput requirement of the wireless transmission. The wireless sensor node design is mainly introduced, including the sensor unit, a processor unit, and wireless module. The sensor node is designed to collect vibration signals and have good signal processing capabilities. The next chapter will study the implementation steps of the envelope analysis, employed and proved effective for bearing fault analysis in Chapter 5. Then, this algorithm will be realized on the designed wireless sensor node in Chapter 8.

Chapter 7
STUDY OF ENVELOPE ANALYSIS IMPLEMENTATION PROCESS

In Chapter 5, through the experimental test, envelope analysis method is proved to be able to extract the simulated bearing fault successfully. Thus, it will be implemented on the newly designed wireless sensor node for extracting bearing fault features. Prior to that, the implementation procedure of this method and the considerations on realizing it on a microcontroller are discussed in this chapter.

7.1 Overall Processing Structure

The implementation of envelope analysis can be divided into three steps, as shown in Figure 7.1. The collected signal firstly passes through a band-pass filter to enhance the signal-to-noise ratio (SNR) of the amplitude modulated resonance signal. Subsequently, the envelope of the modulation signal is obtained to eliminate the high frequency resonance and extract the low frequency fault impulse. Finally, by computing the spectrum of the envelope signal, the frequencies of the impulses are exposed. By comparing the maximum frequency component with the expected characteristic frequency discussed in Section 2.5, the defect component of the bearing can be identified.

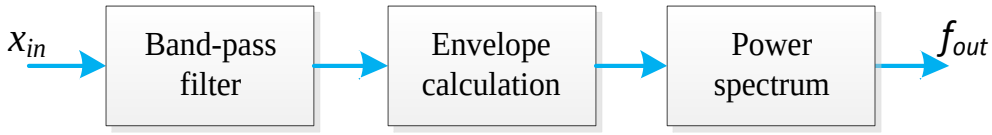

Figure 7.1 Procedures of envelope analysis

In the following sections, these three implementation steps will be explained in detail and the considerations on realizing them on a microcontroller with limited memory size will be discussed.

7.2 Band-pass Filter

A band-pass filter allows the frequency components of the signal in a specific band to pass while the lower and higher frequency components are blocked. As illustrated in Figure 7.2, the frequencies between two cut-off frequencies f_{c1} and f_{c2} pass while frequencies lower than f_{c1} and higher than f_{c2} are rejected. Suppose an input signal has an equal amplitude at frequencies f_1, f_2 and f_3. After passing through the band-pass filter, the output amplitudes at f_1 and f_3 are significantly attenuated while the frequency at f_2 is within the desired range so its signal amplitude passes through unaffected.

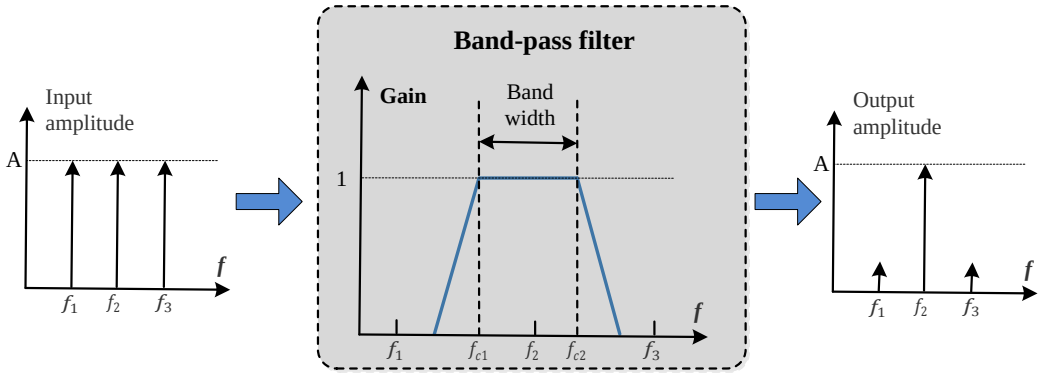

Figure 7.2 Frequency response of band pass filter

7.2.1 FIR filter and IIR Filter

In the digital signal processing area, a band-pass filter can be realized using a Finite Impulse Response (FIR) type filter or an Infinite Impulse Response IIR filter type one. These two types of filters have their own features and are suitable for different application situations.

An FIR filter is one whose impulse response is of finite duration. The filter structure of the FIR filter is shown in Figure 7.3 (a). As demonstrated, the FIR filter's output is determined by the sum of the current and past inputs, each of which is first multiplied by a filter coefficient. The implementation process is actually a convolution process and just includes a series of delay, multiplier and adder. Its corresponding difference equation can be expressed as an equation (7-1).

$$y[n] = \sum_{k=0}^{K} h[k]x[n-k] \qquad (7\text{-}1)$$

Where $x[n]$ and $y[n]$ represent an input and output sequence of index n, respectively: $h[k]$ is the k^{th} tap of the FIR filter coefficient $h[k]$ with the length K and $x[n-k]$ is the filter input delayed by k samples.

Comparatively, an IIR filter is defined as one whose impulse response is of infinite duration. The filter structure of the IIR filter is shown in Figure 7.3 (b). Unlike the FIR filter, the output of the IIR filter not only depends on the past input sequences but also is affected by the past output sequences. Its corresponding difference equation can be expressed as in equation (7-2).

$$y[n] = \sum_{i=1}^{M}(-a[i]y[n-i]) + \sum_{j=0}^{L} b[j]x[n-j]) \qquad (7\text{-}2)$$

Where $a[i]$ is the i^{th} forward coefficient and $b[j]$ is the j^{th} feedback coefficient; L and M are their corresponding tap number.

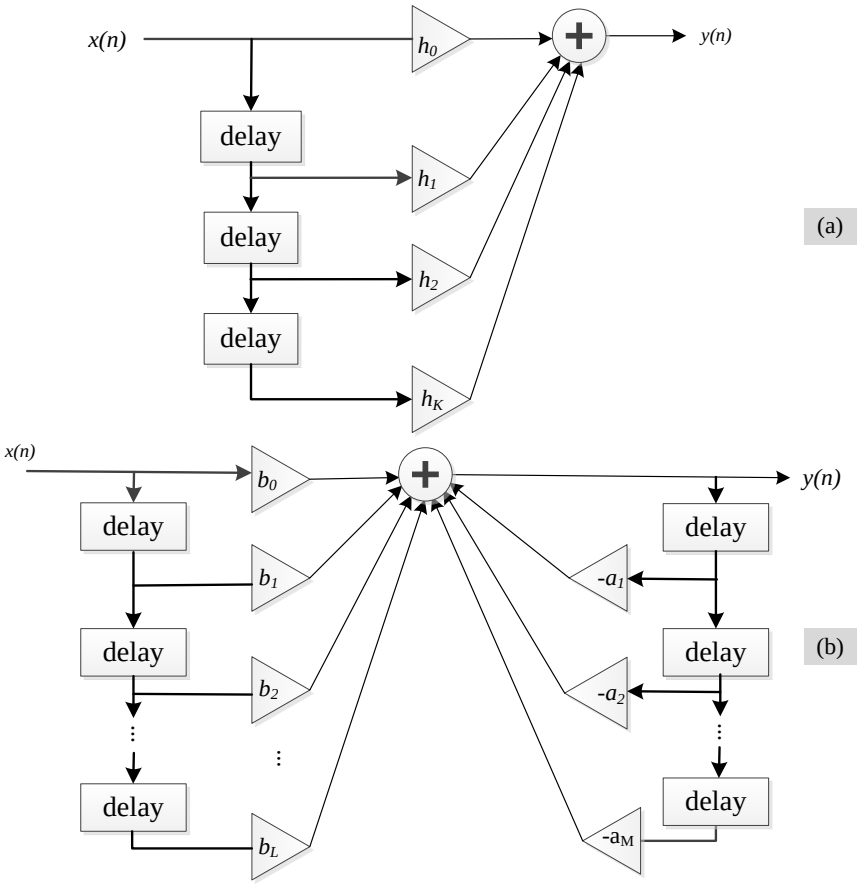

Figure 7.3 (a) FIR filter structure (b) IIR filter structure [116]

Both FIR and IIR filters can be used to implement almost any kind of response filters. However, their difference in the filter structure allows them to have their own advantages. The advantages of FIR filters over the IIR filter are that they are simple to design, linear phase and guaranteed to be stable, less sensitive to noise and errors from finite-precision math and simple implementation. This is a crucial property to have when implementing a filter on a processor or on an integrated circuit. The disadvantages of the FIR filter lies within the fact that they require more computation than an IIR. Thus, the IIR filters are useful for high-speed designs because they typically require a lower number of multiply compared to FIR filters. Unfortunately, IIR filters do not have

linear phase and they can be unstable if not designed properly [117]. Therefore, the FIR type filter is preferred in this design.

7.2.2 Design of FIR Filter

One of the most important advantages of the FIR filter is its ability to have an exactly linear phase response. The linear phase response feature is satisfied when this property is satisfied.

$$h(n) = \pm h(M-1-N), n = 0,1,\dots M-1. \qquad (7\text{-}3)$$

The linear phase FIR filter can be divided into four types as shown in Table 7-1. Among the four types, Type I is most versatile and can be used to design all filter types; Type II is not suitable for high-pass or band-stop filter; Type III can only be used to design band-pass filter and Type IV is not suitable for low-pass or band-stop filters. Thus, the band-pass filter can be realized using any type of filters.

Table 7-1 Linear phase filter types

Type	Impulse response	Number of coefficients	$H(\omega)$
I	$h(n) = h(M-1-n)$	Odd	$H(\omega) = \sum_{n=0}^{N-1} h(n)\cos\left[\left(n - \frac{N-1}{2}\right)\omega\right]$
II	$h(n) = h(M-1-n)$	Even	$H(\omega) = \sum_{n=0}^{N/2} h(n)\cos\left[\left(n - \frac{1}{2}\right)\omega\right]$
III	$h(n) = -h(M-1-n)$	Odd	$H(\omega) = \sum_{n=0}^{(N-1)/2} h(n)\sin(n\omega)$
IV	$h(n) = -h(M-1-n)$	Even	$H(\omega) = \sum_{n=0}^{N/2} h(n)\sin\left[\left(n - \frac{1}{2}\right)\omega\right]$

After several decades' development, the design process of FIR filter has become quite mature. simply, the design methods can be categorized into three types: impulse response truncation method, windowing design method and optimal filter design method, such as the Parks-McClellan exchange FIR filter design method [118].

For practical applications, the FIR filter design can be realized offline using the available scientific software toolboxes, which have been proved to be reliable, such as the fir1, fir2, firpm function provided in matlab from Mathworks. Subsequently, these coefficients can be loaded to the embedded processor for filter calculations.

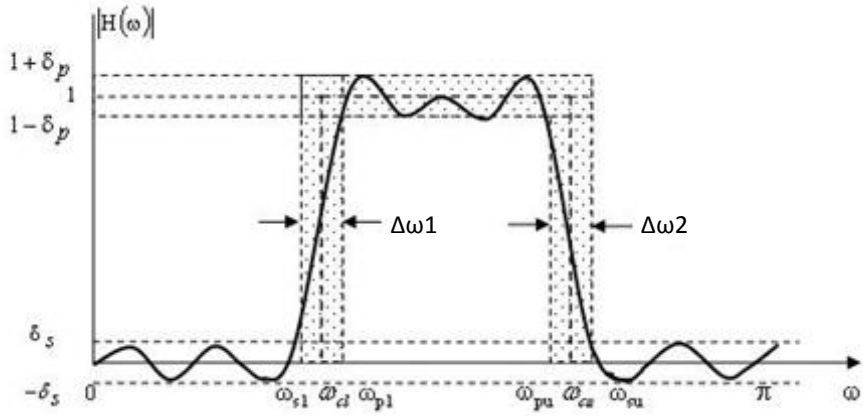

Figure 7.4 Band-pass filter specifications [118].

The detailed specification of a band-pass filter is illustrated in Figure 7.4, where the filter has a pass-band from ω_{pl} to ω_{pu}, stop band at ω_{sl} and ω_{su} and cut-off frequency at ω_{cl} to ω_{cu}. The maximum ripple amplitude in the pass-band and stop-band are expressed as δ_p and δ_s. In practical, the ripples are often expressed in dB using the pass-band ripple and stop-band ripple.

$$\text{pass-band ripple } = 20\ log_{10}\ (1 + \delta_p\ )\ \text{dB} \tag{7-4}$$

$$\text{stop-band attenuation } = -20\ log_{10}\ (\delta_s\ )\ \text{dB} \tag{7-5}$$

Group delay

A constant group delay means a filter has a linear phase response over its pass-band and will induce no phase distortion in its output signals.

For an FIR filter with S tap, the output signal delay in samples is demonstrated below:-

$$\mathrm{G}_{samples} = \frac{S-1}{2} \tag{7-6}$$

Thus, in the case of S being odd, the delay is of integral samples while it is of fractional samples in the case of S is even.

Implementation

Implementing a digital filter in practice typically involves using software to determine the filter coefficients based on various user-defined parameters. The filter design software usually computes and displays the filter coefficients with a high degree of precision. If the digital filter can be implemented using that same degree of precision, then the filter will behave as predicted by the filter design software. In practice, only a

finite number of bits can be used to represent the digital filter coefficients. This reduction in each coefficient's precision causes the frequency response of the filter to differ from the "ideal" response due to coefficient quantization errors. When using B_{coeff} bits to represent the filter coefficients, the total number of possible values that the filter coefficients can take on is 2^{Bcoeff}. Thus, instead of having an infinite range of values for the coefficients, they are instead constrained to one of the 2^{Bcoeff} levels. The location of the poles and zeros of the filters are also quantized. This is because they depend on the value of the filter coefficients. The quantization of the pole and zero locations will typically move the poles and zeros of the filters to locations that are different from the "ideal" setting. This can have drastic effects on the performance of the filter.

7.3 Envelope Detection

The envelope detection process is the heart of the envelope analysis. Simply, it can be implemented using a rectifier and low-pass filter for the analogue amplitude modulated signals. Within the scenario of digital signal processing, it can be implemented using the square-law method and Hilbert transform method.

7.3.1 Square-law Method

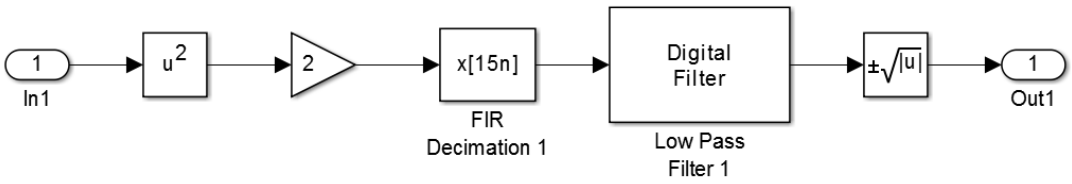

Figure 7.5 The implementation of the envelope detection using the square-law [119]

The block diagram in Figure 7.5 shows the implementation of the envelope detection using the square-law method. For this method, the input signal is firstly squared and passes through a low pass filter. It means that half of the energy of the signal is pushed up to higher frequencies and the other half is shifted down toward DC. Then, the signal is down-sampled to reduce the sampling frequency. Following this, pass the signal through a minimum-phase, low pass filter to remove the high frequency energy.

In order to maintain the correct scale, two additional operations need to be performed. Firstly, the signal is amplified with a factor of two, which will keep only the lower half

of the signal energy, this gain will match the final energy to its original energy. Secondly, the square root of the signal should be applied to reverse the scaling distortion that resulted from squaring the signal.

The squared-law method is easy to implement and can be effective when the sampling rate is much higher than the carrier signal, however, the square operation may cause aliasing problems when the carrier frequency is closer to the sampling frequency [119].

7.3.2 Hilbert Transform Method

Hilbert transform is another common method to produce the envelope. It produces an analytic signal, is a complex signal, of which the real part is the original signal and the imaginary part is the Hilbert transform of the original signal [32]. By calculating the modulus of the analytical signal, the envelope signal can be obtained.

As the measured signal can be considered a complex signal which only has the real part, its Hilbert transform can be realized using Equation (7-10) to (7-10). After the computation, an analytical signal x_{ht} is obtained whose real part is the original data x_{in} while its imaginary part is the Hilbert transformation of x_{in}. Thus, the envelope spectrum can be obtained using Equation (7-10), [113,114].

$$X = fft(x_{in}) \tag{7-7}$$

$$X_h(\mathrm{n}) = \begin{cases} X(n), & n = 0, \frac{N}{2} \\ 2 * X(n), & 1 \le n \le \frac{N}{2} - 1 \\ 0, & \frac{N}{2} + 1 \le n \le N - 1 \end{cases} \tag{7-8}$$

$$x_{ht} = ifft(X_h) \tag{7-9}$$

$$x_{env} = \sqrt{x_{ht} .* conj(x_{ht})} \tag{7-10}$$

$$X_{env} = |fft(x_{env})| \tag{7-11}$$

Where x_{in} is the vibration signal, X is the FFT of x_{in}, X_h is the rectification of X, x_{ht} is the reverse FFT of X_h, $x_{env}$is the analyzed envelope signal and X_{env} is the envelope spectrum. The envelope of the vibration signal and equation presents the

power spectrum of the envelope. Using this method, the computing buffer can be reused which is critical for a processor with limited storage.

7.4 Spectrum Computation

The spectrum of a time sequence can be obtained by performing Discrete Fourier transform (DFT) which is a mathematical procedure used to determine the harmonic, or frequency, content of a discrete signal sequence. The DFT of a discrete sequence $x(n)$ can be defined as:

$$X(m) = \sum_{n=0}^{N-1} x(n) e^{-j2\pi nm/N} \tag{7-11}$$

By calculating the DFT, the signal is converted to the frequency domain - where the signal is represented by a combination of complex sinusoidal. The DFT of a signal is an equivalent representation of the signal but can expose its frequency components much clearer. Just as shown in Figure 7.6, the signal in the frequency domain is just three discrete frequency components, which is much simpler than the waveform in the time domain. The signal can be converted back to its original time domain sequence using Inverse DFT (IDFT).

$$x(n) = \frac{1}{N} \sum_{m=0}^{N-1} x(m) e^{j2\pi nm/N} \tag{7-12}$$

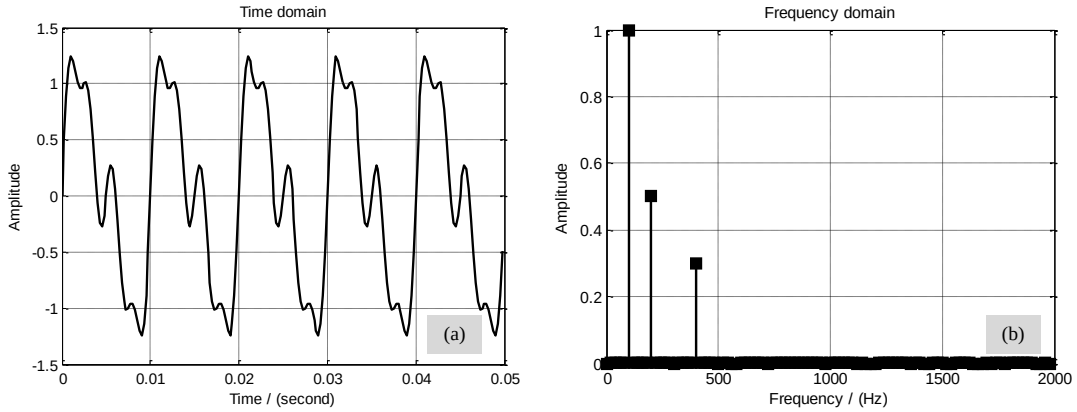

Figure 7.6 Example of DFT (a) time domain (b) frequency domain

For an N-point DFT on a data sequence with the sampling rate f_s, its frequency resolution is f_s/N Hz. Thus, the longer of data sequence for a fixed sampling rate, the

finer of the frequency resolution will be. Thus, in order to obtain satisfactory frequency resolution, the size of DFT calculations should be long enough. However, the calculation of DFT is quite time consuming and its computation time increases quickly with the size of the input sequence. In practice, it is usually implemented using Fast Fourier Transform (FFT), which is exactly equal to the DFT but can be realized as much more efficient.

7.4.1 Fast Fourier Transform (FFT)

The Fast Fourier Transform (FFT) is a faster version of the DFT. It utilizes some clever algorithms to do the same thing as the DTF but in much less time. The FFT can be orders of magnitude faster than the DFT, especially for large sizes. Noticeably, FFT forces one further assumption, that size *N* is an integer multiple of 2. This allows certain symmetries to occur reducing the number of calculations which have to be done [121],[122].

Take the classical radix-2 FFT algorithm for example; it requires the size N to be an integral power of two. For an 8-point data DFT needs N^2 or 64 complex multiplications while the number of multiplication for an N-point radix-2 FFT is just approximately $\frac{N}{2}\log_2 N$ or 12. With the size increases, the advantages of FFT are more obvious.

One thing that needs to be mentioned is the FFT algorithms which internally operate over complex input data sequences. In practice, the collected data only contain the real-valued part and there are some algorithms optimized for real-value data input. One method is just performing complex FFT (CFFT) on the data and therefore, treating the even values in the input array as real and the odd values as imaginary. This results in FFT of N/2 complex points for an input array of length N real points. After the FFT is performed, the result is recombined using a series of pre-calculated coefficients. In this way, only approximately half the operations of the CFFT are required.

7.4.2 DFT leakage and Windowing

Apparently, the DFT convention can only express a limited number of frequency components. The analytical frequencies $f_{analysis}\,(m)$ obtained from an N-point FFT can be calculated with the equation below:

$$f_{analysis}\,(m) = \frac{mf_s}{N}, where\ m = 0,1,2,\dots,N-1 \qquad (7\text{-}13)$$

On the occasion that the input signal has an integral period of samples and its true frequency is at exactly the position of the analytical frequencies, the results are precise. Otherwise, the input signal will show up to some degree in the entire N output analysis frequencies of our DFT. As shown in Figure 7.1, the signal is the time domain and is a pure sinusoidal waveform while its amplitude spectrum is distributed into several frequency components. This is the DFT leakage, which causes DFT results to be only an approximation of the true spectra of the original input signals prior to digital sampling.

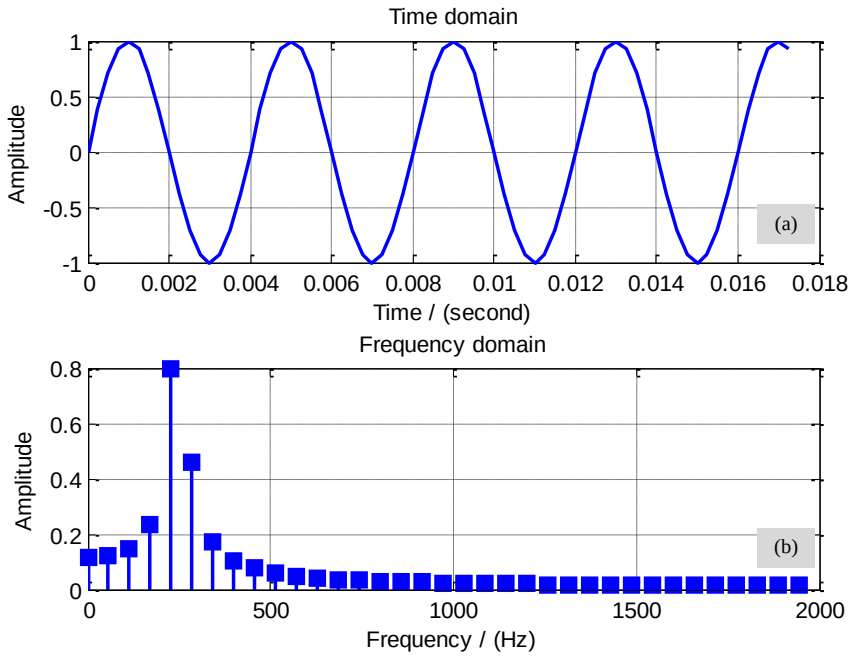

Figure 7.7 DFT leakage example (a) time domain (b) frequency domain

Fortunately, there are several methods to minimize leakage problems . If the frequency of the input signal is known in advance then performing FFT on an integral period of samples can let the frequency components suit at the analytical frequencies. However, the signal from the physical world is uncertain and usually contains multiple frequency components; as a result, it would be hard to perform integral periodical sampling. Increasing the data size for FFT calculation can reduce the leakage and improve the frequency resolution. However, the size increase also means longer computation time and larger memory occupation, which will be quite challenging for the microcontroller.

Windowing is a common remedy to reduce the DFT leakage problem. It reduces DFT leakage by minimizing the magnitude of side lobes. There are several window functions available to achieve various analysis performances, such as: rectangular window, triangular window, Hanning window and Hamming window. Among them, the Hanning window is effective for reducing DFT leakages and is employed in this design. The expression of Hanning window with N points is defined as:

$$w\,(n) = \ 0.5 - 0.5\cos\left(\frac{2\pi n}{N}\right), \qquad n = 0,1,2,\dots,N-1 \tag{7-14}$$

Noticeably, although the DFT leakage can be minimized through these methods, it cannot be eliminated entirely.

7.4.3 Frequency Domain Averaging

Increasing the data size for FFT calculation not only improves the frequency resolution and reduces the DFT leakage but also enables the signals with the lowest energy level possible to be viewed. This is because the noises are random while the true signals are usually periodic for the vibrations from a rotating machine. However, the maximum FFT calculation that a microcontroller can perform is limited to the available memory and larger FFT calculation usually means more computation time.

An alternative way to improve detection sensitivity is to average multiple FFT results, i.e. incoherent average on multiple FFT results. For a series of FFT results Y_m, their averaged results $\bar{Y}$ can be obtained by:

$$\bar{Y}(\mathrm{n}) = \frac{1}{M} \times \sum_{m=1}^{M} Y_m(n)\,, n = 0,1,2,\dots N-1 \tag{7-15}$$

Where $N$the size of FFT and M is the number of FFT calculations. For implementation, it collects a fixed data length of data and performs FFT; therefore, the FFT results have the same frequency resolution bins. Thus, the results for different frames can be added and averaged.

With averaging multiple FFT results, the random noise fluctuations in an FFT's output bins will decrease, while the magnitude of the FFT's signal bin output remains constant. It is quite helpful in filtering out random background vibrations and provides more repeatable results in data collection for early warnings of machine deterioration [123].

The increased FFT sensitivity (or noise variance reduction) due to multiple FFT averaging is also called integration gain. The reduction in the output noise variance $\delta^2{}_{M\ FFTs}$ of the incoherent average of M FFTs is relative to the output noise variance $\delta^2{}_{\text{single } FFTs}$ of a single FFT is expressed as:

$$\frac{\delta^2{}_{M\ FFTs}}{\delta^2{}_{\text{single } FFTs}} = \frac{1}{M} \tag{7-16}$$

As the bearing's state is relatively more stable in a short period when it is running, the frequency domain averaging can be effective for processing the bearing signal. It can be effective for improving the signal-to-noise ratio (SNR) of the processing results and can avoid transmitting much redundant data set. This not only saves the valuable bandwidth in the wireless sensor network but also saves the power of the wireless sensor node.

In implementation, the memory for FFT average calculation can be reused and the computation time is much shorter as the addition is easier and faster to perform than multiplication. Noticeably, the averaging of FFT results reduces the variations in the background noise power but does not reduce the average background noise power.

7.5 Summary

This chapter studies the implementation process of envelope analysis in detail and the considerations on improving the computation results accuracy are discussed. This will improve the implementation and optimization of the signal processing algorithms on the designed microcontroller in the following chapter.

Chapter 8
SOFTWARE DEVELOPMENT ON THE WIRELESS SENSOR NODE

This chapter explains the software development work involved on the wireless sensor node, including the data acquisition process, the implementation of envelope analysis and data transmission. The environment for developing embedded signal processing algorithms are firstly introduced, including the integrated environment code composer studio (CCS), the Tivaware, real time operating system TI-RTOS and the CMSIS DSP library. Then, the data acquisition process is optimized with the help of the execution graph of the TI-RTOS to reduce the CPU interference and improve its signal processing efficacy. On this basis, the envelope analysis is implemented and optimized according to the procedure explained in Chapter 7. Finally, the data transmission requirement for this method is analyzed.

8.1 Introduction to Development Environment

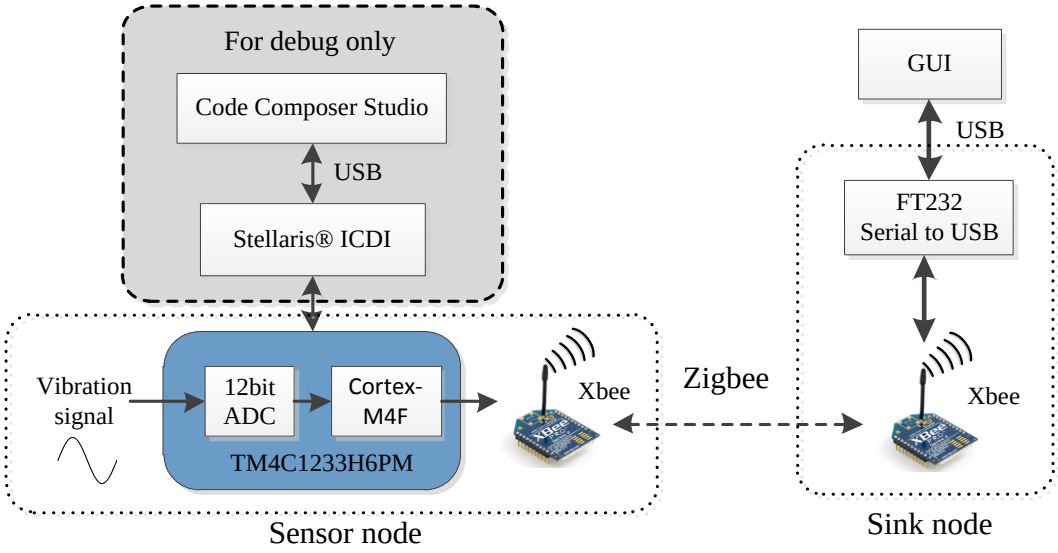

Figure 8.1 Software development environment structure

As illustrated in Figure 8.1 , the proposed wireless measurement system consists of two types of nodes: sensor node and sink node. Thus, the software development involves two parts: the software on the sensor node and the PC host software for communicating with the sink node.

The structure of the software development environment is illustrated in Figure 8.1. On the one hand, the program of the sensor node is debugged via the In-Circuit Debug Interface (ICDI). On the other hand, the data processing results on the sensor node are transmitted through the Zigbee network to the sink node and then routed to the PC for displaying. The ICDI connection is needed only in the debugging process, during which the program can be halted or paused at the break points to peer the processing results online. Furthermore, the processing results can also be transferred over the Zigbee network to the sink node and watched through the graphic user interface (GUI). In the subsequent subsections, the useful tools employed during software development will be briefly introduced.

8.1.1 Code Composer Studio

The Code Composer Studio (CCS) is based on the well-known Eclipse open source software framework, which was developed as an open framework for creating development tools. It combines the advantages of the Eclipse software framework with

advanced embedded debug capabilities from TI resulting in a compelling feature-rich environment for embedded developers. A basic edit perspective of CCS is shown in Figure 8.2. It comprises a suite of tools used to develop and debug embedded applications, including compilers for each of TI's device families, a source code editor, a project build environment, debugger, profiler, simulators, real-time operating system and many other features.

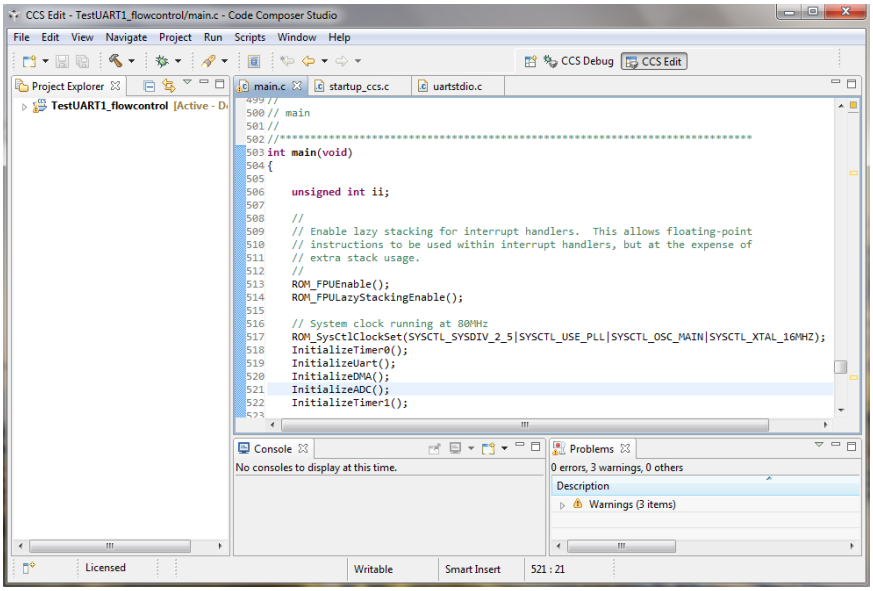

Figure 8.2 Basic edit perspective of the CCS environment

The debugging process of the signal processing algorithms normally needs some modifications of the codes, which is unsatisfactory. CCS provides various useful tools to ease and speed the development process. For example, a break point can be set to halt the program at a desired and to observe the status of the CPU or the processing results. In the debugging process, it is often necessary to view the value of the variables to ensure that the function executes properly. The tools listed below provided by CCS can be helpful in the program debugging process.

Variable Viewer: Variables can be viewed in the watch window when the CPU is halted. The variables in the current context will be automatically added to this viewer, in this way, the program status can be viewed clearly, as shown in Figure 8.3(a).

Expression Viewer: The Expressions view is a typical watch window where variables, expressions and even registers can be monitored. If the required variable is not listed in the variable viewer, the user can add it to the expression viewer, as shown in Figure 8.3(b).

Memory Browser: The memory browser can be used to view the data in the memory. It features multiple viewing formats and types: char, integer (signed/unsigned), float and multiple Hexadecimal data sizes (8 through 64-bits). This is also a useful tool when the variable is a string or an array, one example of which is shown in Figure 8.3(c).

Memory Allocation: The memory allocation provides a cool view of the memory usage of current program for both SRAM and flash, as shown in Figure 8.3 (d). The memory consumption can be clearly viewed, which is helpful in the program optimization stage.

Time Domain Graph: This graph plots the data in the display buffer on a magnitude versus time graph, as shown in Figure 8.3(e). It provides a quick view of the processing results during debugging stage.

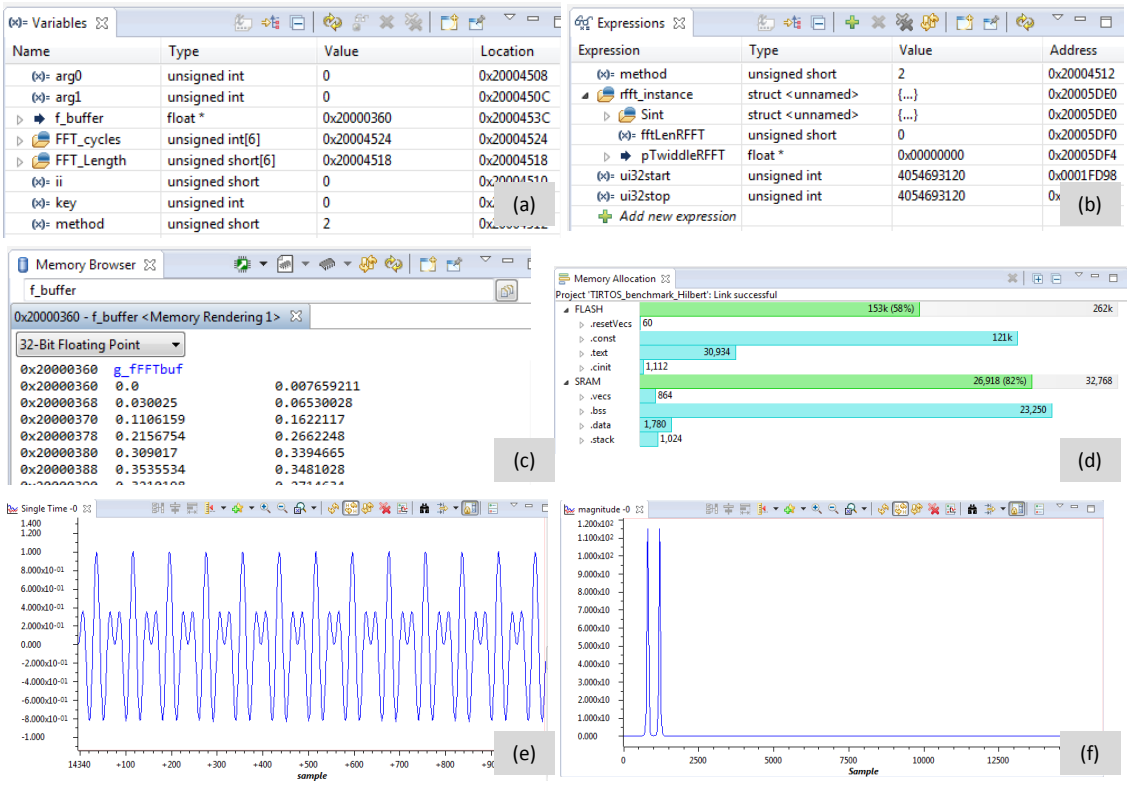

Figure 8.3 Using tools in CCS (a) variable viewer (b) expression viewer (c) memory browser (d) memory allocation (e) time domain graph (f) FFT magnitude graph

FFT Magnitude Graph: This tool can apply FFT on a frame of data and display the spectrum immediately in the debug stage, as shown in Figure 8.3(f). The type of data for analysis can be either real or complex.

Furthermore, the CCS also provides the function to calculate the CPU cycles between two breakpoints, and in this way, the user could easily evaluate the speed performance of an algorithm and ensure whether the real-time requiements are satisfied.

8.1.2 TivaWARE and CMSIS DSP library

TivaWare software is an extensive suite of software tools designed to simplify and speed development of Tiva C Series-based MCU applications. It includes the driver libraries and example codes for the peripherals and typical applications, which allows users to create and build full-function, easy-to-maintain code.

The Cortex Microcontroller Software Interface Standard (CMSIS) DSP library [90] is a library from the ARM company. It provides a suite of common signal processing functions for use on Cortex-M processor based devices and its implementation for Cortex-M4 is optimized for the SIMD instruction set. The library includes over 60 Functions for various data types: fix-point (fractional q7, q15, q31) and single precision floating-point (32-bit). Some of its common functions are listed in Table 8-1. Noticeably, in order to use the CMSIS DSP library for the TIVA C microcontroller, the library needs some modification and to be recompiled in the CCS, which can be found in [125].

Table 8-1 Functions in CMSIS DSP library

Categories	**Description**
Basic math	Vector addition, dot multiplication, shift, scale and offset
Fast math	A fast approximation to sine, cosine, and square root
Complex math	Conjugate, dot product, magnitude, multiplication
Filters	IIR filter, FIR filter, LMS filter
Matrix	Addition, inverse, multiplication, scale, transpose
Transforms	Complex FFT, real FFT
Motor control	PID, vector Clarke transform, vector Park transform
Statistical	Maximum, mean, minimum, power, RMS, standard deviation
Support	Vector copy, vector fill, format converting functions
Interpolation	Linear interpolation, Bilinear interpolation

8.1.3 Real time Operating System - TI-RTOS

Traditionally, the program on a microcontroller doesn't need an operating system because the resources on the microcontroller are usually limited and the tasks are quite simple. With the fast development in micro-electronics, more and more functions have been integrated into the microcontroller, which makes the programming challenging. Based on this, the utilization of real time operating system (RTOS) on the microcontroller has become a developing trend.

In this design, the TI-RTOS is employed for development, which is a complete real-time operating system for TI microcontrollers based on a preemptive multithreading kernel. It combines a real-time multitasking kernel SYS/BIOS with additional middleware components including TCP/IP and USB stacks, a FAT file system, and device drivers, enabling the researcher to focus on differentiating their application: see Figure 8.4. It is built on existing proven software components such as SYS/BIOS, TivaWare software and controlSUIT software to ensure reliability and quality. [126].

With combination of CCS, several useful tools are quite helpful for development. For example, the RTOS object viewer (ROV) can be used to examine the state of operating system objects, such as tasks and semaphores, and detect why a task is not executing as expected; through the RTOS analyzer, the CPU load and the thread execution sequence can be viewed; the timestamp can be employed to measure the execution time of the program.

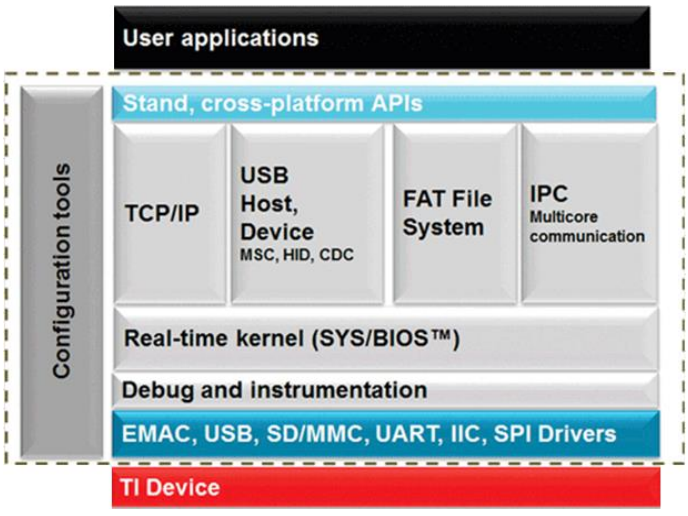

Figure 8.4 Block diagram of TI-RTOS [126].

8.2 Data Acquisition Process and Optimization

The data from the vibration sensor is in analogue electric form. Before carrying out digital signal processing, the analogue signal should be digitized. The analogue signal digitization theory is firstly explained in the following subsections, and then three data acquisition mechanisms are realized and compared for optimizing this process with the help of the TI-RTOS.

8.2.1 Analogue Signal Digitization Theory

As shown in Figure 8.5, a continuous analog signal $x(t)$ is converted to a time-discrete form $x(n)$ by sampling its value in periodical intervals of duration T_s. The value-continuous samples are rounded to a value-discrete binary number. The quality of the converter's approximation of the input will improve when the converter resolution *n* is larger, since the rounding error is smaller. This rounding error, called the quantization error, which has a range of $\pm\frac{1}{2}$ LSB (least significant bit), where oneLSB $= \frac{V_{ref}}{2^N}$.

The sampling rate is defined as

$$f_s = \frac{1}{T_s} \tag{8-1}$$

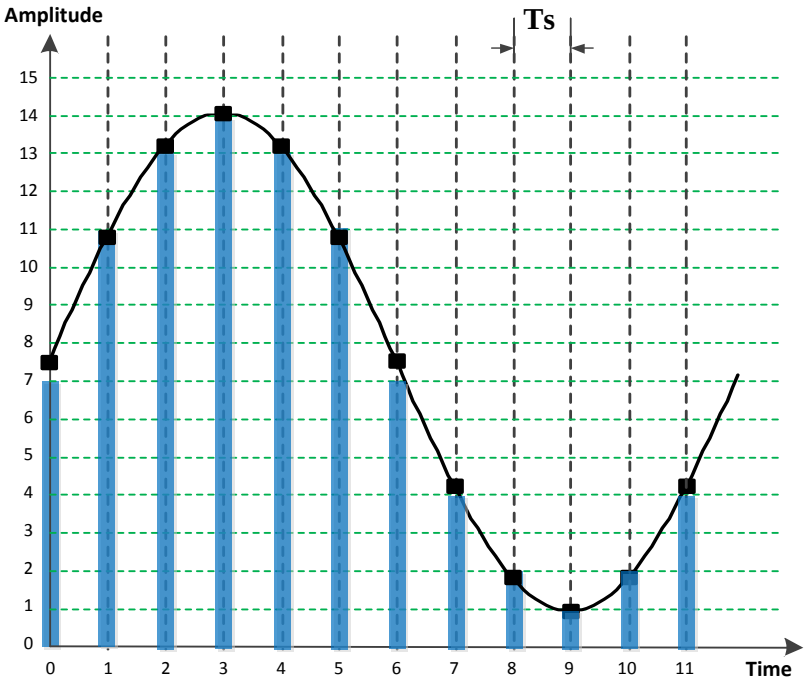

Figure 8.5 Conversion of an analog to a time-discrete signal (sampling)

In order to reconstruct the original signal from the sampled digital sequence, the analog signal $x(t)$ must be band limited and the sampling frequency f_s must satisfy the Nyquist sampling theory [127]

$$f_s \geq 2f_{max} \tag{8-2}$$

Where f_{max} represents the maximum frequency of the analog signal $x(t)$.

Otherwise, aliasing problem may happen and the sampled data sequence is not trustworthy anymore. For this reason, an analogue low-pass filter is usually included in the signal conditioning chain so as to limit the bandwidth of the input signal.

8.2.2 Timer Triggered Interrupt Sampling Method

As shown in Figure 8.5, in the data conversion process, the time interval between each sampling point should be precisely equal. One way to promise the interval equality is using a timer to trigger an interrupt as presented in Figure 8.6(a), inside which the CPU will start the ADC, wait for the data conversion to finish and read the sampling results. For each time the timer triggers the interrupt, one data sample is collected. After the required amount of data is collected, a semaphore will be posted to inform the process task that the data is ready for process. Then, the process will be released from its block status and the acquired data dealt with.

The execution graph of employing this method to sample an analogue signal is illustrated in Figure 8.7. From the execution graph, the thread running sequences are clear, which helps to ensure that the program is running as expected. As shown in Figure 8.7, a timer interrupt happens periodically and the time interval between each interrupt is about 31 μs, corresponding to the sampling frequency at around 32 kHz. The execution time for each interrupt is approximately 8 μs while the time for the last interrupt is relatively longer; this is because it needs to execute one more operation to post the data ready for processing semaphore. After the semaphore is posted by the last timer interrupt, the BIOS scheduler runs to reschedule the threads, immediately after which, the process task starts running. This is exactly as we expected in Figure 8.6.

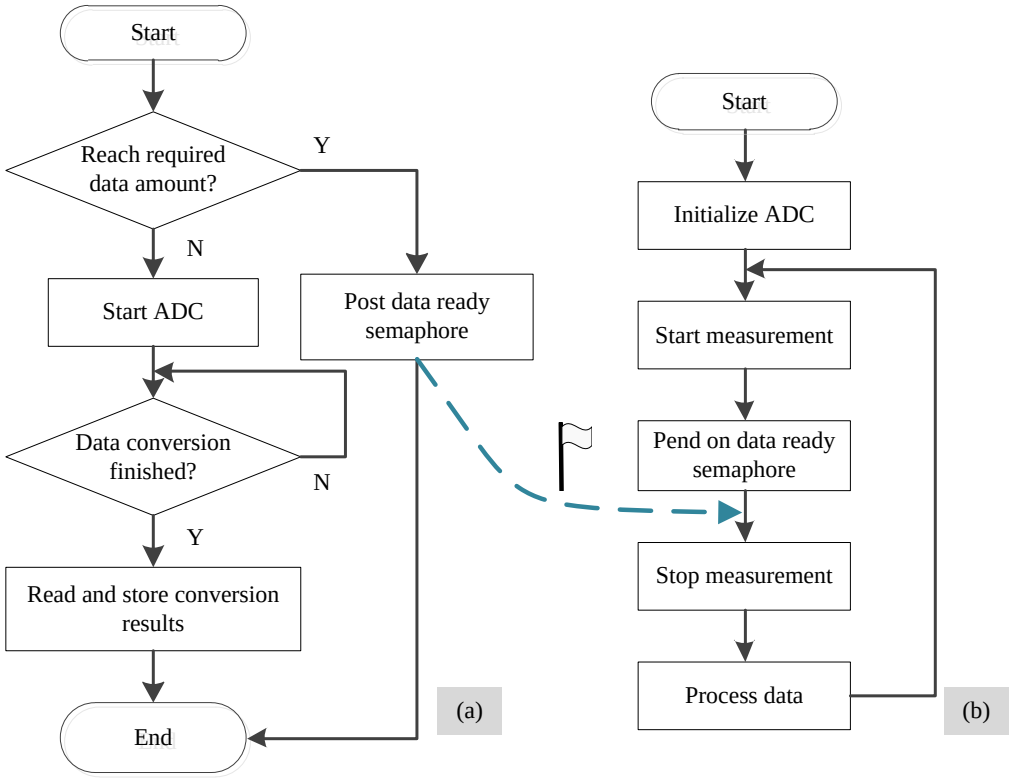

Figure 8.6 Flowchart of timer triggered interrupt sampling method
(a) timer ISR (b) process task

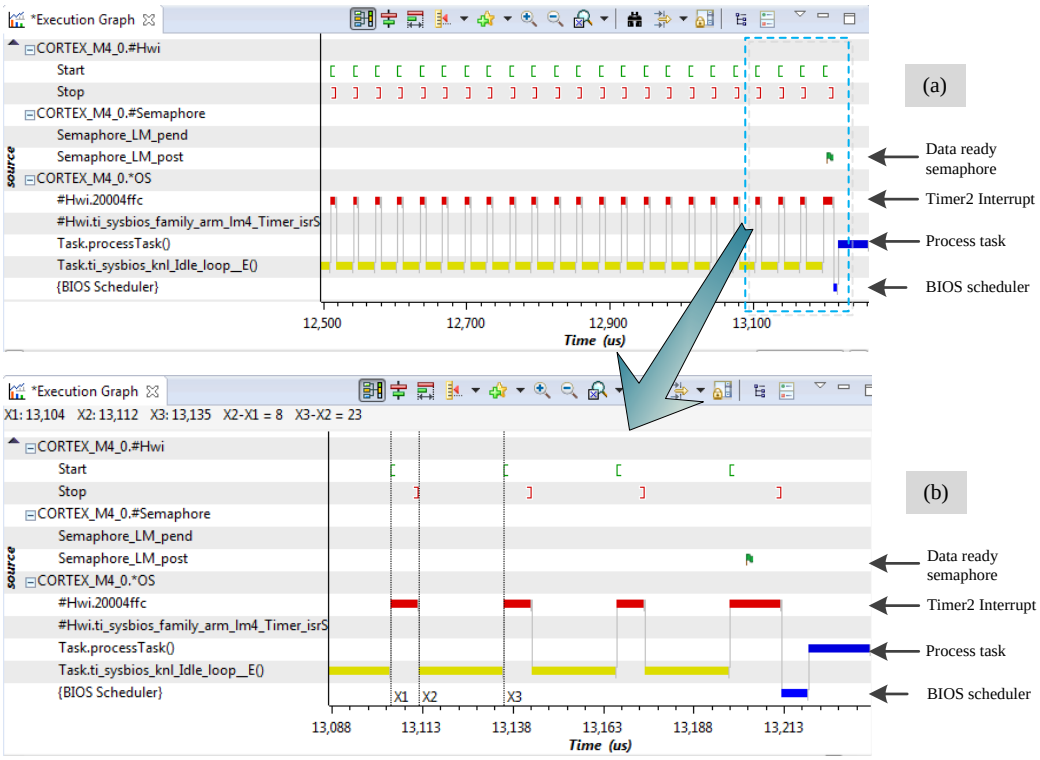

Figure 8.7 Execution graph of timer triggered interrupt sampling method
(a) full view (b) magnified view

8.2.3 ADC Triggered Interrupt Sampling Method

In the timer triggered interrupt sampling method, the ADC is triggered by the CPU and considerable time is spent waiting for the ADC conversion to finish inside the timer interrupt: this delay needs to be overcome.

In order to eliminate the waiting time, an extra ADC interrupt routine is specially added to read the conversion results. In this way, the CPU does not need to wait while the ADC is converting the data. The execution graph by adopting this idea is presented in Figure 8.8. As expected, after triggering the timer interrupts, an ADC interrupt follows to read the data conversion results. As illustrated in Figure 8.8 (b), the execution time for the timer ISR is reduced from 8 µs to 5 µs. Meanwhile, it can be noticed that the execution time for the ADC interrupt is also 5 µs. Thus, the total time spent on sampling one data point is about 10 µs. This means the CPU efficacy has decreased by employing this method, which is unexpected. The reason may lie in that the time spent on entering and exiting a hardware interrupt is more than the time spent inside the ISR, which is true for the hardware interrupt based on an RTOS. However, for the program without an RTOS, this method still has the potential to shorten the sampling time.

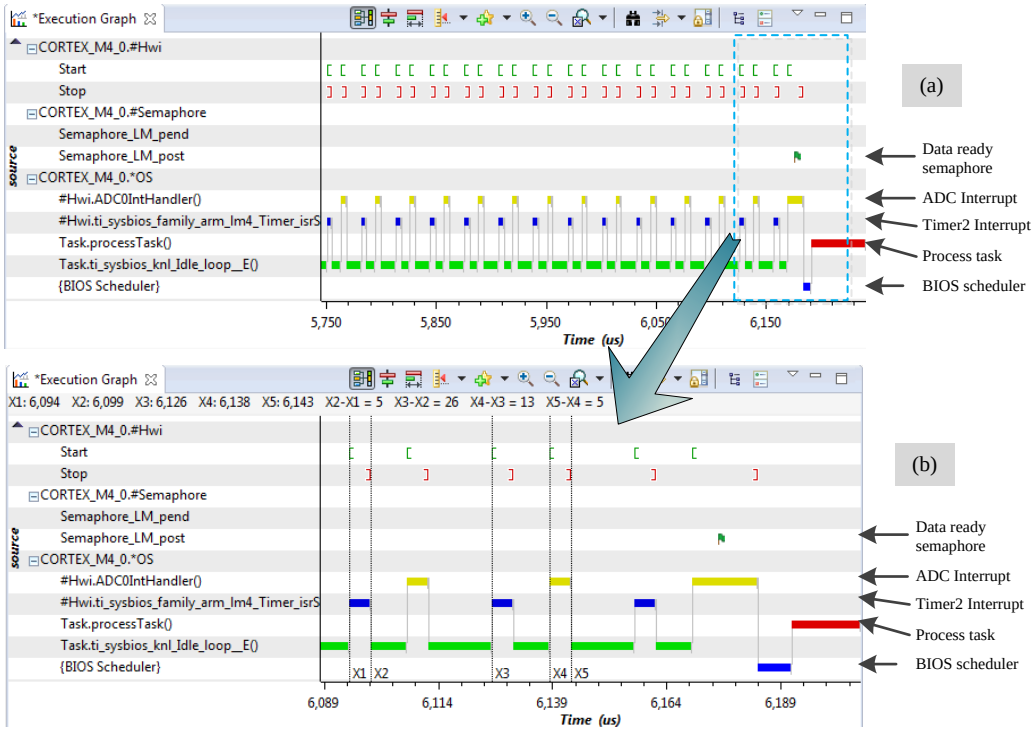

Figure 8.8 Execution graph of timer triggered interrupt sampling method
(a) full view (b) magnified view

Noteworthy, in the above method, the timer interrupt service routine (ISR) is utilized to finish one task, which is to trigger the ADC. So, a method of using the timer event to trigger the ADC directly is used, in which way, the timer ISR can be avoided. Fortunately, according to the introduction in Section 6.3.1, the ADC module does have the option to be triggered by a timer overflow event. As shown in Figure 8.9(b), the ADC and timer peripheral are properly initialized, and then the ADC interrupt (shown in Figure 8.9(a)) will be triggered periodically after the conversion is completed.

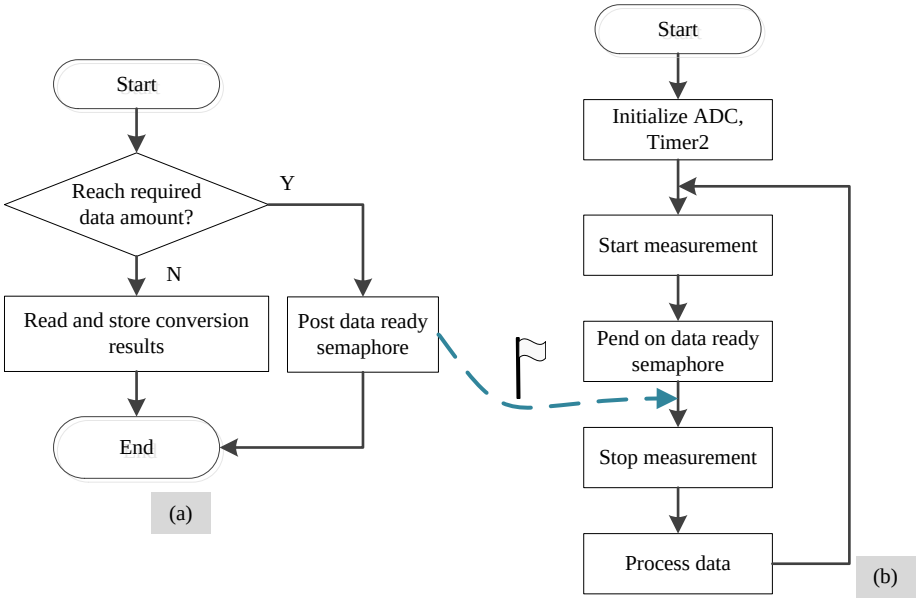

Figure 8.9 Flowchart of ADC triggered interrupt sampling method
(a) ADC interrupt routine (b) process task

The execution graph of using this method is presented in Figure 8.10. As it shows, the ADC interrupt only happens periodically. The execution time for the ADC interrupt remains 5 μs, therefore, the total time spent on sampling one data point is reduced to 5 μs. This result is better.

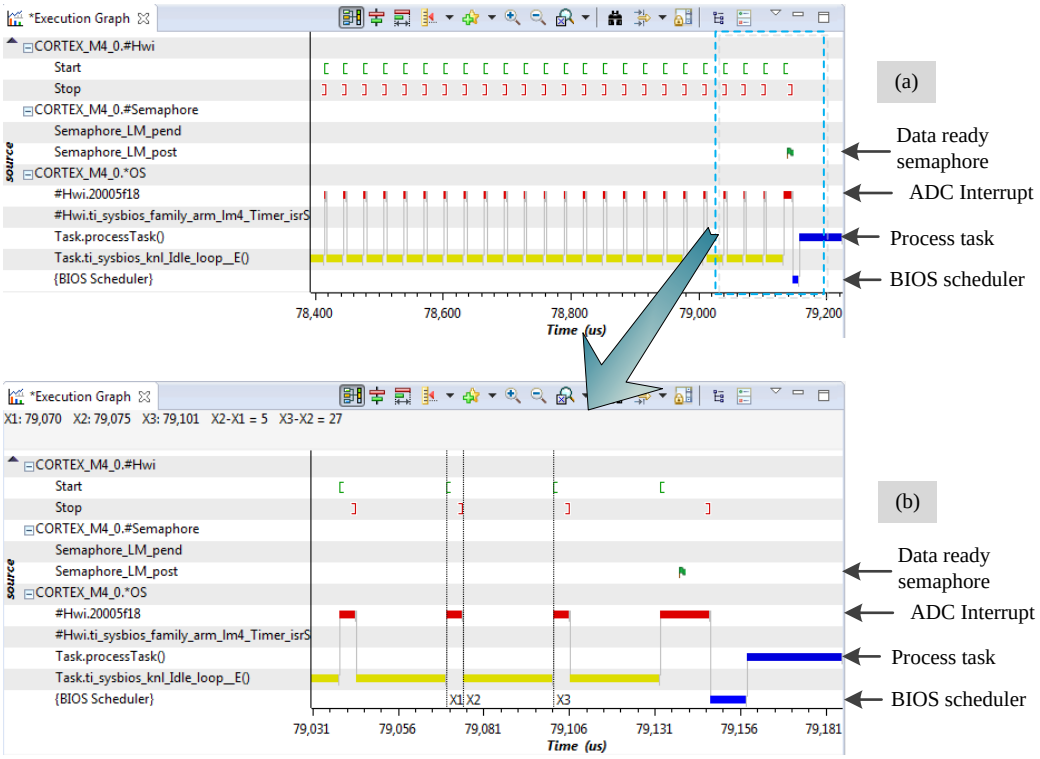

Figure 8.10 Execution graph of ADC triggered interrupt sampling method
(a) full view (b) magnified view

8.2.4 DMA Triggered Interrupt Sampling Method

As discussed in the above Section 8.2.3, by using the timer overflow event to start the ADC directly, the execution time spent on each sampling time point has been effectively shortened. It can be observed that the ADC ISR is just responsible for moving conversion results from the ADC result register to the internal RAM. For this kind of data movement, another peripheral DMA can help.

The execution graph of using the DMA triggered interrupt method is presented in Figure 8.11, in which 1024 points of data are sampled with the sampling frequency at 32 kHz. As it shows, there is only one interrupt generated for this sampling period excluding the system tick interrupts. Compared with the method in Section 8.2.3, which needs 1024 interrupts, the advantages of the DMA triggered interrupt sampling method is obvious. By using the DMA to help move data, the interrupt times can be greatly reduced and the CPU can be liberated from frequently responding to the interrupts.

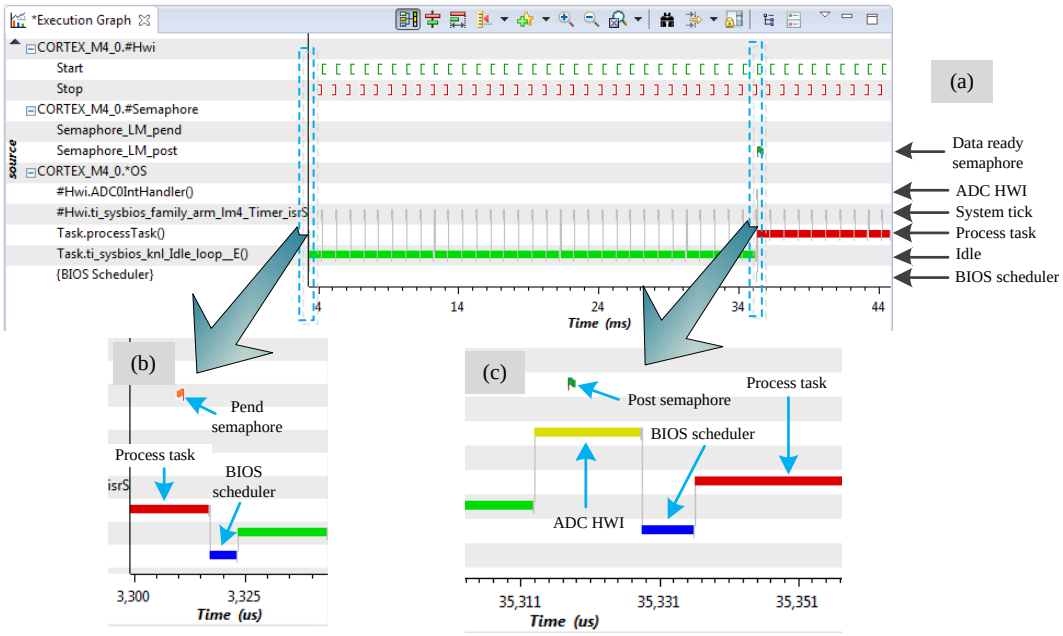

Figure 8.11 Execution graph of DMA triggered interrupt sampling method
(a) full view and (b) magnified view

By connecting a 200Hz sinusoidal waveform to the input of the ADC, a frame of data with 1024 points is acquired using the DMA triggered method and is displayed using the graph tool in Figure 8.12. As it shows, the signal is continuous and quite smooth, which implies the equality between the sampling intervals. The period of the acquired waveform is about 5 ms, as depicted in Figure 8.12. This is in accordance with the input sine wave's frequency, i.e. 200 Hz.

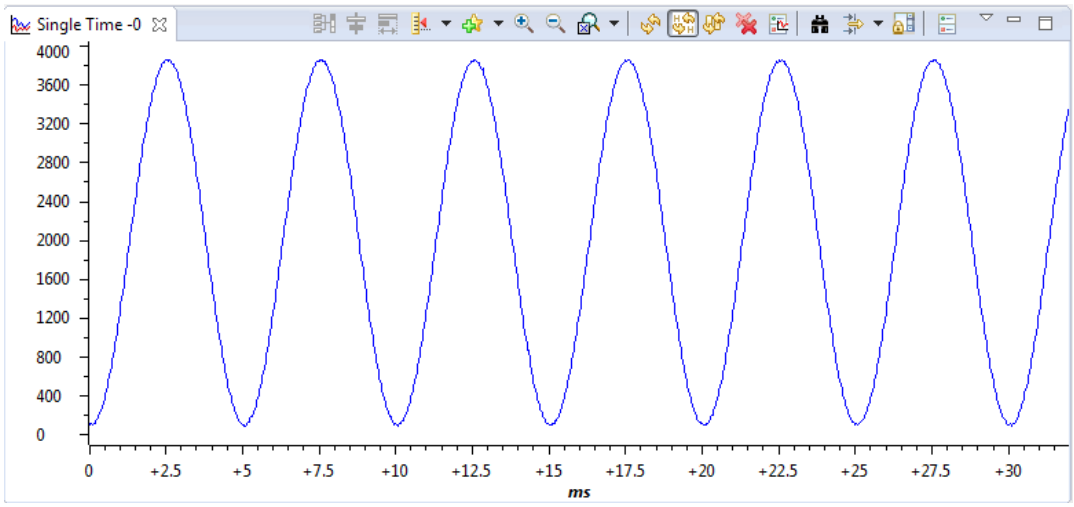

Figure 8.12 A waveform of 1024 points acquired using the DMA triggered method

8.3 Signal Processing Algorithms Implementation and Optimization

After one frame of data is acquired, the next step is to process it them using the envelope analysis explained in Chapter 7. The detailed implementation and optimization on the TIVA Launchpad board is introduced below.

8.3.1 Band-pass Filter

As discussed in Section 7.2, the FIR filter is employed to filter the data. The coefficients of the filter are calculated offline and stored as a constant table in the flash to save RAM memory. The coefficients are stored in single floating point format, thus, the preciseness for computation can be promised.

Recalling the bearing fault characteristic frequencies in Table 5-2, the maximum fault frequency is the inner race fault at 135.5 Hz, whose third harmonic is at around 406.5 Hz. As the characteristic frequency resides on the two sides of the resonance signal, they should be contained by the band-pass filter. A band-pass filter with 1 kHz bandwidth would enclose the first three harmonics of all the fault characteristic frequencies. Thus, the band-width of the band-pass filter is designed as close to 1 kHz. The frequency and phase response of the designed 81-tap band-pass is presented in Figure 8.13, which has a flat amplitude response and a linear phase response from 1 kHz to 2 kHz.

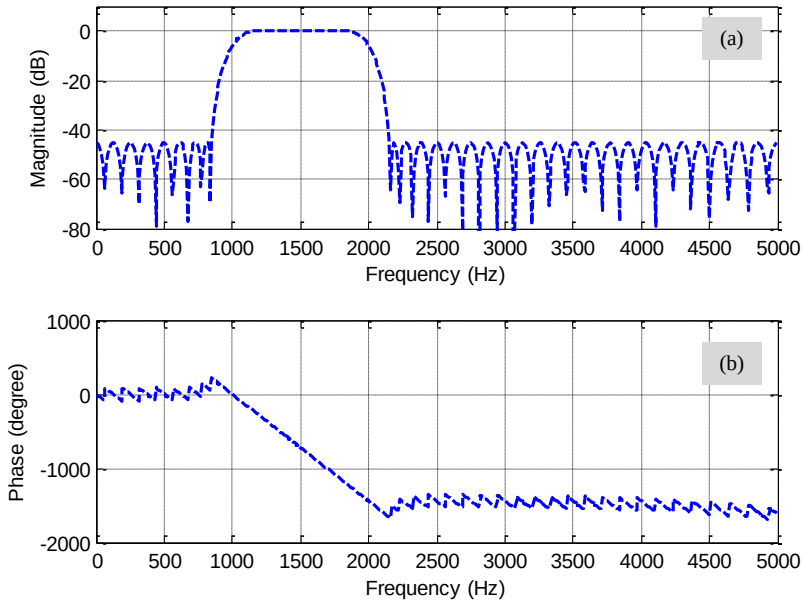

Figure 8.13 Frequency response of the designed band-pass filter (a) magnitude and (b) phase

The detailed measure of the designed band-pass filter is listed in Table 8-2. As it shows, the ripple in the pass-band is less than 0.1 dB and the attenuation ratio for the stop-band signal is up to 45 dB.

Table 8-2 Measure of the designed band-pass filter

Parameter	**Value**
First 3-dB point	1.04kHz
Second 3-dB point	1.96 kHz
Pass-band ripple	0.097 dB
First stop-band attenuation	45 dB
Second stop-band attenuation	45 dB
First transition width	300 Hz
Second transition width	300 Hz

On implementation, the signal computations are implemented using single floating point, in which way the integrated FPU unit on the microcontroller can show its power. The preciseness of computation can be promised and there are concerns about overflowing problems, which is common problem for fixed-point digital signal processing. Therefore, the collected data sequence is firstly converted from *unsinged int* format to *single precision floating point* format.

Two functions *arm_fir_init_f32* and *arm_fir_f32* from the CMSIS DSP library are employed to achieve the FIR filtering process. In order to save memory, the large frame of data is further divided into small blocks, which are then processed by the filter function. Specifically, the output data of the FIR filter are delayed by $(81-1)/2 = 40$ samples according to equation (7-6), which also implies that the first 40 samples output of the FIR filter are invalid.

8.3.2 Spectrum Calculation

The spectrum calculation is explained earlier as it is part of the Hilbert transform. As shown in Table 5-2, the minimum difference between the four types of fault frequencies is 35.1 Hz, which indicates the frequency resolution should be larger than this value in order to distinguish the four bearing faults. On the case the sampling frequency at 10 kHz, the FFT size should be larger than $10000/35.1 \approx 285$. As the FFT size should be the power of 2, this means the FFT size should be larger than 512. According to the

discussion in Section 7.4.2, the FFT size is expected to be larger to get the benefit from higher frequency resolution and lower spectrum leakage.

On implementation, two functions *arm_cfft_f32* and *arm_cfft_radix2_f32* are available for complex type FFT calculations. Comparatively, the *arm_cfft_f32* is faster than the *arm_cfft_radix2_f32*, which employs the traditional radix2 algorithm. Besides, two functions *arm_rfft_f32* and *arm_rfft_fast_f32* are available for real-valued FFT calculations. As their name implies, the later one is faster than the first one.

Based on the test, it is found that the input and output buffer for the two complex FFT functions can be the same while they must be different for the two real-valued FFT functions. This means the buffer for the FFT calculation is at least double the size of the input data sequence. As the data for computation is in single floating point format, one data occupies four bytes. Therefore, for an N-point FFT calculation, the buffer should be larger than $4N \times 2 = 8N$ bytes. According to the introduction on the microcontroller in Section 6.3, the SRAM memory size is 32 kB. Considering the buffer should be smaller than the SRAM memory size, the FFT size N should be smaller than 4k, i.e. 4096. As other computations also consume SRAM memory, this means the maximum allowable FFT size in single floating point format is 2048 point.

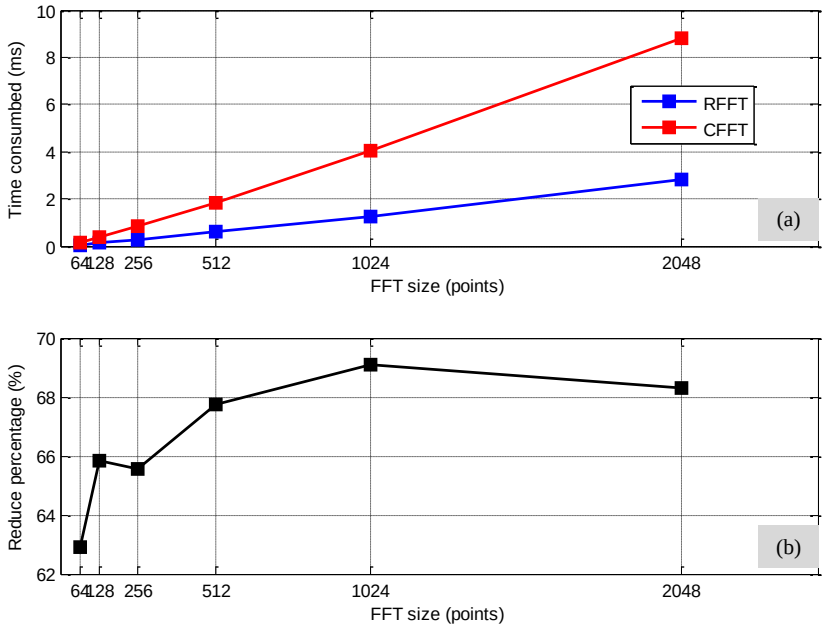

Figure 8.14 (a) FFT computation speed comparison between RFFT and CFFT using radix-2 and (b) time reduction percentage

Figure 8.14 shows the computation time spent by using the *arm_cfft_radix2_f32* function (CFFT) and the *arm_rfft_fast_f32* function (RFFT). The execution time is measured using the timestamp function provided in the TI-RTOS. As it shows, the RFFT method is much faster than the CFFT method for the same FFT size and it could save nearly 70% of the computation time. The improvement in computation time is quite helpful in reducing the power consumption of the wireless sensor node.

One concern to be dealt with is the spectrum leakage. Table 8-3 shows the periods of fault signals that can contain in one maximum FFT computation frame, i.e. 2048 points. It can be observed that the periods for the fault signal BSF and FTF are ahort. In order to minimize the spectrum leakage, a Hanning window is applied to the signal before spectrum calculation.

Table 8-3 Periods included in one frame

Fault type	Fault frequency (Hz)	Periods in one frame (2048 points)
BPFI	135.5	27.7
BPFO	83.5	17.1
BSF	48.4	9.9
FTF	9.3	1.9

8.3.3 Hilbert Transform

Hilbert transform is a crucial procedure in obtaining the envelope and it is also the most time consuming part because it involves a forward and an inverse FFT calculation as discussed in Section 7.3.2. As the data for Hilbert transform are real-valued, the forward FFT can be computed using either the complex or the real-valued FFT functions. However, for the inverse FFT, the result is the analytic signal which contains both the real and imaginary part. Thus, the inverse FFT can only be computed using the complex FFT function. A computation speed comparison result is presented in Figure 8.15, where the red line indicates the computation time for the method using pure complex FFT function: the blue line represents that for the method combining the real-valued FFT and complex FFT. As shown in Figure 8.15 (b), the computation speed improvement is up to nearly 33%, which is worthy for the optimization.

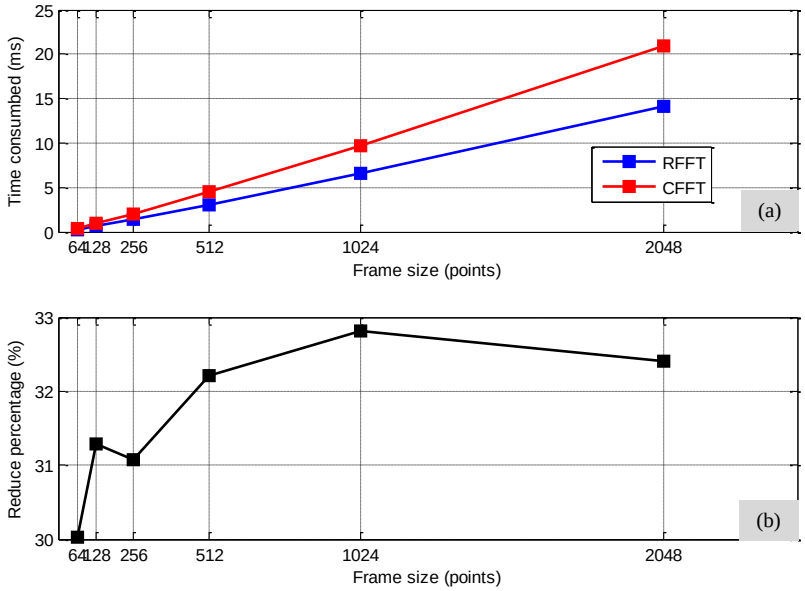

Figure 8.15 (a) Hilbert transform computation speed comparison between RFFT and CFFT using radix-2 and (b) time reduction percentage

8.3.4 Overall Signal Processing Flow

Now the picture for the overall signal processing flow becomes clear, and this is presented in Figure 8.16. The collected vibration signal is processed frame by frame, each of which is composed of 2048 points. Firstly, the data are converted from 16-bit unsigned integer to 32-bit single floating-point format. In order to maintain high accuracy, the computation is achieved in floating point and the FPU unit integrated on the microcontroller is utilized to speed up the floating point calculations. The following calculations are carried out in a large buffer with the size of 16 kB, which is twice of the frame size. The reason for using a double sized buffer has been explained in 8.3.2.

After format conversion, the data passes through an FIR band-pass filter whose coefficients have been computed and stored in the flash. When implementing FIR filter, the data frame is divided into several smaller sub-frames with a fixed size, which then pass through the FIR filter in sequence. This allows the filtering to be accomplished using a relatively smaller buffer. The Hilbert transform is chosen to detect the envelope due to its preciseness. HT is then carried out on the filtered signal to obtain the analytic signal. After the Hilbert transform, the envelope is acquired by simply calculating the magnitude of the analytic signal. As we are only interested in the AC components of the obtained envelope signal, the DC component of the envelope is removed; otherwise, the large DC component might leak to the nearby frequency bins.

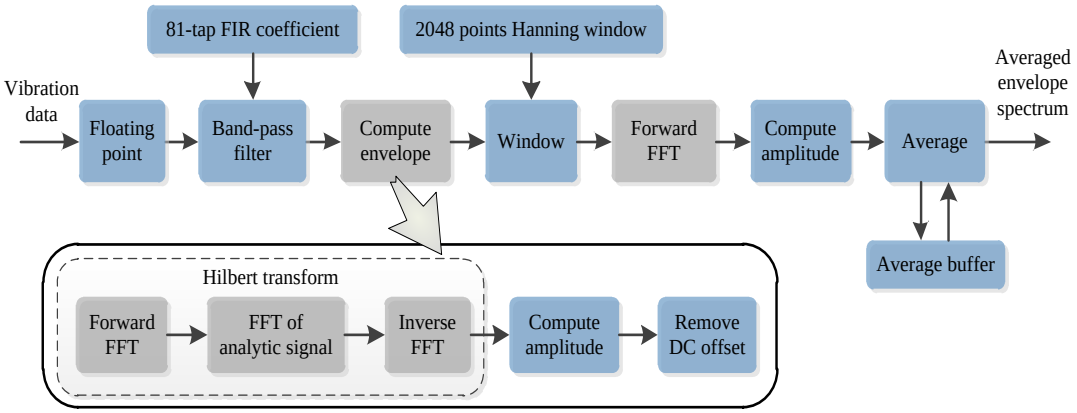

Figure 8.16 Data flow of envelope analysis

Finally, a Hanning window is applied to the calculated envelope signal and its amplitude spectrum is obtained with a forward FFT calculation. At the end of signal process chain, an average process is added to improve the accuracy of the processing results as discussed in Section 7.4.3.

8.4 Data Transmission

After the averaging process, the resulting data are converted into a 16-bit unsigned integer format and transmitted to the wireless module. It is obvious that the data size will be much smaller when only the result of averaged envelope spectrum is sent out, compared with that of sending the results of multiple envelope spectra which are based on calculating the averaged result.

Recalling the bearing fault frequencies in Table 5-2, the maximum fault frequency is the inner race fault at 135.5 Hz, whose third harmonic is around 406.5 Hz. As after the envelope analysis, the high frequency resonances have been removed and only the low frequency fault frequency components exist in the computed envelope spectrum. This means, there is no need to transfer the data of the entire spectrum. For example, we may just transmit the spectrum under 500 Hz, which is about 103 points of spectrum data. This would save quite a lot of bandwidth.

Figure 8.17 presents the comparison of effective data amount that needs to be transmitted in different processing phases. Provided all the transmission data are stored with 16-bit resolution, the raw data per frame (2048 points) occupy as much as 4096 bytes, and the envelope spectrum needs to send half of that, since the spectrum is

symmetric, a reduction of 50%. For the envelope spectrum, only 103 points of spectrum data (206 bytes) need to be transmitted, contributing a significant reduction of nearly 95%. In this case, the data output rate is reduced to approximately 8 kbps, which will be a much lighter weight for the Zigbee network and real-time transmission could be achieved.

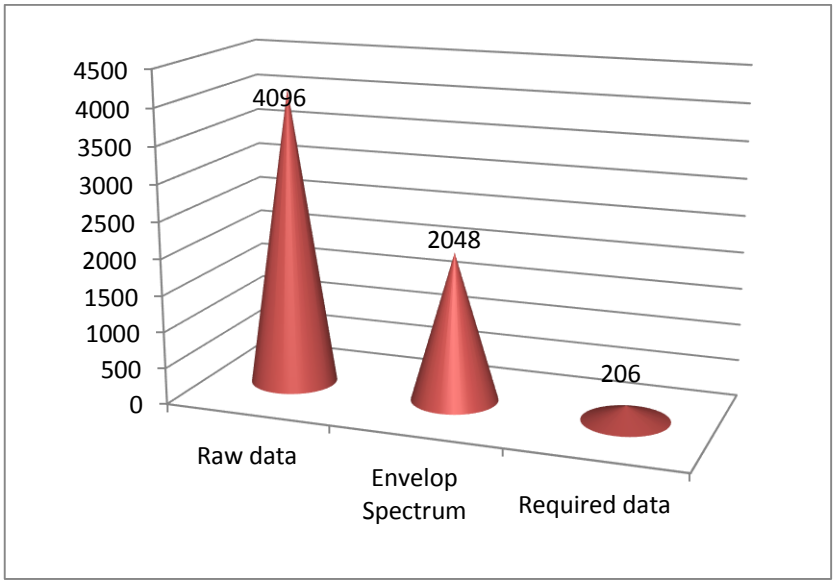

Figure 8.17 Comparison of the data amount

8.5 Summary

In this chapter, an automatic data acquisition process is achieved on a real time operating system, and in this way the CPU is allowed to focus on the intensive signal processing. On this basis, envelope analysis is implemented and the embedded processor is optimized to be able to carry out envelope analysis on a frame length of 2048 points, which is enough to extract the bearing fault features under the sample rate at 10 kHz. Finally, the effective data transmission requirement are analyzed, which shows the data amount for the envelope analysis result is reduced by nearly 95% compared to the raw data set. Therefore, the data throughput of the wireless network can be effectively reduced and such multiple nodes are allowed to coexist in the same network.

Chapter 9
PERFORMANCE ANALYSIS AND AUTOMATIC BAND-PASS FILTER SELECTION

In the previous chapter, the envelope analysis is implemented on the proposed wireless sensor node. In this chapter, the local processing results of the implemented algorithm on the wireless sensor node are firstly verified online under the CCS development environment. Then, the wireless sensor node is further evaluated for detecting two other kinds of common bearing faults. Based on the experiments, a simple and yet effective band-pass filter selection algorithm is developed to automatically determine an optimal band for envelop analysis.

9.1 Local Processing Results Verification

To verify the processing results of the implemented envelope analysis from the wireless sensor node, the wireless sensor node is used to collect a typical bearing vibration signal connected with an outer race fault. Below, the key processing results of the envelope analysis are viewed under the CCS development environment online. The processing results are viewed by setting breakpoints at relevant computation stages and displaying the results via the graph tool. In the test, the sampling rate is set at 10 kHz and 2048 points of data are processed per frame.

The collected raw vibration signal and its spectrum are presented in Figure 9.1 (a) and (b), respectively. The Direct Current (DC) offset is removed from the raw signal in order to highlight the Alternating Current (AC) spectrum. Some spikes show up periodically in the time domain signal, which indicates the existence of a bearing fault. It can be observed that the amplitude around 1500 Hz is relatively higher, which might be one of the resonant frequencies of the bearing house. Therefore, a band-pass filter with the pass-band from 1 kHz to 2 kHz (designed in Section 8.3.1) is applied to filter the raw vibration signal.

The filtered signal and its spectrum are displayed in Figure 9.2(a) and (b). From the figure, it can be seen that the signal has become much smoother and is well limited at the frequency band from 1000 Hz to 2000 Hz. With a careful comparison with the raw signal in Figure 9.1 (a), a small delay explained in Section 7.2.2 can be noticed.

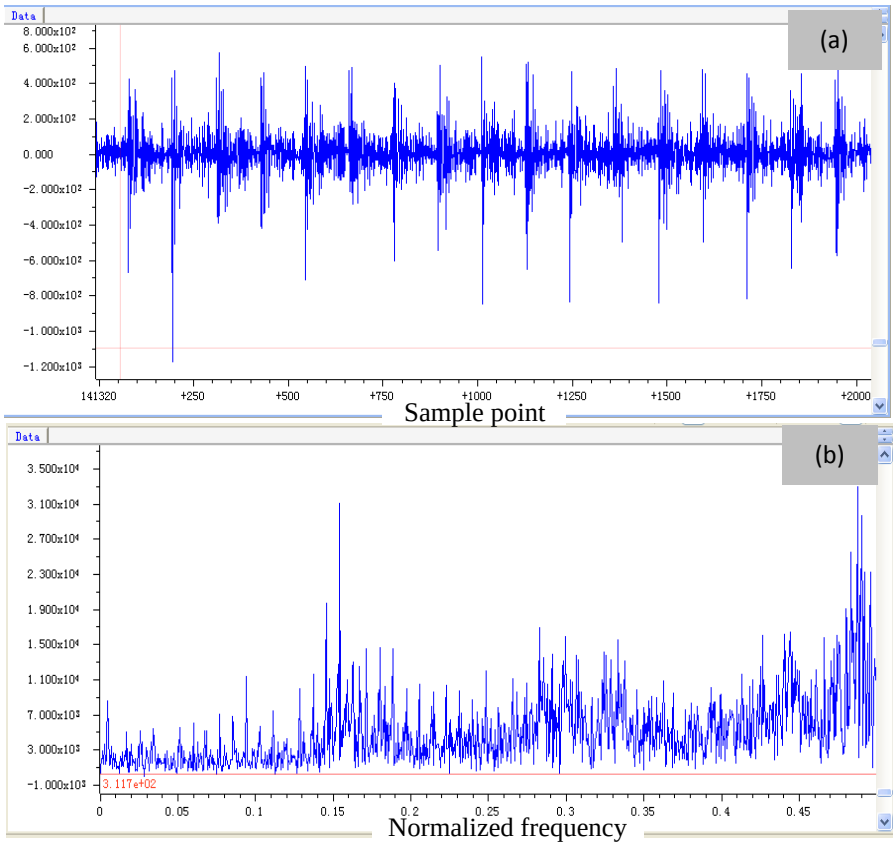

Figure 9.1 Raw signal (a) time domain (b) frequency domain

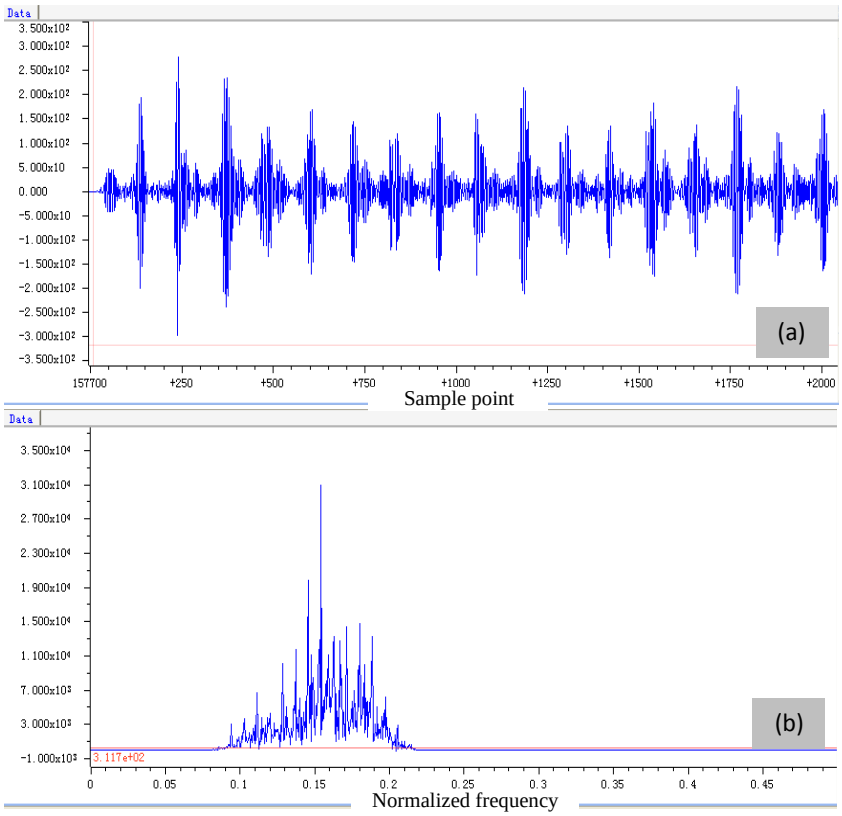

Figure 9.2 Filtered signal (a) time domain (b) frequency domain

The computed envelope is shown in Figure 9.3 (a), which roughly matches the outline of the filtered signal in Figure 9.2 (a). This confirms the correctness of the envelope calculation programs. The calculated spectrum of the envelope signal is illustrated in Figure 9.3 (b), where the frequency resolution is 4.9Hz per bin. As seen in the figure, there are three distinctive spectral peaks at data samples 18, 36 and 54, whose corresponding frequencies are 87.9 Hz, 170.9 Hz and 258.8 Hz, respectively. Compared with Table 5-2, these frequencies agree with the first three harmonics of the characteristic frequency of the outer race fault. Therefore, the spectrum feature indicates the existence of an outer race fault on the roller bearing.

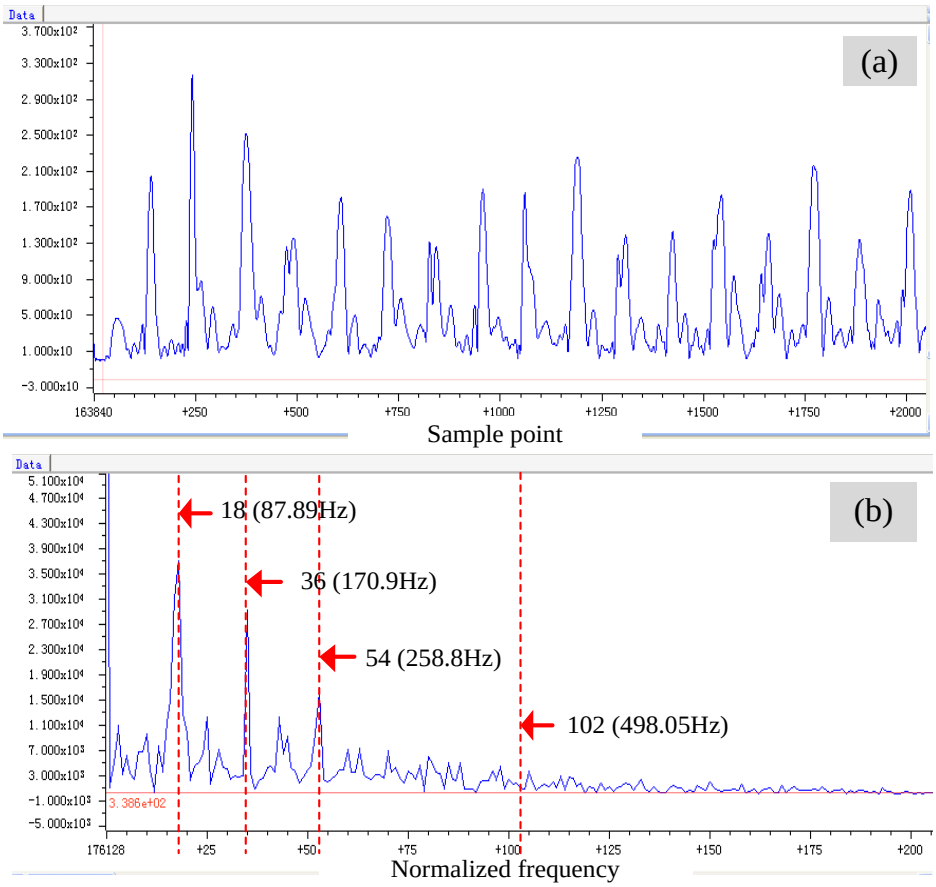

Figure 9.3 Envelope and its spectrum (a) envelope (b) magnified envelope spectrum

The above analysis verifies both the correctness of the implementation program of envelope analysis and its effectiveness for extracting bearing fault features. Figure 9.4 presents the averaged envelope spectrum which is obtained after four averages on the sensor node and transferred to the remote host machine. As it shows, the spectral peaks of interest become more distinctive and the background random components are

effectively suppressed compared with that of Figure 9.3. This has allowed a more reliable diagnostic result to be obtained.

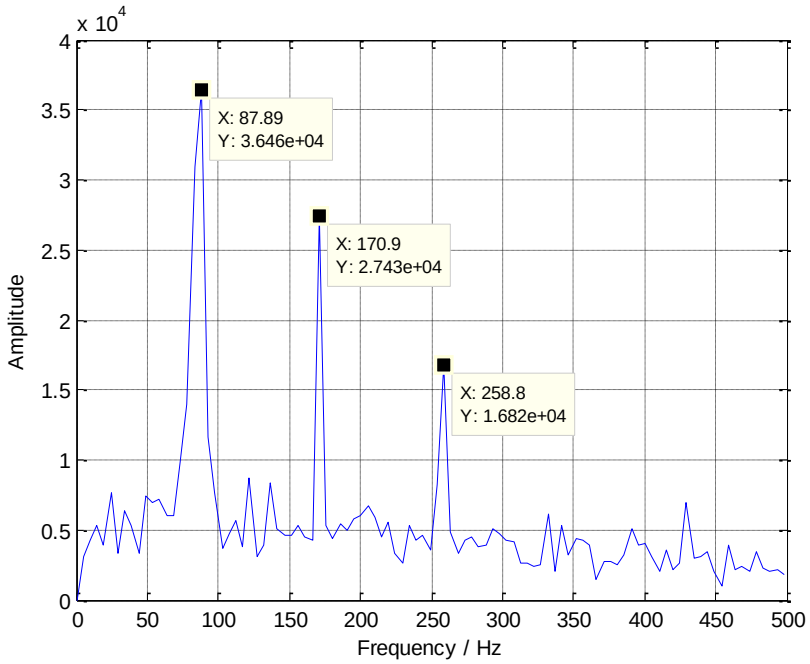

Figure 9.4 Averaged results by four times

9.2 Performance Analysis on Bearing Fault Diagnosis

For ease of evaluation, a graphical user interface (GUI) is developed as shown in Figure 9.5. By using this tool, the running signal processing algorithm and current effective band-pass filter can be controlled directly on the GUI. The data for transmission can be raw data, filtered data, envelope and their spectrums. The processing results can be viewed online and saved for post processing.

The amplitude of the signal is converted to the true acceleration according to the signal sensitivity and calculation methods. By using this tool, data from two types of bearing faults are measured via the proposed wireless condition monitoring system and analyzed in the following subsections.

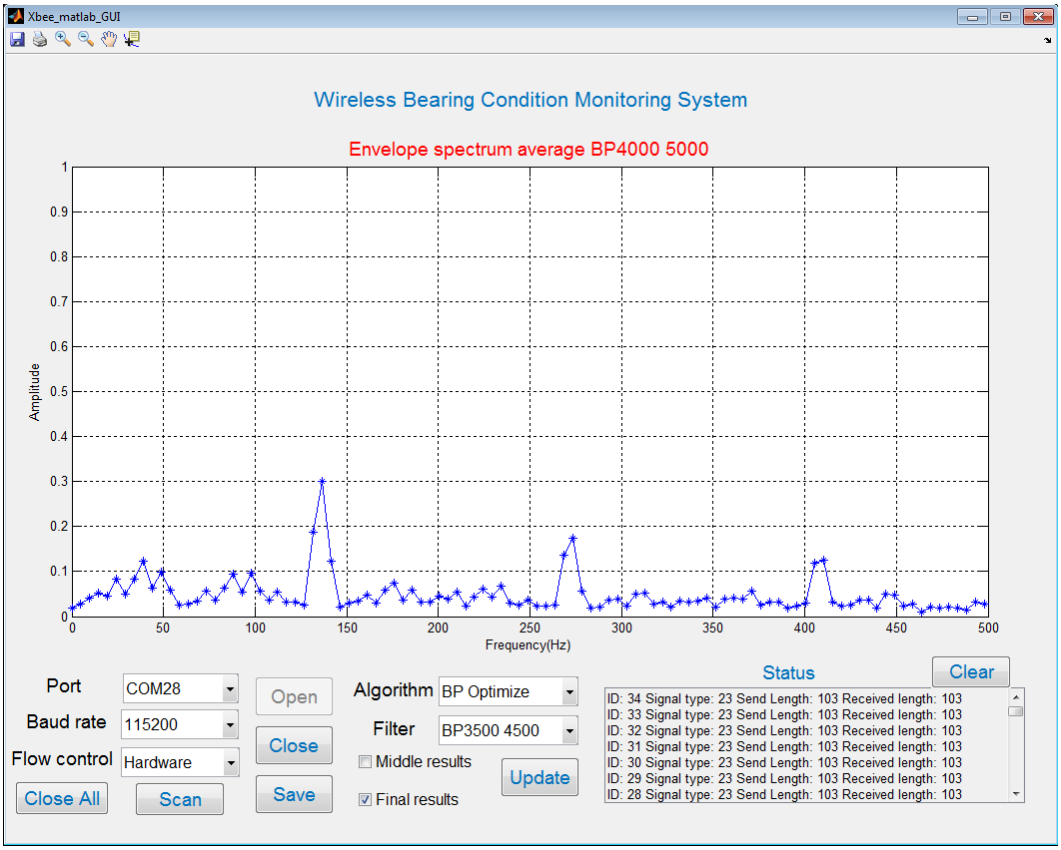

Figure 9.5 GUI for wireless bearing condition monitoring

9.2.1 Roller Fault

The processing results for the bearing with roller fault are presented in Figure 9.6. For evaluation purposes, the raw data and middle processing results are all transmitted. These results are for the same frame of raw signal. It can be observed that the outline of the raw signal, filtered signal and envelope signal are quite similar, which confirms the correctness of the calculation program. . It is noteworthy that the filtered signal and the envelop signal are lagged behind by the raw signal in some samples, which is the effect of the FIR filter.

It can be seen from the spectrum of the raw signal that the band from 4000 Hz to 5000 Hz is higher than the other bands, thus, the raw signal is filtered using a band-pass filter at this pass-band. In the envelope spectrum, the characteristic frequency for the roller can be clearly viewed up to its 4^{th} harmonics. Therefore, the roller fault feature is well contained in the calculated envelope spectrum.

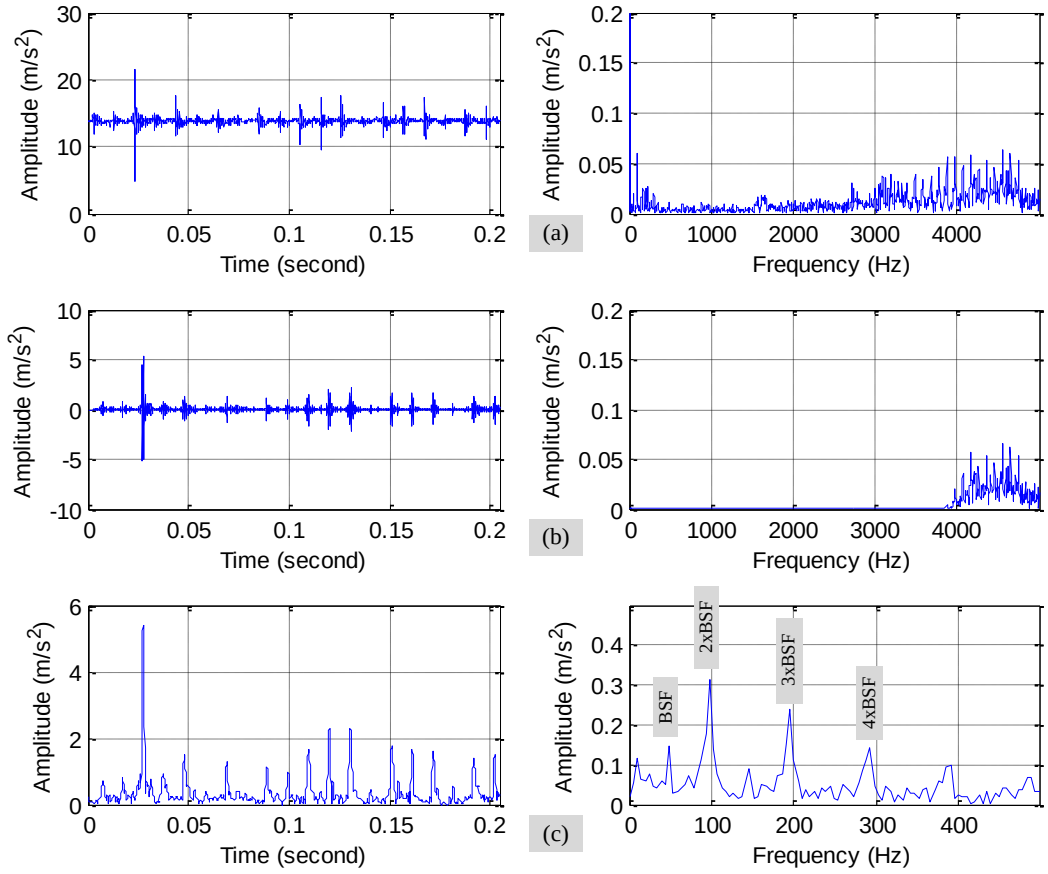

Figure 9.6 Processing results for vibration signal from bearing with roller fault (a) raw signal and its spectrum, (b) filtered signal and its spectrum (c) envelope and its spectrum

9.2.2 Inner Race Fault

Similarly, the processing results for the bearing with the inner race fault are presented in Figure 9.7. From the raw signal, a series of impulses can be observed; however, it is not easy to tell the fault type. From its spectrum, it can be seen the obvious harmonics are more likely to exist on the pass band from 3500 Hz to 4500 Hz. Thus, a band-pass filter for this pass-band is chosen to filter the raw data. As it shows, the impulses become more obvious after filtering.

Finally, from the calculated envelope spectrum, the first three harmonics for inner race fault characteristic frequency can be clearly observed, which confirms the existence of an inner race fault. Obviously, it is much easier to observe the existing faults from the envelope spectrum instead of looking the raw data, spectrum, filtered data or even the envelope meanwhile the dataset of the envelope spectrum is much smaller than the other

kind of datasets. This means the envelope spectrum is much more informative than the other kind of datasets.

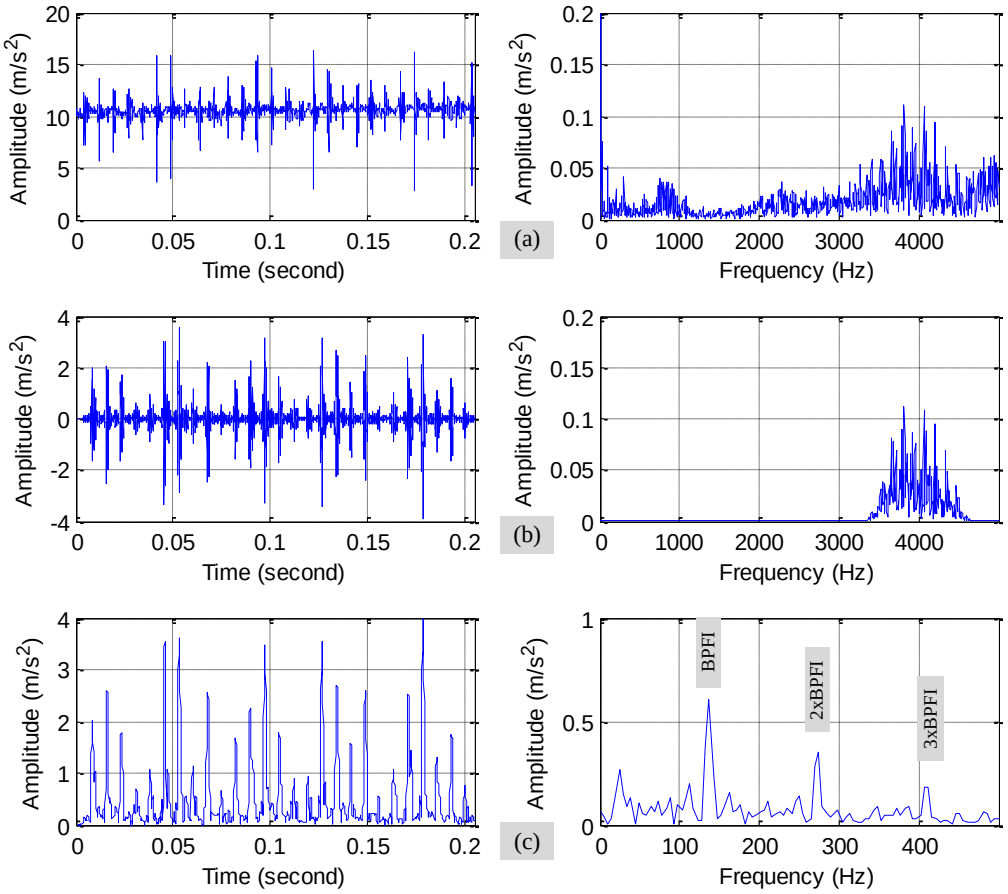

Figure 9.7 Processing results for vibration signal from bearing with inner race fault (a) raw signal and its spectrum, (b) filtered signal and its spectrum (c) envelope and its spectrum

9.3 Amplitude based Band Selection Algorithm

According to the discussion in Chapter 7, the band-pass filter plays an important role in the envelope analysis process. In order to acquire good results, a proper band-pass filter needs to be selected.

As explained in Section 2.5, an extremely short impulse is generated as the bearing rotates over the localized fault, whose energy is distributed across a very wide frequency range. These results in various resonances of the bearing and the surrounding structure being excited. Therefore, the resonances for different bearing systems vary and may change with the bearing system conditions. Traditionally, the optimal resonant frequencies are acquired through impact tests or excitation measurement. During an

impact test, a special hammer is employed to excite the bearing structure. A force sensor is fitted on the hammer for measuring the dynamic force of the excitation and a vibration sensor is mounted on the object bearing structure for obtaining the vibration response of the structure. These two signals are acquired simultaneously, based on which the frequency response function (FRF) of the bearing structure can be calculated. By analyzing the spectrum function, the resonances of the bearing structure can be obtained and thus, a proper band-pass filter can be selected to filter the signals around the resonances.

The disadvantage of the impact test is that it is time consuming and needs to be carried out by experienced engineers. Furthermore, the bearing resonances might change with the running condition, in which case the impact test has to be repeated and a new proper band-pass filter may need to be selected. For this reason, several methods have been developed to automatically select the optimal band-pass filter. For example, the so-called "spectral kurtosis" gives a very similar indication of the band to be demodulated without requiring historical data and a fast version of this algorithm, fast kurtogram, has been available for online condition monitoring implementation [134] [135].

However, it is still quite challenging to implement the complicated fast kurtogram on an embedded processor as it involves complex filtering process and consumes a large amount memory as it actually decomposes the signal into many levels in order to find the most effective one. For this reason, a simple band-pass filtering mechanism has been developed in this thesis, for realizing the automatic band-pass filter selection on the MCU. The implementation processes is depicted below:

Step 1, compute spectra for successive 8 frames to obtain an average spectrum. In this way, the random noises are suppressed to a certain degree and the true signals are enhanced as discussed in Section 7.4.3;

Step 2, calculate the mean of the spectrum in a wide frequency range from 1000 Hz to 5000 Hz, where the bearing impulse responses more significant. Then take the mean value as a threshold for selecting a narrower band;

Step 3, calculate the sum of the amplitude higher the threshold in each sub-band, shown listed in Table 9-1 and store their summation values in an array. Note that the band-pass filters have an overlapped bandwidth of 500 Hz;

Table 9-1 Band-pass filter-for comparison

Index	0	1	2	3	4	5	6
Pass-band (Hz)	1k-2k	1.5k-2.5k	2k-3k	2.5k-3.5k	3k-4k	3.5k-4.5k	4k-5k

Step 4, divide the summation value in the array by the total sample points in each sub-band and the result are then taken as the characteristic value for determining the optimal pass-band;

Step 5, find the maximum characteristic value among the characteristic value sequence and its corresponding pass-band is then considered as the effective one and a band-pass filter with this pass-band will be employed to filter the signal.

A group of band-pass (or high-pass) filters are designed according to the sub-band parameters listed in Table 9-1 and their frequency responses are shown in Figure 9.8. As it shows, the corresponding band-pass filter has a flat amplitude response and linear phase response for the desired pass-band.

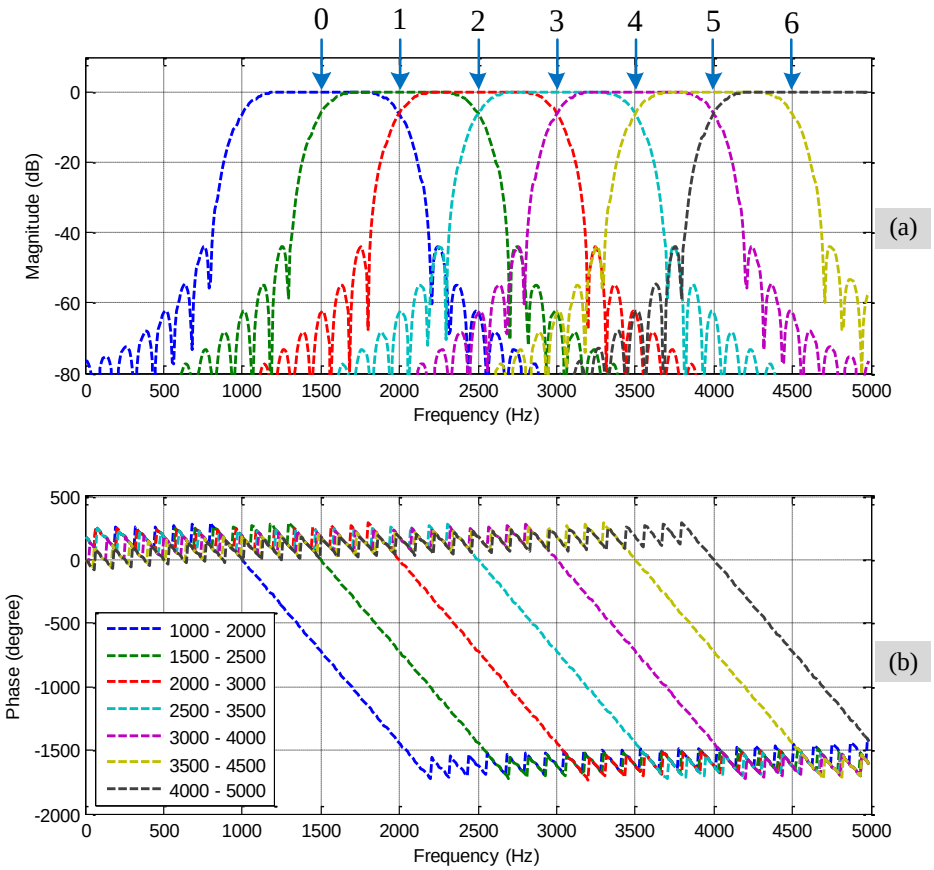

Figure 9.8 Frequency response of the band-pass filters (a) amplitude response (b) phase response

As shown in the selection process, the computation involves only basic arithmetic operations. These can be efficiently implemented by the MCU, compared with implementing more complicated algorithms such as the fast kurtogram and possible hardware based filter banks.

9.4 Performance Evaluation

Figure 9.9 presents an optimised result for the inner race fault signal. The computations are implemented on the wireless sensor node and the results are transmitted to the host side for verification. It shows the characteristic value for the optima band between 3500Hz and 4500 Hz is the largest one, which is in accordance with the selection in Section 9.2.2.

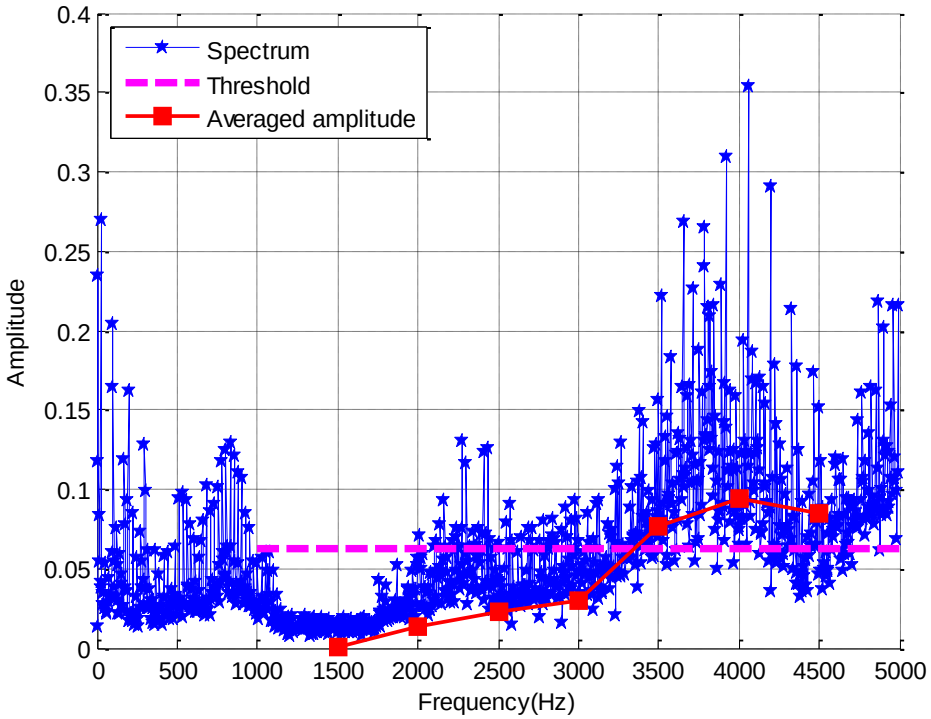

Figure 9.9 Band-pass filter optimization result for bearing with inner race fault

For verification, the band-pass filters for two bands: 3500-4500Hz and 4000-5000Hz are employed to process the same vibration signal and the computed envelope spectra are presented in Figure 9.10. It can be seen that the amplitude at the first harmonic obtained by using the 3500-4500Hz pass-band is higher than that of using 4000-5000Hz one. This verifies the effectiveness of the band-pass optimization process.

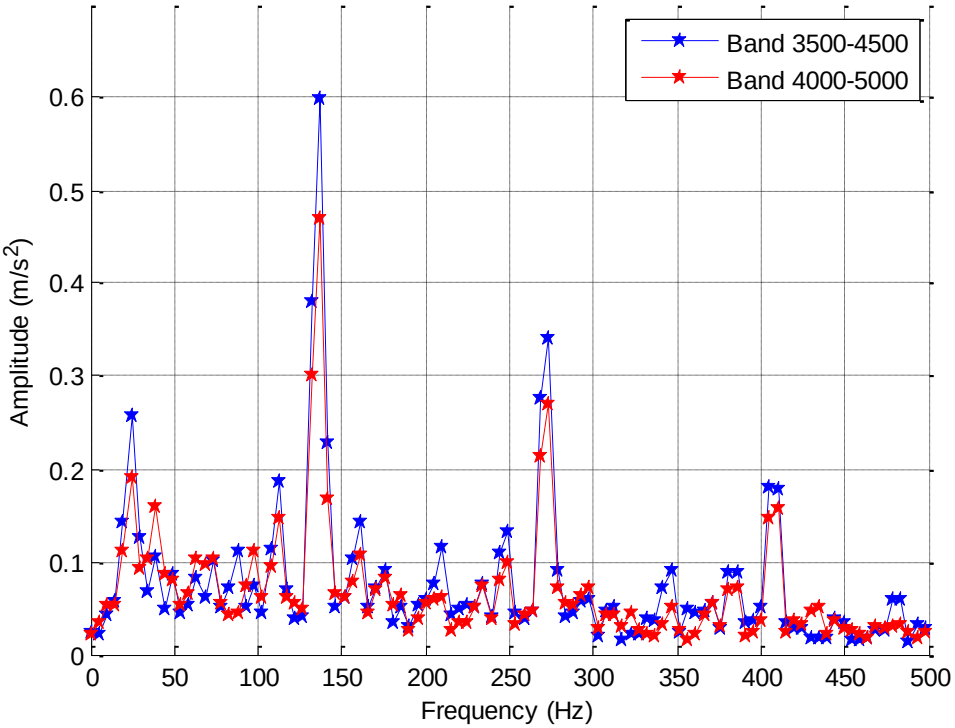

Figure 9.10 Envelope spectrum result comparison for the bearing with inner race fault

Similarly, the optimization is employed to process the vibration signal from the bearing with the roller fault. As shown in Figure 9.11, the pass-band of 4000-5000Hz is selected. This is consistent with the visual observations that frequency band of 4000-5000Hz is relatively more impulsive than other bands. The envelope spectrum employing the pass-band 3500-4500Hz and 4000-5000Hz are shown in Figure 9.12. As it shows, the highest frequency component for the 4000-5000Hz band-pass filter is larger than that for the 3500-4500Hz band-pass filter.

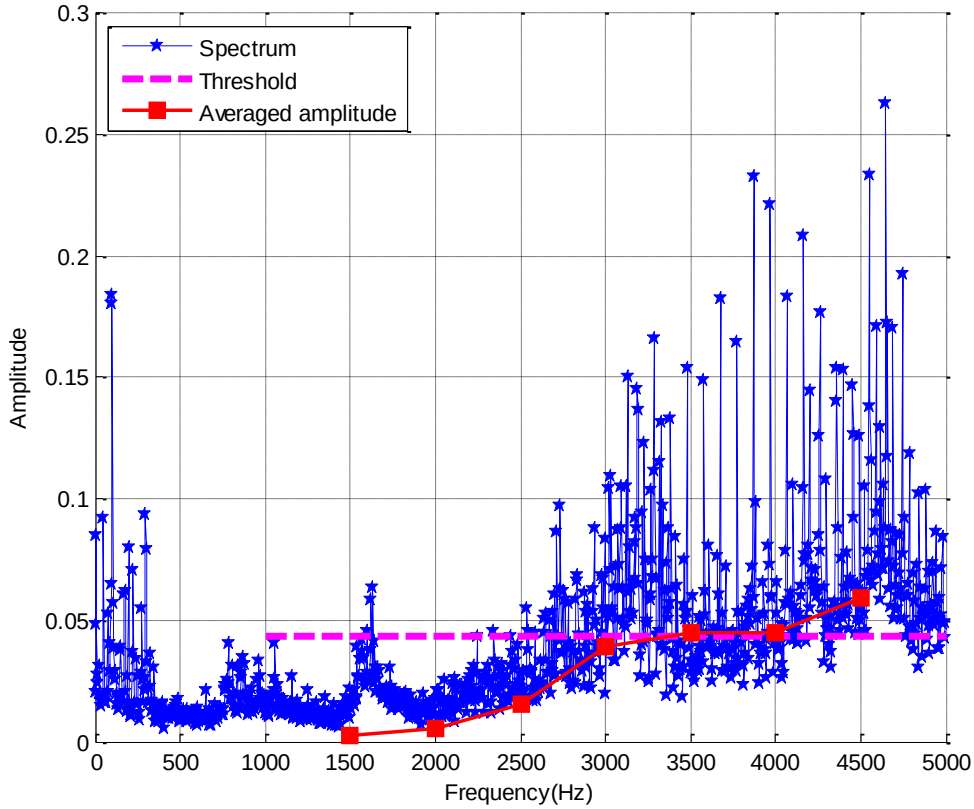

Figure 9.11 Band-pass filter optimization result for bearing with roller fault

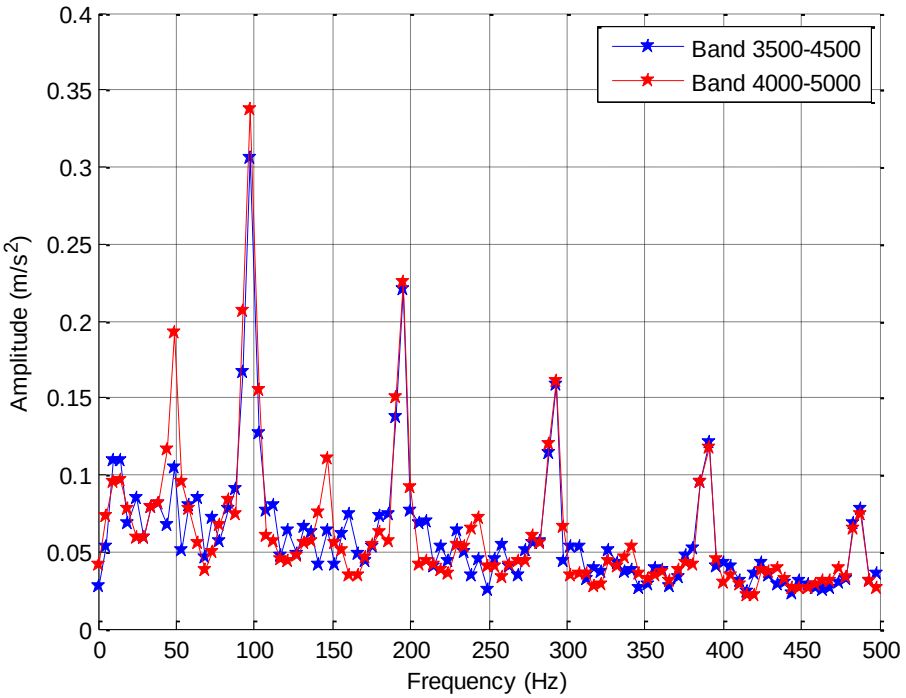

Figure 9.12 Envelope spectrum results comparison for the bearing with roller fault

To further evaluate the performance of the automatic band-pass filter selection algorithm, a bearing with both outer race and inner race fault is employed for testing. The optimization result for the combined fault is presented in Figure 9.13. It can be seen that the outline of the spectrum is slightly different from that in Figure 9.9 and Figure 9.11. According to the selection result, the band from 4000 Hz to 5000 Hz is an optimal one.

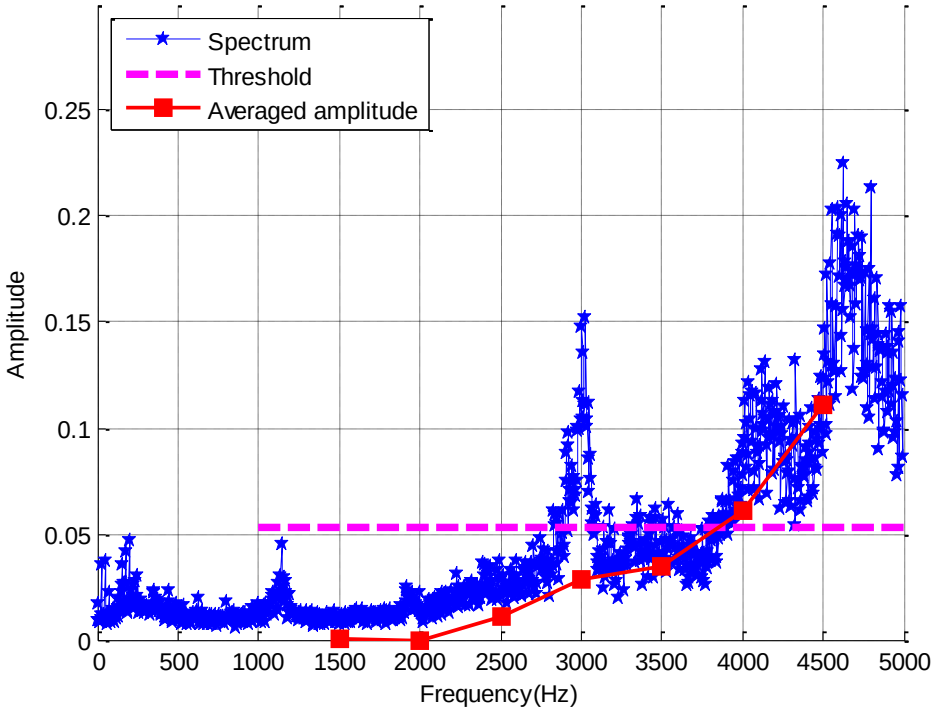

Figure 9.13 Band-pass filter optimization result for bearing with both outer race fault and inner race fault

To verify the effectiveness of the chosen band-pass filter, the same vibration signal is processed using the band-pass filter of 3500-4500Hz and 4000-5000Hz and the calculated envelope spectrum are given in Figure 9.14. It can be seen that the harmonics for the outer race fault (around 84 Hz) and inner race fault (around 137 Hz) both appear in the two spectra. Furthermore, the harmonics in the 4000-5000Hz result are relatively higher than those in the 3500-4500Hz one. This proves the proposed band-pass optimization process also works for the combined fault case.

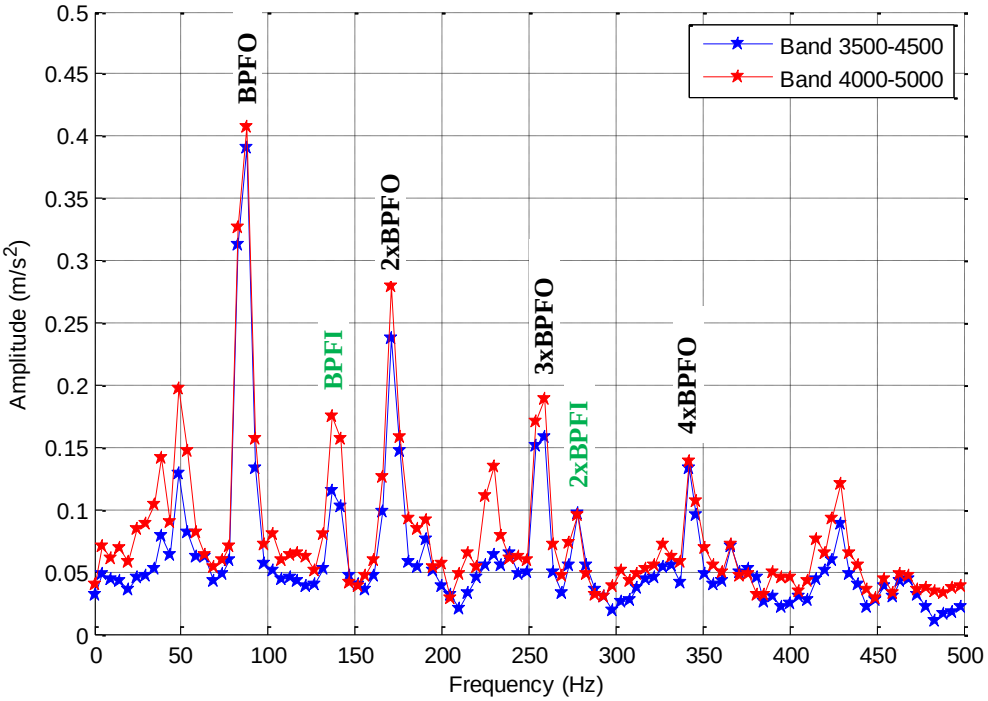

Figure 9.14 Envelope spectrum results comparison for the bearing with both outer fault and inner race fault

9.5 Summary

In this chapter, the signal processing programs are firstly validated online by viewing the processing results directly on the processor memory in the debugging environment. It shows that the embedded program can calculate the envelope spectrum correctly and the simulated outer race fault feature is successfully identified from the calculated envelope spectrum. Then, a GUI is developed to help more efficiently view the processing results. On this basis, two other common bearing faults, roller fault and inner race fault, are examined and it is proved that the simulated fault can also be successfully detected from the resultant small dataset containing envelope spectrum. In addition, a simple but effective band-pass selection algorithm is developed and embedded on the wireless sensor node to automatically select the effective band-pass filter; in this way the envelope analysis results can be more effective.

Chapter 10
CONCLUSIONS AND FUTURE WORK

This chapter summarizes the achievements of this research and draws conclusions based on the results obtained from the entire research project. It then presents a summary of the novel contributions of the research conducted by the author. Finally, suggestions are given for the future work which could advance the explorations presented in this thesis.

10.1 Summary

This research focused on the exploration of employing the cost effective wireless sensor network to conduct condition monitoring for rolling element bearings. It is expected to significantly reduce the cost on maintenance for industrial machines. Vibration was chosen as the measurement parameter because it has long been proved sensitive and effective for various types of machinery faults. As an important component in the rotating machines, bearing has been widely used in the industrial area and also accounts for a high percentage of machinery faults. For this reason, bearing has been selected as the study target in this thesis.

According to the investigation on the current popular wireless protocols, Zigbee is a good candidate for industrial condition monitoring because of its inherent features like low power consumption, low cost and its capability to contain tens or even hundreds of sensor nodes. This is just suitable for the data measurement in a factory, where a lot of machine signals needs to be measured.

A comparison made between wired and wireless measurement system has found that the Zigbee based wireless measurement system is deficient in streaming long continuous data of raw vibration signals due to limited bandwidth. Moreover, it can have problems with data loss due to inevitable ambient interference. Therefore, a new wireless sensor node is designed, which embed signal processing algorithms and transfer the processed results of much smaller data size. Thereby the conflict between large data set and restricted bandwidth can be reduced significantly. A state-of-the-art Cortex-M4F processor is employed as the core processor on the wireless sensor node to achieve advanced signal processing.

The implementation detail and considerations of envelope analysis are discussed in detail in Chapter Seven and Chapter Eight and several optimizations have been employed to achieve high performance.

From the experimental results, it can be seen that the simulated bearing faults can be successfully diagnosed from the resultant small data set that contains the envelope spectrum and the data throughput requirement is reduced by nearly 95% compared with the raw data transmission. Finally, a simple but effective band-pass filter selection

algorithm is developed and implemented on the wireless sensor to achieve automatic band-pass filter selection.

10.2 Review of Research Objective and Achievements

This research is motivated by both the potential benefits and great challenges of implementing wireless sensor network for low cost remote condition monitoring. The main achievements of this work have been presented below in the same order they appear in Section 1.5.

Objective one: Investigate the popular condition monitoring techniques and select an effective one to monitor the health status of the bearing.

Achievement one: In Chapter one, a number of effective techniques for machinery condition monitoring are reviewed and it is found that vibration has been the most widely employed one in the industry because both of its high sensitivity to the machinery faults, which can find the machinery fault in an early stage, and its nonintrusive characteristic, which allows the online condition monitoring while the machine is running.

Objective two: Investigate the fundamentals of rolling bearings, including bearing types, components and common failures, and explore the fault generation mechanisms.

Achievement two: According to the investigation in Chapter two, bearing fault accounts for a high percentage of electrical machine failures and is concerned mostly by industries. Then, the common bearing types, components, failure types and fault generation mechanism of the localized faults are studied. On this basis, it is found the localized faults are usually detected and diagnosed by their unique characteristic frequencies.

Objective three: Review the popular signal processing algorithms and select effective signal processing algorithms for bearing fault feature extraction and diagnosis.

Achievement three: In Chapter three, the popular signal processing algorithms in the time domain, frequency domain and time-frequency domain are reviewed. It is found that these signal processing techniques have their unique advantages in extracting some specific features and the envelope analysis is able to find the localized bearing faults at

an early stage and thus has been widely employed in different the industrial areas and continuously improved by many researchers.

Objective four: Study current popular wireless protocols, their development trends and any existing applications for condition monitoring and choose a wireless protocol for the different industrial environments.

Achievement four: From the investigation in Chapter 4, it is found the different wireless communication protocols have been developed according to the unique application requirement. For condition monitoring, the IEEE802.15.4 is proved to be more suitable because of its inherent features like the ability to establish large network, low cost, low power, and low latency and so on. Moreover, several more advanced protocols like ISA100.11a and WirelessHART based on IEEE802.15.4 have been developed to satisfy the special industrial applications requirements.

Objective five: Make a comparison test between a wired and wireless condition monitoring system and evaluate the performance of the wireless measurement system.

Achievement five: A wireless measurement system based on Zigbee and a traditional wired online data acquisition system are employed to collect the vibration signal from a bearing test rig with simulated outer race fault. From the analysis results, it can be seen that the simulated bearing fault can be detected and diagnosed by utilizing envelope analysis algorithm to analyse both signals. However, it is also found that the wireless data transmission is not reliable due to both the noisy factory environment and the bandwidth limitation of the Zigbee network. Moreover, because of the large dataset of the vibration signal, it is difficult to establish a reliable network containing multiple sensor nodes.

Objective six: On-board local data processing is an effective way to reduce the data throughput of the wireless network and thus solve the bandwidth limitations of the Zigbee network. In order to implement customizable signal processing algorithms, the wireless sensor node is redesigned.

Achievement six: In Chapter six, a prototype wireless sensor node with good signal processing capability is designed to collect and process the vibration signal on the node

itself. A state-of-the-art Cortex-M4F processor is employed as the core processor to achieve the relative complicated signal processing algorithms and a wireless module with embedded Zigbee stack is chosen to establish the wireless network.

Objective seven: Study the implementation procedure of envelope analysis algorithm and the considerations on realizing it on an embedded processor with limited memory and computing capability.

Achievement seven: In Chapter seven, the three main procedures of envelope analysis are studied in detail. On this basis, the FIR filter is employed to implement the band-pass filter because its capability to produce linear phase response and the Hilbert transform is chosen to detect the envelope due to its preciseness. In addition, several techniques that might improve the performance are also discussed, such as using the real-valued FFT algorithm to achieve faster computation speed, using a proper window function to reduce the DFT leakage and utilizing the frequency domain averaging to reduce the random noise and thus improve the signal to noise ratio.

Objective eight: Implement and optimize the envelope analysis on the designed wireless sensor node.

Achievement eight: In chapter eight, an automatic data acquisition process is achieved on the designed wireless sensor node running a real time operating system, in which way the CPU is allowed to focus on the intensive signal processing. On this basis, envelope analysis is implemented and the embedded processor is optimized to carry out envelope analysis on a frame length of 2048 points, which is enough to extract the bearing fault features under the sample rate at 10 kHz. With the on-board envelope analysis, it shows the effective data transmission requirement is reduced by nearly 95% compared to the raw data set. Thereafter, multiple such nodes are allowed to coexist in the same network.

Objective nine: Evaluate the wireless sensor node with embedded envelope analysis and examine its performance for bearing fault diagnosis.

Achievement nine: In chapter nine, the signal processing programs are firstly examined online by viewing the processing results directly on the processor memory in the

debugging environment. Then, a GUI is developed to help more efficiently view the processing results. On this basis, two other common bearing faults are examined and it is proved that the simulated fault can be successfully detected from the small dataset of envelope spectrum. Furthermore, a simple but effective band-pass selection algorithm is embedded on the wireless sensor node to automatically select the effective band-pass filter, in which way; the envelope analysis results can be more effective.

10.3 Contributions to Knowledge

The novel aspects of the research can be summarised as follows:

First contribution: The IEEE802.15.4 is proved to be more suitable for vibration based condition monitoring applications because of its inherent features like the ability to establish large network, low cost, low power, and low latency and so on. It also shows that two IEEE802.15.4 based protocols: ISA100.11a and WirelessHART under development are more potential for the special industrial application requirements.

Second contribution: It has found that the Zigbee based wireless measurement system can be employed to transfer raw vibration signal for bearing condition monitoring. However, due to both noisy factory environment and bandwidth limitation, it is difficult to maintain the reliability and efficiency for data transfer, and thereby to allow multiple such sensor nodes to coexist in the same network.

Third contribution: A new wireless sensor node is designed to entitle the capability of implementing customizable signal processing algorithms and thus reduce the data amount though the wireless sensor network. A state-of-art Cortex-M4F processor is validated to be an efficient core processor as it allows a number of common signal processing algorithms to be embedded and uses low power consumption. Not just for this thesis, it can also be employed for developing other kinds of advanced signal processing algorithms such as cepstrum, bispectrum and so on for more comprehensive advanced applications.

Forth contribution: An automatic data acquisition process that combines Timer, ADC and DMA is developed on the designed wireless sensor node running a real time operating system. Its performance and reliability is validated with the help of the execution graph of the real time operating system.

Fifth contribution: The computation speed of FFT and Hilbert transform utilizing the CMSIS DSP library is compared for various frame sizes. This has provided a consult for related signal processing algorithm development based on Cortex-M4F processor. On this basis, the implementation of envelope analysis on an embedded processor is optimized and a 2048-point envelope analysis calculation in the single precision floating point format is achieved on a processor with just 32 kB memory.

Sixth contribution: With the experimental test, the envelope analysis is proved to be an effective and efficient processing algorithm for wireless sensor nodes in characterising periodic impulsive signals for bearing fault diagnosis. It can effectively reduce the data throughput by nearly 95% with the signal sample rate at 10 kHz. Therefore, multiple such sensor nodes are allowed to coexist in the same low data band-with wireless network for plant monitoring.

Seventh contribution: An amplitude based optimal band selection algorithm is developed, which choose one of concessive sub-bands as the optimal one if it has the highest amplitude, and thus needs small amount of arithmetic operations and can be embedded on the wireless sensor node to yield desired performance of bearing fault detection and diagnosis.

10.4 Recommended Future Work

Although the proposed system can be employed successfully for diagnosing bearing faults, there is still some limitations for the proposed system, such as only limited features have been extracted for fault detection, the power management is still not optimized for long-time battery operation. Based on studies and progress made in this PhD programme, a number of key recommendations are suggested for future works in this area with a view to improving the application:

First suggestion: New features can be extracted out to detect and classify other rolling bearing defects such as misalignment, unbalance, looseness, and lack of lubrication, etc.

Second suggestion: Other advanced signal processing techniques such as wavelet, cepstrum can be implemented on the sensor nodes for the condition monitoring and fault diagnosis of other kinds of machines.

Third suggestion: The emerging energy harvesting techniques can be employed to provide power supply to the wireless sensor node, in which way the sensor node can be even battery-less and further reduce the human interposes on the maintenance.

Fourth suggestion: Multiple sensor nodes can be added to the same network for monitoring the status of various machines.

Appendix A CODE COMPOSER STUDIO

Code Composer Studio (CCS) is Texas Instruments' integrated development environment (IDE) for developing routines on a wide variety of their DSPs. Code Composer Studio is TI's Eclipse based Integrated Development Environment (IDE). You might also think of IDE as meaning, "Integrated Debugger and Editor. You can select the target DSP, adjust the optimization parameters, and set the user preferences as you desire. An application is developed based on the concept of a project, where the information in the project determines what source code is used and how it will be processed.

A.1 Running an Application in CCS

To start build the project, select Project from the main menu and click Build Project. CCS will now compile and link the project files to produce an executable file. If all is well, the console window will show "Build Finished". Note that CCS has many menu buttons that have the same function as the menu commands as shown in Figure A.10.1.

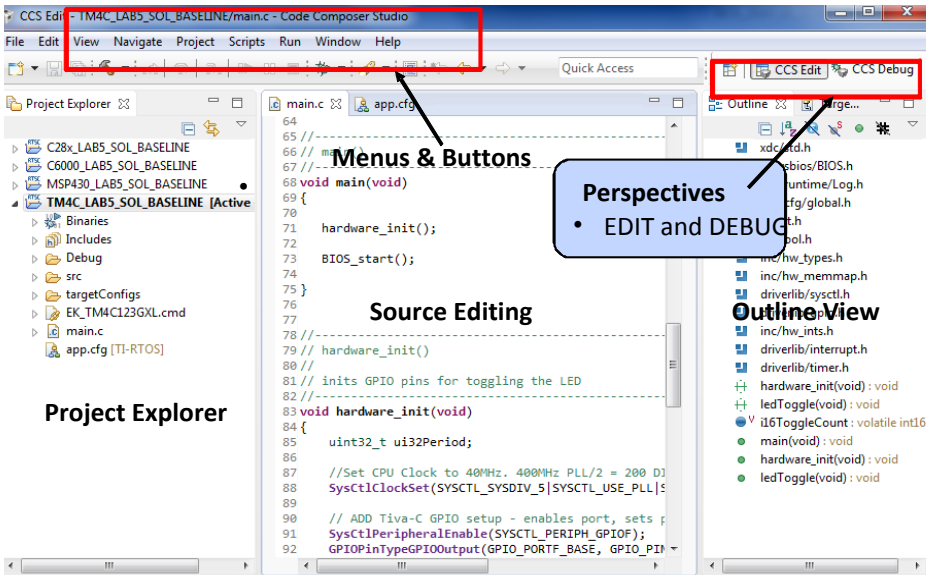

Figure A.10.1 CCSv6 GUI – EDIT Perspective

A.2 Debugging an Application in CCS

Here, by clicking on the Debug icon. It will load the program and switches you to the "Debug" perspective. Choosing the breakpoints you can follow the code.

There are several various tools provided with XDCtools and SYS/BIOS to debug the application. Figure A.10.2 .shows more detailed of CCSv6 GUI – DEBUG Perspective. To terminate the debug session, select Run from the main menu and click Terminate. You may modify and rebuild your code even while the hardware is running. You must rebuild and reload a program after any changes are made in the code if you wish to see the results of these changes.

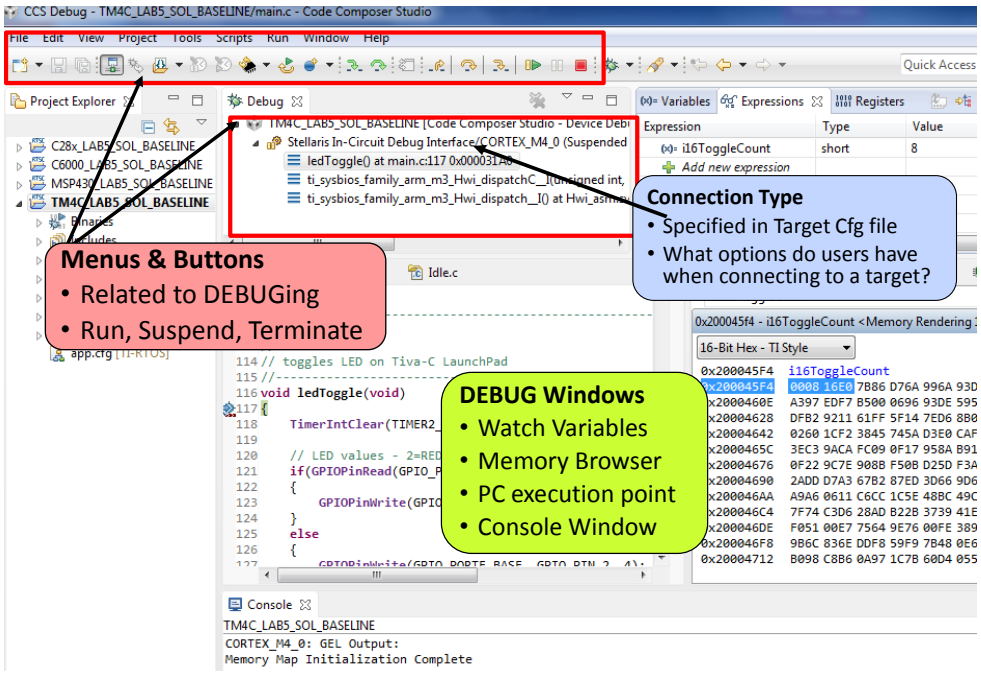

Figure A.10.2 CCSv6 GUI – DEBUG perspective

A.3 Measure Execution Time

The code composer studio provides a tool to measure the time consumed by a piece of code. This is achieved by using the breakpoint to act as a CPU counter, which can count the CPU cycles consumed between two break points.

The watchpoint can be further customized, if needed, by right-clicking on the watchpoint and selecting Properties. The code composer studio provides a tool to measure the time consumed by a piece of code. This is achieved by using the breakpoint to act as a CPU counter, which can count the CPU cycles consumed between two break points.

Count Event can be used to measure clock cycles between two points in the code. Since these are all implemented internally by the hardware and require on-chip analysis resources, there is usually a limit to the maximum number of events that can be enabled at one time.

By enter right-click on count event view, and select Properties and check the box marked Reset Count on Run. This will make the Event counter reset every time the processor is put to run, therefore allowing counting events within breakpoint boundaries. FigureA.10.3 show three breakpoints to count the number of cycles between two places in your code enable the count event, it shows three values for each breakpoint which is as following 1st run = 55342, 2nd run =12292 and 3rd run = 24580.

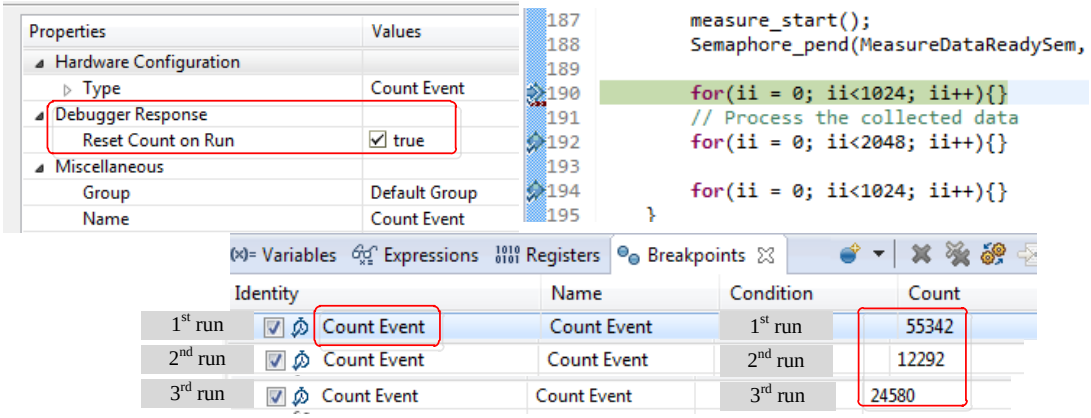

FigureA.10.3 Measure the count event

A.4 View a signal and its spectrum

FigureA.10.4 (a) plot the data in the display buffer on a magnitude versus time graph. It provides a quick view of the processing results during debugging stage. In addition the FFT can be applied on a frame of data and display the spectrum immediately in the debug stage as shown in FigureA.10.4 (b). The data for analysis can be either real or complex type.

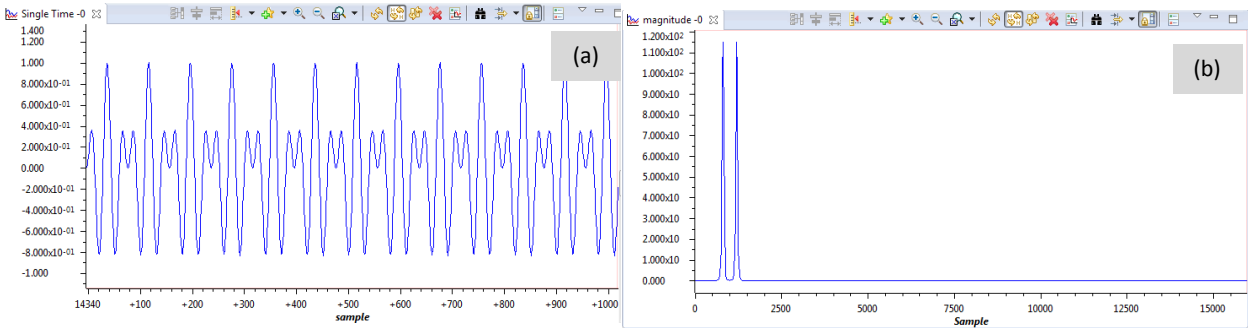

FigureA.10.4 sing tools in CCS (a) time domain graph (b) FFT magnitude graph

Appendix B TI-RTOS

This appendix begins with a general introduction about real-time operating system for TI microcontrollers. It combines a real-time multitasking kernel with additional middleware components. SYS/BIOS provide pre-emptive multitasking, communication and synchronization primitives, and memory management. Here the thread types Hwi, Swi, Task a, Idle are explained.

B.1 Introduction of SYS/BIOS

SYS/BIOS are a inaccessible real-time kernel. It is developed for uses that require real-time scheduling and synchronization or real-time instrumentation. SYS/BIOS provide pre-emptive multithreading, hardware abstraction, real-time analysis, and configuration tools. SYS/BIOS can help to minimize memory and CPU requirements on the target.

TI-RTOS is a scalable, one-stop embedded tools ecosystem for TI devices. It scales from a real-time multitasking kernel (SYS/BIOS) to a complete RTOS solution including additional middleware components and device drivers. By providing essential system software components that are pre-tested and pre-integrated, TI-RTOS enables you to focus on differentiating your application. The thread types Hwi, Swi, Task and Idle are explained briefly below.

The Hwi priority only applies to the order in which multiple interrupts that are ready on a given CPU cycle are serviced by the CPU. Hardware interrupts are pre-empted by another interrupt unless interrupts are globally disabled or when specific interrupts are individually disabled. Hwi threads are used to perform time critical tasks that are subject to hard deadlines.

A Swi function in progress can be preempted at any time by a Hwi; the Hwi completes before the Swi function resumes. The Clock module automatically creates a Swi for its use and run the Clock functions within that Swi. The priority of the Swi used by Clock can be changed by configuring Clock.swiPriority. To handle Swi functions, the Swi manager uses Swi objects. If a Swi is posted, it runs only after all pending Hwis have run.

SYS/BIOS task objects are threads that are managed by the Task module. Tasks have higher priority than the Idle Loop and lower priority than hardware and software interrupts. The Task module provides a set of functions that manipulate task objects.

Idle threads execute at the lowest priority in a SYS/BIOS. Idle threads run sequentially at the same priority. Idle threads may use to reduce power needs when other processing is not being performed.

B.2Time-Stamp Module

Timestamp module, as the name suggests, provides time stamping services. The Timestamp module can be used for benchmarking code and adding timestamps to logs. Calls to the Timestamp module function are forwarded to a platform-specific Timestamp Provider implementation.

The information that is displayed is the Live Session View contains every BIOS event in the system along with a time stamp. Time column on the left in Figure B.1 shows the time stamp in NANOSECONDS.

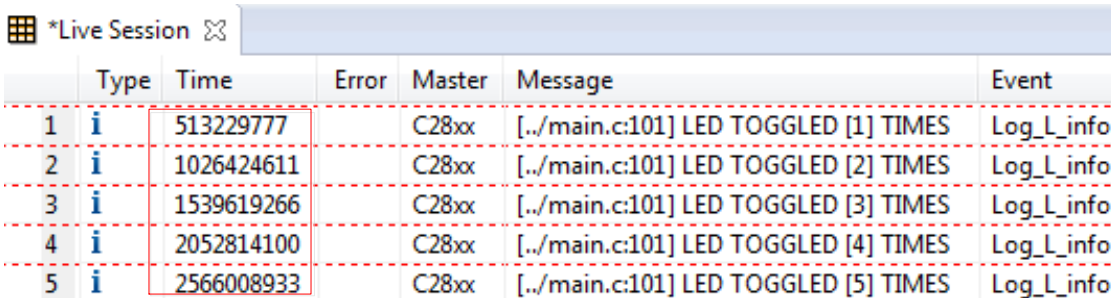
*Live Session

	Type	Time	Error	Master	Message	Event
1	i	513229777		C28xx	[../main.c:101] LED TOGGLED [1] TIMES	Log_L_info
2	i	1026424611		C28xx	[../main.c:101] LED TOGGLED [2] TIMES	Log_L_info
3	i	1539619266		C28xx	[../main.c:101] LED TOGGLED [3] TIMES	Log_L_info
4	i	2052814100		C28xx	[../main.c:101] LED TOGGLED [4] TIMES	Log_L_info
5	i	2566008933		C28xx	[../main.c:101] LED TOGGLED [5] TIMES	Log_L_info

Figure B.1 Time stamp in Nano second

You would need to DIVIDE this number by the number of nanoseconds in one CPU clock cycle to get the cycle number. The previous tools in the older DSP/BIOS RTOS did not provide time stamps.

B.3Execution Graph

RTOS Analyser use to perform execution sequence analysis on SYS/BIOS applications. The execution sequence and start/stop benchmarking events are shown in the Execution Graph. The Execution Graph, Concurrency, CPU Load, Task Load, and Printf Logs features display information automatically provided by SYS/BIOS. The Task Profiler, Duration, Context Aware Profile, and Count Analysis features display data only if you

have modified target code to instrument the required events. Figure B.2 shows the configuration of the execution analysis.

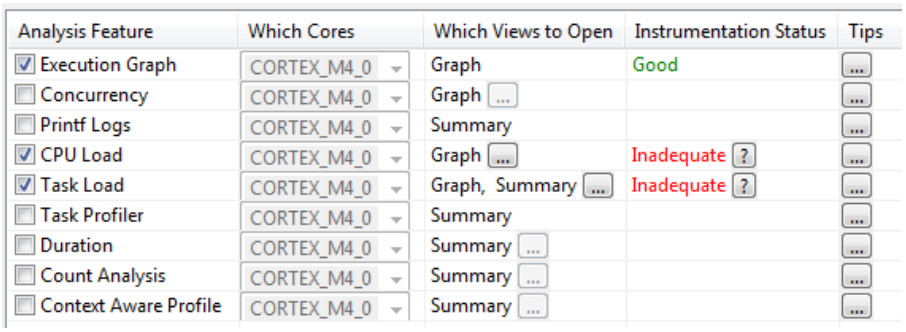

Figure B.2 configuration of the execution analysis

By selecting the execution graph .it will display the events in your system via a graph. The SCOPE of what you are looking at varies depending on the frequency of the events. You can zoom in or zoom out and take measurements on the graph for profiling when events occur.

To magnify the graph by using zoom out to match approximately the execution graph in Figure B.3. It shows the Post, Start and Stop of the ADC conversion. Also you can see the ledToggle routine running and the Scheduler run between the Post and Start of the Clock Swi. And, of course, Idle is the dominant thread running here.

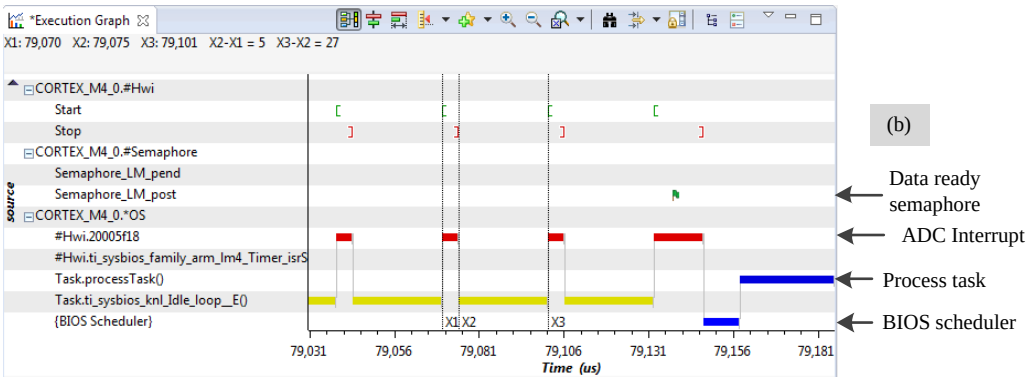

Figure B.3 Execution graph

There is a measurement marker that you can use to benchmark how long this routine took on your target. You will lay down TWO markers and the tool will take a measurement between them as shown in **Error! Reference source not found.** . By Selecting the measurement marker (X1 and X2) on the left and right respectively, then you'll see in the top left-hand corner a benchmark X1= 79.070 and X2 = 79.75 the difference will be X2-X1=5. The execution time for

REFERENCES

[1] L. Jiang, X. Fu, J. Cui, and Z. Li, "Fault detection of rolling element bearing based on principal component analysis," in *Control and Decision Conference (CCDC), 2012 24th Chinese*, 2012, pp. 2944–2948.

[2] J. M. Rybak, "Remote condition monitoring using open-system wireless technologies," *Sound Vib.*, vol. 40, no. 2, p. 16, 2006.

[3] L. Hou and N. W. Bergmann, "Novel Industrial Wireless Sensor Networks for Machine Condition Monitoring and Fault Diagnosis," *IEEE Trans. Instrum. Meas.*, vol. 61, no. 10, pp. 2787–2798, Oct. 2012.

[4] A. Kelly, *Maintenance Strategy*. Elsevier, 1997.

[5] G. Dalpiaz and A. Rivola, "CONDITION MONITORING AND DIAGNOSTICS IN AUTOMATIC MACHINES: COMPARISON OF VIBRATION ANALYSIS TECHNIQUES," *Mech. Syst. Signal Process.*, vol. 11, no. 1, pp. 53–73, Jan. 1997.

[6] R. S. Beebe, *Predictive Maintenance of Pumps Using Condition Monitoring*. Elsevier, 2004.

[7] M. El Hachemi Benbouzid, "A review of induction motors signature analysis as a medium for faults detection," *Ind. Electron. IEEE Trans. On*, vol. 47, no. 5, pp. 984–993, 2000.

[8] H. Bloch and H. P. Block, *Practical Machinery Management for Process Plants: Volume 1: Improving Machinery Reliability: Improving Machinery Reliability Vol 1*, 3 edition. Houston, Tex: Gulf Professional Publishing, 1998.

[9] L. (Weidong) and U. of M. M. S. of Engineering, *A Study of Diesel Engine Acoustic Characteristics*. University of Manchester, 2000.

[10] D. H. Shreve, "Introduction to vibration technology," *IRD Mechanalysis Inc Columb.*, 1994.

[11] S.-G. Liu, L.-Y. Ding, and H.-H. Zeng, "Design and implementation of integrated protection apparatus in prefabricated substation," in *Proceedings of 2004 International Conference on Machine Learning and Cybernetics, 2004*, 2004, vol. 5, pp. 2804–2808 vol.5.

[12] S. Patidar and P. K. Soni, "An overview on Vibration analysis techniques for the diagnosis of rolling element bearing faults," *Int. J. Eng. Trends Technol. IJETT*, vol. 4, no. 5, pp. 1804–1809, 2013.

[13] Z. Pei, Z. Deng, B. Yang, and X. Cheng, "Application-oriented wireless sensor network communication protocols and hardware platforms: A survey," in *Industrial Technology, 2008. ICIT 2008. IEEE International Conference on*, 2008, pp. 1–6.

[14] B. Li, M.-Y. Chow, Y. Tipsuwan, and J. C. Hung, "Neural-network-based motor rolling bearing fault diagnosis," *Ind. Electron. IEEE Trans. On*, vol. 47, no. 5, pp. 1060–1069, 2000.

[15] H. Monavar, H. Ahmadi, and S. Mohtasebi, "Prediction of Defects in Roller Bearings Using Vibration Signal Analysis." 2008.

[16] N. A. Chang and S. L. Ceccio, "The acoustic emissions of cavitation bubbles in stretched vortices," *J. Acoust. Soc. Am.*, vol. 130, no. 5, pp. 3209–3219, 2011.

[17] X. Liu, X. Wu, and C. Liu, "A comparison of acoustic emission and vibration on bearing fault detection," in *2011 International Conference on Transportation, Mechanical, and Electrical Engineering (TMEE)*, 2011, pp. 922–926.

[18] L. M. Rogers, "The application of vibration signature analysis and acoustic emission source

location to on-line condition monitoring of anti-friction bearings," *Tribol. Int.*, vol. 12, no. 2, pp. 51–58, Apr. 1979.

[19] N. Tandon and B. C. Nakra, "Comparison of vibration and acoustic measurement techniques for the condition monitoring of rolling element bearings," *Tribol. Int.*, vol. 25, no. 3, pp. 205–212, Jun. 1992.

[20] N. T. A. Choudhury, "Application of acoustic emission technique for the detection of defects in rolling element bearings. Tribology Int," *Tribol. Int.*, vol. 33, no. 1, pp. 39–45, 2000.

[21] C. James Li and S. Y. Li, "Acoustic emission analysis for bearing condition monitoring," *Wear*, vol. 185, no. 1–2, pp. 67–74, Jun. 1995.

[22] J. Miettinen and P. Andersson, "Acoustic emission of rolling bearings lubricated with contaminated grease," *Tribol. Int.*, vol. 33, no. 11, pp. 777–787, Nov. 2000.

[23] N. Tandon and A. Choudhury, "A review of vibration and acoustic measurement methods for the detection of defects in rolling element bearings," *Tribol. Int.*, vol. 32, no. 8, pp. 469–480, 1999.

[24] X. Liu, X. Wu, and C. Liu, "A comparison of acoustic emission and vibration on bearing fault detection," in *Transportation, Mechanical, and Electrical Engineering (TMEE), 2011 International Conference on*, 2011, pp. 922–926.

[25] V. C. Gungor and G. P. Hancke, "Industrial Wireless Sensor Networks: Challenges, Design Principles, and Technical Approaches," *IEEE Trans. Ind. Electron.*, vol. 56, no. 10, pp. 4258–4265, Oct. 2009.

[26] H. Hayashi, T. Hasegawa, and K. Demachi, "Wireless technology for process automation," in *ICCAS-SICE, 2009*, 2009, pp. 4591–4594.

[27] J. Yick, B. Mukherjee, and D. Ghosal, "Wireless sensor network survey," *Comput. Netw.*, vol. 52, no. 12, pp. 2292–2330, Aug. 2008.

[28] A. Bogias, "A wireless 802.11 condition monitoring sensor for electrical substation environments," phd, Cardiff University, 2012.

[29] B. Lu, L. Wu, T. G. Habetler, R. G. Harley, and J. A. Gutierrez, "On the application of wireless sensor networks in condition monitoring and energy usage evaluation for electric machines," in *Industrial Electronics Society, 2005. IECON 2005. 31st Annual Conference of IEEE*, 2005, p. 6–pp.

[30] S. Giannoulis, C. Koulamas, C. Emmanouilidis, P. Pistofidis, and D. Karampatzakis, "Wireless Sensor Network Technologies for Condition Monitoring of Industrial Assets," in *Advances in Production Management Systems. Competitive Manufacturing for Innovative Products and Services*, Springer, 2013, pp. 33–40.

[31] J. Lin, Q. Chen, X. Tian, and F. Gu, "Fault diagnosis of rolling bearings using multifractal detrended fluctuation analysis and Mahalanobis distance criterion," in *Automation and Computing (ICAC), 2012 18th International Conference on*, 2012, pp. 1–6.

[32] X. X. Zheng, H. S. Xu, and others, "Fault diagnosis of wind turbine rolling bearing based on wavelet and Hilbert transforms," in *Control Conference (CCC)*, 2012, pp. 24–26.

[33] Y. Cai, C. Lu, and H. Liu, "Incipient fault detection of rolling bearing based on duffing oscillator," in *Reliability, Maintainability and Safety, 2009. ICRMS 2009. 8th International Conference on*, 2009, pp. 858–863.

[34] M. Li, "An intelligent fault diagnosis system of rolling bearing," in *Transportation, Mechanical, and Electrical Engineering (TMEE), 2011 International Conference on*, 2011, pp. 544–547.

[35] P. J. Tavner, "Review of condition monitoring of rotating electrical machines," *IET Electr. Power*

Appl., vol. 2, no. 4, p. 215, 2008.

[36] O. V. Thorsen and M. Dalva, "A survey of faults on induction motors in offshore oil industry, petrochemical industry, gas terminals, and oil refineries," *Ind. Appl. IEEE Trans. On*, vol. 31, no. 5, pp. 1186–1196, 1995.

[37] P. J. Tavner and J. P. Hasson, "Predicting the design life of high integrity rotating electrical machines," 1999.

[38] IAS Motor Reliability Working Group, "report of large motor reliability survey of industrial and commercial installations." Aug-1985.

[39] P. F. Albrecht, J. C. Appiarius, R. M. McCoy, E. L. Owen, and D. K. Sharma, "Assessment of the reliability of motors in utility applications-Updated," *Energy Convers. IEEE Trans. On*, no. 1, pp. 39–46, 1986.

[40] O. V. Thorsen and M. Dalva, "A survey of faults on induction motors in offshore oil industry, petrochemical industry, gas terminals, and oil refineries," *Ind. Appl. IEEE Trans. On*, vol. 31, no. 5, pp. 1186–1196, 1995.

[41] P. F. Albrecht, J. C. Appiarius, R. M. McCoy, E. L. Owen, and D. K. Sharma, "Assessment of the reliability of motors in utility applications-Updated," *Energy Convers. IEEE Trans. On*, no. 1, pp. 39–46, 1986.

[42] L. Wang and R. X. Gao, *Condition Monitoring and Control for Intelligent Manufacturing*. Springer Science & Business Media, 2006.

[43] "Classification and Characteristics of Rolling Bearings," *Classification and Characteristics of Rolling Bearings*, 04-Aug-2013. [Online]. Available: http://www.ntn.co.jp/english/products/catalog/pdf/2202E_a01.pdf.

[44] "Bearing self-study guide," *Expanding your knowledge of bearings and related components.* [Online]. Available: http://www.skf.com/binary/12-69177/457640.pdf [Accessed: 01-Jan-2011].

[45] Houghton, P. S, "Ball and Roller Bearings." Applied Science Publishers Ltd, 1976.

[46] Karim Nice, "HowStuffWorks 'How Bearings Work,'" *HowStuffWorks*. [Online]. Available: http://science.howstuffworks.com/transport/engines-equipment/bearing.htm. [Accessed: 01-Aug-2014].

[47] S. A. McInerny and Y. Dai, "Basic vibration signal processing for bearing fault detection," *IEEE Trans. Educ.*, vol. 46, no. 1, pp. 149–156, Feb. 2003.

[48] "BEARINGFAILURE: CAUSES AND CURES." .

[49] S. A. McInerny and Y. Dai, "Basic vibration signal processing for bearing fault detection," *IEEE Trans. Educ.*, vol. 46, no. 1, pp. 149–156, 2003.

[50] P. P. Kharche and S. V. Kshirsagar, "Review of Fault Detection in Rolling Element Bearing," 2014.

[51] S. . McInerny and Y. Dai, "Basic vibration signal processing for bearing fault detection," *IEEE Trans. Educ.*, vol. 46, no. 1, pp. 149–156, Feb. 2003.

[52] I. Howard, "A Review of Rolling Element Bearing Vibration'Detection, Diagnosis and Prognosis'," DTIC Document, 1994.

[53] N. Tandon and A. Choudhury, "AN ANALYTICAL MODEL FOR THE PREDICTION OF THE VIBRATION RESPONSE OF ROLLING ELEMENT BEARINGS DUE TO A LOCALIZED DEFECT," *J. Sound Vib.*, vol. 205, no. 3, pp. 275–292, Aug. 1997.

[54] A. V. Dube, L. S. Dhamande, and P. G. Kulkarni, "Vibration Based Condition Assessment Of Rolling element Bearings With Localized Defects," *Int. J. Sci. Technol. Res.*, vol. 2, no. 4, 2013.

[55] Mao Kunli and Wu Yunxin, “Fault Diagnosis of Rolling Element Bearing Based on Vibration Frequency Analysis,” 2011, pp. 198–201.

[56] F. Immovilli, M. Cocconcelli, A. Bellini, and R. Rubini, “Detection of Generalized-Roughness Bearing Fault by Spectral-Kurtosis Energy of Vibration or Current Signals,” *IEEE Trans. Ind. Electron.*, vol. 56, no. 11, pp. 4710–4717, Nov. 2009.

[57] P. Večeř, M. Kreidl, and R. Šmíd, “Condition Indicators for Gearbox Condition Monitoring Systems,” 06-Jan-2005. [Online]. Available: https://ojs.cvut.cz/ojs/index.php/ap/article/view/782. [Accessed: 04-Aug-2014].

[58] M. Lebold, K. McClintic, R. Campbell, C. Byington, and K. Maynard, “Review of vibration analysis methods for gearbox diagnostics and prognostics,” in *Proceedings of the 54th Meeting of the Society for Machinery Failure Prevention Technology*, 2000, vol. 634.

[59] J. P. Dron, F. Bolaers, and l. Rasolofondraibe, “Improvement of the sensitivity of the scalar indicators (crest factor, kurtosis) using a de-noising method by spectral subtraction: application to the detection of defects in ball bearings,” *J. Sound Vib.*, vol. 270, no. 1–2, pp. 61–73, Feb. 2004.

[60] S. Al-Arbi, “Condition Monitoring of Gear Systems using Vibration Analysis,” University of Huddersfield, 2012.

[61] F. De Lorenzo and M. Calabro, “Kurtosis: A statistical approach to identify defect in rolling bearing,” *Kurtosis: A statistical approach to identify defect in rolling bearing*. [Online]. Available: http://www.icmrt07.unina.it/Proceedings/Papers/A/84.pdf. [Accessed: 10-May-2013].

[62] S. Jaehong, “On-line machinery health diagnosis and prognosis for predictive maintenance and quality assurance of equipment functioning,” 2001.

[63] A. K. S. Jardine, D. Lin, and D. Banjevic, “A review on machinery diagnostics and prognostics implementing condition-based maintenance,” *Mech. Syst. Signal Process.*, vol. 20, no. 7, pp. 1483–1510, Oct. 2006.

[64] B. D. Forrester, “Advanced vibration analysis techniques for fault detection and diagnosis in geared transmission systems,” 1996.

[65] R. B. Randall, “A New Method of Modeling Gear Faults,” *J. Mech. Des.*, vol. 104, no. 2, pp. 259–267, Apr. 1982.

[66] P. Fidler, “THEORETICAL VERIFICATION OF ENVELOPE ANALYSIS OF ROLLING ELEMENT BEARINGS WITH USING MATLAB,” 2009.

[67] R. Rubini and U. Meneghetti, “APPLICATION OF THE ENVELOPE AND WAVELET TRANSFORM ANALYSES FOR THE DIAGNOSIS OF INCIPIENT FAULTS IN BALL BEARINGS,” *Mech. Syst. Signal Process.*, vol. 15, no. 2, pp. 287–302, Mar. 2001.

[68] Y.-T. Sheen, “An envelope analysis based on the resonance modes of the mechanical system for the bearing defect diagnosis,” *Measurement*, vol. 43, no. 7, pp. 912–934, Aug. 2010.

[69] R. B. Randall and J. Antoni, “Rolling element bearing diagnostics—A tutorial,” *Mech. Syst. Signal Process.*, vol. 25, no. 2, pp. 485–520, Feb. 2011.

[70] Y. Yunlong and Z. Zhenxiang, “Fault diagnosis of rolling rearing based on the wavelet analysis,” in *2010 2nd International Asia Conference on Informatics in Control, Automation and Robotics (CAR)*, 2010, vol. 1, pp. 257–260.

[71] V. N. Patel, N. Tandon, and R. K. Pandey, “Defect detection in deep groove ball bearing in presence of external vibration using envelope analysis and Duffing oscillator,” *Measurement*, vol. 45, no. 5, pp. 960–970, Jun. 2012.

[72] Y.-T. Sheen, “An envelope detection method based on the first-vibration-mode of bearing vibration,” *Measurement*, vol. 41, no. 7, pp. 797–809, Aug. 2008.

[73] B. Claudio, I. Fabio, C. Marco, R. Riccardo, and B. Alberto, “Fault Detection of Linear Bearings in Brushless AC Linear Motors by Vibration Analysis.” IEEE, 2010.

[74] W. Taiyong and L. Jinzhou, “Fault Diagnosis of Rolling Bearings Based on Wavelet Packet and Spectral Kurtosis,” 2011, pp. 665–669.

[75] A. K. S. Jardine, D. Lin, and D. Banjevic, “A review on machinery diagnostics and prognostics implementing condition-based maintenance,” *Mech. Syst. Signal Process.*, vol. 20, no. 7, pp. 1483–1510, Oct. 2006.

[76] J. Altmann and J. Mathew, “MULTIPLE BAND-PASS AUTOREGRESSIVE DEMODULATION FOR ROLLING-ELEMENT BEARING FAULT DIAGNOSIS,” *Mech. Syst. Signal Process.*, vol. 15, no. 5, pp. 963–977, Sep. 2001.

[77] X. Lou and K. A. Loparo, “Bearing fault diagnosis based on wavelet transform and fuzzy inference,” *Mech. Syst. Signal Process.*, vol. 18, no. 5, pp. 1077–1095, Sep. 2004.

[78] S. Tyagi, “Wavelet Analysis And Envelope Detection For Rolling Element Bearing Fault Diagnosis ø e A Comparative Study,” 2003.

[79] N. E. Huang, Z. Shen, S. R. Long, M. C. Wu, H. H. Shih, Q. Zheng, N.-C. Yen, C. C. Tung, and H. H. Liu, “The empirical mode decomposition and the Hilbert spectrum for nonlinear and non-stationary time series analysis,” *Proc. R. Soc. Lond. Math. Phys. Eng. Sci.*, vol. 454, no. 1971, pp. 903–995, Mar. 1998.

[80] N. E. Huang, Z. Shen, and S. R. Long, “A NEW VIEW OF NONLINEAR WATER WAVES: The Hilbert Spectrum [1],” *Annu. Rev. Fluid Mech.*, vol. 31, no. 1, pp. 417–457, Jan. 1999.

[81] L. J. Hadjileontiadis, “A Novel Technique for Denoising Explosive Lung Sounds Emnpirmical Mode Decompiosition and Fractal Dimension Foilter,” *Eng. Med. Biol. Mag. IEEE*, vol. 26, no. 1, pp. 30–39, 2007.

[82] Y. Kopsinis and S. McLaughlin, “Development of EMD-Based Denoising Methods Inspired by Wavelet Thresholding,” *IEEE Trans. Signal Process.*, vol. 57, no. 4, pp. 1351–1362, Apr. 2009.

[83] C. Junsheng, Y. Dejie, and Y. Yu, “A fault diagnosis approach for roller bearings based on EMD method and AR model,” *Mech. Syst. Signal Process.*, vol. 20, no. 2, pp. 350–362, Feb. 2006.

[84] Z. K. Peng, P. W. Tse, and F. L. Chu, “A comparison study of improved Hilbert–Huang transform and wavelet transform: Application to fault diagnosis for rolling bearing,” *Mech. Syst. Signal Process.*, vol. 19, no. 5, pp. 974–988, Sep. 2005.

[85] Bin Lu and V. C. Gungor, “Online and Remote Motor Energy Monitoring and Fault Diagnostics Using Wireless Sensor Networks,” *IEEE Trans. Ind. Electron.*, vol. 56, no. 11, pp. 4651–4659, Nov. 2009.

[86] J. Cheng, J. Jin, and L. Kong, “Wireless distributed monitoring and centralized controlling system for prefabricated substations in China,” in *IEEE International Conference on Industrial Technology, 2005. ICIT 2005*, 2005, pp. 45–50.

[87] H. Wu, L. Liu, and X. Yuan, “Remote Monitoring System of Mine Vehicle Based on Wireless Sensor Network,” in *2010 International Conference on Intelligent Computation Technology and Automation (ICICTA)*, 2010, vol. 2, pp. 1015–1019.

[88] K. R. Rao, Z. S. Bojkovic, and D. A. Milovanovic, *Wireless Multimedia Communications: Convergence, DSP, QoS, and Security*. CRC Press, 2008.

[89] P. Radmand, A. Talevski, S. Petersen, and S. Carlsen, "Comparison of industrial WSN standards," in *2010 4th IEEE International Conference on Digital Ecosystems and Technologies (DEST), IEEE, Dubai, United Arab Emirates*, 2010, pp. 632–637.

[90] "Introduction to Wireless LAN Measurements," *Introduction to Wireless LAN Measurements*, 03-Sep-2015. [Online]. Available: http://download.ni.com/evaluation/rf/Introduction_to_WLAN_Testing.pdf. [Accessed: 09-Mar-2015].

[91] "SmarTrend Web Vibration Monitoring Systems from Diagnostic Solutions | Diagnostic Solutions." .

[92] G. P. Hancke and B. Allen, "Ultrawideband as an Industrial Wireless Solution," *IEEE Pervasive Comput.*, vol. 5, no. 4, pp. 78–85, Oct. 2006.

[93] C. Zinner and W. Kubinger, "ROS-DMA: A DMA Double Buffering Method for Embedded Image Processing with Resource Optimized Slicing," in *Proceedings of the 12th IEEE Real-Time and Embedded Technology and Applications Symposium, 2006*, 2006, pp. 361–372.

[94] A. Mainwaring, D. Culler, J. Polastre, R. Szewczyk, and J. Anderson, "Wireless sensor networks for habitat monitoring," in *Proceedings of the 1st ACM international workshop on Wireless sensor networks and applications*, 2002, pp. 88–97.

[95] J. P. Lynch, "An overview of wireless structural health monitoring for civil structures," *Philos. Trans. R. Soc. Math. Phys. Eng. Sci.*, vol. 365, no. 1851, pp. 345–372, Feb. 2007.

[96] A. Carullo, S. Corbellini, M. Parvis, and A. Vallan, "A Wireless Sensor Network for Cold-Chain Monitoring," *IEEE Trans. Instrum. Meas.*, vol. 58, no. 5, pp. 1405–1411, May 2009.

[97] H.-C. Lee, A. Banerjee, Y.-M. Fang, B.-J. Lee, and C.-T. King, "Design of a Multifunctional Wireless Sensor for In-Situ Monitoring of Debris Flows," *IEEE Trans. Instrum. Meas.*, vol. 59, no. 11, pp. 2958–2967, Nov. 2010.

[98] N. Aakvaag, M. Mathiesen, and G. Thonet, "Timing and power issues in wireless sensor networks - an industrial test case," in *International Conference Workshops on Parallel Processing, 2005. ICPP 2005 Workshops*, 2005, pp. 419–426.

[99] D. Dzung, C. Apneseth, J. Endresen, and J.-E. Frey, "Design and implementation of a real-time wireless sensor/actuator communication system," in *10th IEEE Conference on Emerging Technologies and Factory Automation, 2005. ETFA 2005*, 2005, vol. 2, p. 10 pp.–442.

[100] "Wireless Sensors & Measurement Systems - GST." [Online]. Available: http://www.globalsensortech.com/wireless-sensors-measurement-systems. [Accessed: 03-Aug-2014].

[101] "HART Overview." [Online]. Available: http://en.hartcomm.org/hcp/tech/aboutprotocol/aboutprotocol_what.html. [Accessed: 03-Aug-2014].

[102] Montenegro, N. Kushalnagar, J. Hui, and D. Culler, "RFC 4944 - Transmission of IPv6 Packets over IEEE 802.15.4 Networks," 2007. [Online]. Available: http://www.rfc-base.org/rfc-4944.html. [Accessed: 24-Sep-2014].

[103] N. Q. Dinh, S.-W. Kim, and D.-S. Kim, "Performance evaluation of priority CSMA-CA mechanism on ISA100.11a wireless network," in *2010 5th International Conference on Computer Sciences and Convergence Information Technology (ICCIT)*, 2010, pp. 991–996.

[104] H. Hayashi, T. Hasegawa, and K. Demachi, "Wireless technology for process automation," in

ICCAS-SICE, 2009, 2009, pp. 4591–4594.

[105] Honeywell Inc., "XYR 6000 Wireless Transmitters - Accurate, Cost-Effective Process Monitoring." 2009.

[106] K. Al-Agha, M.-H. Bertin, T. Dang, A. Guitton, P. Minet, T. Val, and J.-B. Viollet, "Which Wireless Technology for Industrial Wireless Sensor Networks? The Development of OCARI Technology," *IEEE Trans. Ind. Electron.*, vol. 56, no. 10, pp. 4266–4278, Oct. 2009.

[107] "China Sensor, Measurement, Wireless Sensor supplier - Beijing Beetech Inc." [Online]. Available: http://www.made-in-china.com/showroom/beetech-beijing. [Accessed: 20-Jan-2015].

[108] W. Zhishen and A. Masato, *Structural Health Monitoring and Intelligent Infrastructure*, vol. 1. Tokyo, Japan: Taylor & Francis, 2003, 2003.

[109] V. P. Raj, K. Natarajan, and T. G. Girikumar, "Induction motor fault detection and diagnosis by vibration analysis using MEMS accelerometer," in *2013 International Conference on Emerging Trends in Communication, Control, Signal Processing Computing Applications (C2SPCA)*, 2013, pp. 1–6.

[110] R. B. Randall and J. Antoni, "Rolling element bearing diagnostics—A tutorial," *Mech. Syst. Signal Process.*, vol. 25, no. 2, pp. 485–520, Feb. 2011.

[111] "Tiva™ TM4C1233H6PM Microcontroller data sheet," *Tiva™ TM4C1233H6PM Microcontroller*. [Online]. Available: http://www.ti.com/lit/ds/symlink/tm4c1233h6pm.pdf.

[112] "XBee® ZB - Digi International." [Online]. Available: http://www.digi.com/products/wireless-wired-embedded-solutions/zigbee-rf-modules/zigbee-mesh-module/xbee-zb-module#overview. [Accessed: 28-Mar-2013].

[113] "XBee®/XBee-PRO® ZB RF Modules," *XBee®/XBee-PRO® ZB RF Modules*. [Online]. Available: https://www.adafruit.com/datasheets/XBee%20ZB%20User%20Manual.pdf. [Accessed: 09-Mar-2014].

[114] X. Liu, H. Chen, M. Wang, and S. Chen, "An XBee-Pro based energy monitoring system," in *Telecommunication Networks and Applications Conference (ATNAC), 2012 Australasian*, 2012, pp. 1–6.

[115] Digi International Inc., "XBee®/XBee-PRO® ZB RF Modules." Digi International Inc., 08-May-2013.

[116] D. Grover and J. R, *Digital Signal Processing and the Microcontroller*. 1998.

[117] "Robotic Embedded Systems Lab Yunlin: November 2007." [Online]. Available: http://smartrobot.blogspot.co.uk/2007_11_01_archive.html. [Accessed: 13-May-2015].

[118] R. G. Lyons, *Understanding digital signal processing*, 3rd ed. Upper Saddle River, NJ: Prentice Hall, 2011.

[119] "Envelope Detection - MATLAB & Simulink Example - MathWorks United Kingdom." [Online]. Available: http://uk.mathworks.com/help/dsp/examples/envelope-detection.html?requestedDomain=www.mathworks.com. [Accessed: 09-Jan-2015].

[120] S. Holm, "FFT pruning applied to time domain interpolation and peak localization," *IEEE Trans. Acoust. Speech Signal Process.*, vol. 35, no. 12, pp. 1776–1778, 1987.

[121] H. V. Sorensen, D. L. Jones, M. Heideman, and C. S. Burrus, "Real-valued fast Fourier transform algorithms," *Acoust. Speech Signal Process. IEEE Trans. On*, vol. 35, no. 6, pp. 849–863, 1987.

[122] G. D. Bergland, "A guided tour of the fast Fourier transform," *Spectr. IEEE*, vol. 6, no. 7, pp. 41–52,

1969.

[123] D. H. Shreve, “Signal processing for effective vibration analysis,” *IRD Mechanalysis Inc Columb. Ohio*, 1995.

[124] “TM4C ARM Cortex-M4 Microcontrollers - Tools & Software - TI.com.” [Online]. Available: http://www.ti.com/lsds/ti/microcontroller/tiva_arm_cortex/c_series/tm4c_arm_cortex-m4/tools_software.page#tivaware. [Accessed: 03-Jun-2013].

[125] “CMSIS DSP Software Library.” [Online]. Available: http://www.keil.com/pack/doc/CMSIS/DSP/html/index.html. [Accessed: 31-May-2015].

[126] “TI-RTOS - Texas Instruments Wiki.” [Online]. Available: http://processors.wiki.ti.com/index.php?title=TI-RTOS. [Accessed: 30-Mar-2015].

[127] J. Corcoran, *Electronic Instrument Handbook*, Third Edition. Palo Alto, California: Agilent Technologies, 2004.

[128] J. Antoni, “Fast computation of the kurtogram for the detection of transient faults,” *Mech. Syst. Signal Process.*, vol. 21, no. 1, pp. 108–124, Jan. 2007.

[129] J. Antoni, “The spectral kurtosis: a useful tool for characterising non-stationary signals,” *Mech. Syst. Signal Process.*, vol. 20, no. 2, pp. 282–307, Feb. 2006.